

A Study of Lipid-Protein Binding Assays With α -Tocopherol Transfer Protein Using Surface
Plasmon Resonance

Jennifer Kujani, BSc

Biotechnology

Submitted in partial fulfillment of the requirements for the degree of

Master of Science

Faculty of Mathematics and Science, Brock University

St. Catharines, Ontario

© Jennifer Kujani 2025

Abstract

Vitamin E is an essential micronutrient required both in early embryonic development, as well as into adulthood for proper neurological function and to prevent cell damage due to oxidative stress. Of its eight naturally occurring forms, the *RRR*- α -tocopherol isomer is selectively retained and used as an antioxidant in mammalian tissues. The α -tocopherol transfer protein (α -TTP) localized in the liver is responsible for the uptake and transport of *RRR*- α -tocopherol to the plasma membrane of hepatocytes to be secreted and delivered to target tissues throughout the body via systemic circulation. Despite knowing the bioactive role of vitamin E for centuries, the complete cyclic transport of α -tocopherol within hepatocytes remains unknown. This study investigates the binding interactions between recombinantly expressed wildtype α -TTP and unilamellar plasma membrane lipid vesicles containing various phosphatidylinositol phosphates to elucidate the mechanism of binding between α -TTP and its proposed secondary ligand – PI(4,5)P₂. Using surface plasmon resonance binding assays, wildtype α -TTP alone or preincubated with α -tocopherol was injected onto lipid vesicles containing either PI(4,5)P₂, PI(3,4)P₂, or PI(3)P. Based on association rate constants (k_{on} , s⁻¹), wtTTP preferentially bound to lipid vesicles containing 4% PI(3,4)P₂ (0.01896 s⁻¹) and 4% PI(4,5)P₂ (0.01174 s⁻¹) instead of 4% PI(3)P (0.00750 s⁻¹). In addition, concentration-dependence was observed for the rate of binding to lipid vesicles containing 2%, 4%, or 6% PI(4,5)P₂. All binding assays with wtTTP preincubated with α -tocopherol produced rate constants almost three times greater than their non-preincubated counterparts. However, while wtTTP preincubated with α -tocopherol still associated fastest to lipid vesicles containing PI(3,4)P₂, there was no correlation between rate of binding and increased PI(4,5)P₂ concentrations. The results found in this study provide further insight into the mode of α -tocopherol transport and ligand exchange facilitated by α -TTP in hepatocytes.

Acknowledgements

I would like to express my gratitude to Dr. Jeffrey Atkinson for being a wonderful supervisor throughout my graduate studies and for allowing me the opportunity to join his amazing laboratory group. Thank you to my committee members, Dr. Dustin Duncan and Dr. Stephen Glasgow, for their invaluable contributions.

Special words of appreciation go to Dr. Candace Panagabko for her outstanding guidance throughout my research journey. Your laboratory expertise and brilliance in problem solving are incomparable. I am extremely thankful for all the research skills you have taught me, even more so for the daily support and personal conversations we have shared about pets, childhood, life, and everything in between.

Thank you to the extraordinary group members, Natalie Boccalon and Morgan Robinson, whose camaraderie and continued support reminded me that self-care is just as important as a strong work ethic. Special thanks to Raissa Sultana for her friendship, wisdom, reassurance, and our coffee runs. I would also like to thank the Yan group for being exemplary lab mates with whom we shared space, instruments, reagents, and the ups and downs of research.

Finally, I am forever grateful to my family for their unwavering support throughout my entire university career. Thank you to my sister for inspiring me to pursue a life in science, and to my brother for challenging my views and introducing me to the thrilling world of motorcycles. Thank you to my parents who believed in me even when I doubted myself and always encouraged me to see how far I could go. To everyone – thank you with all my heart. I could never have gotten here without you all, and I will never forget everything that has been done for me as I continue in the future.

Table of Contents

Abstract.....	
Acknowledgements	
I. List of Figures	
II. List of Tables	
III. List of Abbreviations	
1 Introduction	1
1.1 Vitamin E.....	1
<u>1.1.1 History.....</u>	<u>1</u>
<u>1.1.2 Biochemistry</u>	<u>1</u>
<u>1.1.3 Dietary Sources and Transport.....</u>	<u>5</u>
1.2 α -TTP	10
<u>1.2.1 Localization and Function.....</u>	<u>10</u>
<u>1.2.2 Structure and α-Tocopherol Binding.....</u>	<u>10</u>
<u>1.2.3 α-TTP's Secondary Ligand</u>	<u>14</u>
<u>1.2.4 The α-Tocopherol Transport Cycle Model in Hepatocytes.....</u>	<u>16</u>
1.3 Ataxia with Vitamin E Deficiency	21
1.4 Surface Plasmon Resonance.....	24
<u>1.4.1 History.....</u>	<u>24</u>
<u>1.4.2 Principles and Experimentation</u>	<u>24</u>
<u>1.4.3 SPR Experimentation Used in this Project</u>	<u>25</u>
1.5 Project Outlines and Objectives	27
<u>1.5.1 Objectives</u>	<u>27</u>
<u>1.5.2 Project Outlines.....</u>	<u>31</u>
2 Experimental.....	33
2.1 Instruments	33
2.2 Software	34
2.3 Materials.....	35
2.4 Bacterial Strains	36
2.5 Chemicals, Reagents, Buffers, and Solutions	36
<u>2.5.1 Protein Expression, Purification, and Quantification Reagents.....</u>	<u>36</u>
<u>2.5.2 Protein Expression Solutions</u>	<u>37</u>
<u>2.5.3 Protein Purification Buffers</u>	<u>37</u>

2.5.4	<u>SDS-PAGE Chemicals</u>	38
2.5.5	<u>SDS-PAGE Solutions</u>	38
2.5.6	<u>Protein Binding Assay Buffer</u>	39
2.5.7	<u>Lipid Membrane Vesicle Reagents</u>	39
2.5.8	<u>SPR Reagents</u>	39
2.5.9	<u>SPR Buffers</u>	40
2.5.10	<u>SPR Chip Derivatization Reagents</u>	40
2.5.11	<u>SPR Chip Derivatization Solutions</u>	40
2.6	<u>Methods</u>	41
2.6.1	<u>α-TTP Transformations</u>	41
2.6.2	<u>Protein Expression</u>	41
2.6.3	<u>Protein Purification via Glutathione S-Transferase Affinity Chromatography</u>	42
2.6.4	<u>Protein Concentration Quantification</u>	44
2.6.5	<u>SDS-PAGE</u>	45
2.6.5.1	<i>13% Acrylamide Gel Casting</i>	45
2.6.5.2	<i>Gel Electrophoresis</i>	45
2.6.6	<u>α-TTP and NBD-α-Tocopherol Binding Assays</u>	46
2.6.6.1	<i>NBD-α-Tocopherol Quantification</i>	46
2.6.6.2	<i>Microplate Reader Binding Assay</i>	47
2.6.6.2.1	<u><i>Experimental Procedure</i></u>	47
2.6.6.2.2	<u><i>Data Analysis</i></u>	48
2.6.6.3	<i>Fluorometer Binding Assay</i>	49
2.6.6.3.1	<u><i>Experimental Procedure</i></u>	49
2.6.6.3.2	<u><i>Data Analysis</i></u>	51
2.6.7	<u>Lipid Membrane Vesicle Preparation</u>	51
2.6.8	<u>Wildtype α-TTP Preincubations with α-Tocopherol</u>	52
2.6.9	<u>Gold SPR Sensor Slide Derivatization</u>	52
2.6.10	<u>SPR Injection Procedure</u>	53
2.6.10.1	<i>SPR Injection Protocol</i>	53
2.6.10.2	<i>SPR Injection Conditions</i>	57
2.6.11	<u>SPR Data Analysis</u>	57

2.6.11.1	<i>SPR Data Extraction</i>	57
2.6.11.2	<i>SPR Data Analysis</i>	58
3	Results and Discussion	59
3.1	α -TTP Expression and Purification	59
3.2	SPR Concentration Binding Curve Using Wildtype α -TTP.....	67
3.3	SPR Injections Using Wildtype α -TTP, α -Tocopherol, and Lipid Vesicles with PIPs ...	70
3.3.1	<u>Wildtype α-TTP Injections</u>	<u>70</u>
3.3.2	<u>Wildtype α-TTP Preincubated with α-Tocopherol Injections</u>	<u>73</u>
3.4	SPR Troubleshooting	77
3.5	Wildtype α -TTP Binding Assays.....	81
3.6	Remaining SPR Issues	85
4	Conclusion and Future Directions	Error! Bookmark not defined.
5	References	91
6	Appendix	95

I. List of Figures

Figure 1. Natural Vitamin E Structures.....	2
Figure 2. Schematic Diagram of the Antioxidant Bioactivity of α -Tocopherol.	5
Figure 3. Digestive Transport of Vitamin E.....	8
Figure 4. Schematic Example of Hepatic γ -Tocopherol Metabolism.	9
Figure 5. Interactions of α -TTP's Binding Site and α -Tocopherol.	12
Figure 6. Closed and Open Conformations of α -TTP.....	13
Figure 7. The Different Forms of Phosphatidylinositol.....	15
Figure 8. Surface Topology of α -TTP.	16
Figure 9. α -Tocopherol Transport into and out of Hepatocytes.....	18
Figure 10. Proposed Mechanistic Model for the α -Tocopherol Transport Cycle via α -TTP.....	20
Figure 11. TTPA Gene.....	22
Figure 12. SPR Detector Report.	25
Figure 13. SPR Experiment and Sensor Chip Schematic.....	27
Figure 14. Single Point Mutations of α -TTP.....	31
Figure 15. Binding Assay Plate Configuration.....	48
Figure 16. Detector Scan Data Trace.....	54
Figure 17. wtTTP Expression Using Different Cell Lines.	60
Figure 18. Schematic Diagram of GST Affinity Purification.....	61
Figure 19. α -TTP Purification via GST Affinity Chromatography Pre-Optimization.....	63
Figure 20. α -TTP Purification via GST Affinity Chromatography Post-Optimization.	67
Figure 21. wtTTP Concentration Binding Curve.....	69
Figure 22. Injections of wtTTP onto PM with PIPs.....	71
Figure 23. One-Way ANOVA Test of Rate Constants and B_{\max} Values of wtTTP Injections.....	73
Figure 24. Injections of wtTTP Preincubated with α -Tocopherol onto PM with PIPs.....	74
Figure 25. One-Way ANOVA Test of Rate Constants and B_{\max} Values of wtTTP Preincubation Injections.	76
Figure 26. Lipid and Protein Injection Issues.	78
Figure 27. Binding Assays Performed Using wtTTP Purified with Triton X-100.....	82
Figure 28. Binding Assays Performed Using wtTTP Purified without Triton X-100.	85
Figure 29. BSA Standard Injection.	86
Figure 30. Representative Sensorgram of SPR Injections and Chip Regeneration Cycle... ..	95
Figure 31. Raw Data Used to Generate the Concentration Binding Curve in Figure 21.....	95
Figure 32. Raw Data of SPR Injections of wtTTP Used to Generate Figure 22.....	96
Figure 33. Non-normalized SPR Injections of wtTTP Used to Generate Figure 22.....	96
Figure 34. SPR Injections of wtTTP Depicting Error Bars Used to Generate Figure 22.....	97
Figure 35. Raw Data of SPR Injections of wtTTP Preincubated with α -Tocopherol Used to Generate Figure 24.	100
Figure 36. Non-normalized SPR Injections of wtTTP Preincubated with α -Tocopherol... ..	100
Figure 37. SPR Injections of wtTTP Preincubated with α -Tocopherol Depicting Error Bars Used to Generate Figure 24.....	101
Figure 38. Mass Spectrum of NBD- α -Tocopherol Stock Solution.	104

II. List of Tables

Table 1. Mutations Found in the TTPA Gene	22
Table 2. Planned SPR Experiments using wtTTP and K217A	29
Table 3. Concentration of NBD-α-Tocopherol During Fluorometer Binding Assays	50
Table 4. Plasma Membrane Lipid Composition	51
Table 5. SPR Injection Syringe Cleaning Protocol	55
Table 6. α-TTP Purification Optimization Strategies	66
Table 7. SPR Troubleshooting Methods	80
Table 8. Parameter Values of wtTTP Injections	98
Table 9. P Values of Rate Constants for wtTTP Injections	99
Table 10. P Values of B_{\max} Values for wtTTP Injections	99
Table 11. Parameter Values of wtTTP Preincubated with α-Tocopherol Injections	102
Table 12. P Values of Rate Constants for wtTTP Preincubated with α-Tocopherol Injections	103
Table 13. P Values of B_{\max} Values for wtTTP Preincubated with α-Tocopherol Injections	103

III. List of Abbreviations

ABCA1	ATP-binding cassette transporter A1
APS	Ammonium persulfate
ATP	Adenosine triphosphate
AVED	Ataxia due to vitamin E deficiency
BSA	Bovine serum albumin
CRALBP	Cellular retinaldehyde binding protein
CEHC	Carboxyethyl hydroxychromanol
CMR	Chylomicron remnant
DF	Dilution factor
DMSO	Dimethyl sulfoxide
DOPA	1,2-dioleoyl-sn-glycero-3-phosphate
DOPC	1,2-dioleoyl-sn-glycero-2-phosphocholine
DOPE	1,2-dioleoyl-sn-glycero-3-phosphoethanolamine
DOPS	1,2-dioleoyl-sn-glycero-3-phospho-L-serine
DTT	DL-Dithiothreitol
EDC	<i>N</i> -(3-dimethylaminopropyl)- <i>N</i> '-ethylcarbodiimide
EDTA	Ethylenediaminetetraacetic acid
ER	Endoplasmic reticulum
FIVE	Familial isolated vitamin E deficiency
Frq1	Frequenin
GST	Glutathione <i>S</i> -transferase
HDL	High-density lipoprotein
HEPES	4-(2-hydroxyethyl)piperazine-1-ethanesulfonic acid
IPTG	Isopropyl- β -D-thiogalactopyranoside
K ₂ HPO ₄	Dipotassium phosphate
KH ₂ PO ₄	Monopotassium phosphate
LB+	Luria Bertani plus
LDL	Low-density lipoprotein
LE/L	Late endosome/lysosome
MS	Mass spectrometry
NaCl	Sodium chloride
NBD	4-chloro-7-nitro-2,1,3-benzoxadiazole
NHS	<i>N</i> -hydroxysuccinimide
NPC1L1	Niemann-Pick C1-like protein 1
OD	Optical density
PA	Phosphatidic acid
PAGE	Polyacrylamide gel electrophoresis
PBS	Phosphate buffered saline
PC	Phosphatidylcholine
PE	Phosphatidylethanolamine
PI	Phosphatidylinositol
PI(3)P	Phosphatidylinositol-3-phosphate
PI(3,4)P ₂	Phosphatidylinositol-3,4-bisphosphate
PI(4,5)P ₂	Phosphatidylinositol-4,5-bisphosphate

PI4KIII β	Phosphatidylinositol 4-kinase type III beta protein
PIP ₂	Phosphatidylinositol biphosphates
PIPs	Phosphatidylinositol phosphates
PITPs	Phosphatidylinositol/phosphatidylcholine transfer proteins
PM	Plasma membrane
PMSF	Phenylmethylsulfonyl fluoride
PS	Phosphatidylserine
PUFA	Polyunsaturated fatty acid
RIU	Refractive index unit
ROS	Reactive oxygen species
SDS	Sodium dodecyl sulfate
SM	Sphingomyelin
SOC	Super optimal growth medium with catabolic repressor
SPF	Supernatant protein factor
SPR	Surface plasmon resonance
SR-B1	Scavenger receptor class type B1
TB	Terrific broth
TCE	Trichloroethylene
TEMED	Tetramethylethylenediamine
UV	Ultraviolet
VLDL	Very low-density lipoprotein
wtTTP	Wildtype α -tocopherol transfer protein
α -TTP	α -Tocopherol transfer protein

1 Introduction

1.1 Vitamin E

1.1.1 History

Vitamin E was discovered in 1922 by Herbert Evans and Katherine Bishop who were investigating the dietary requirements for producing healthy, fertile rats on vegetable-deficient diets (Niki & Traber, 2012). In this preliminary research it was discovered that rats raised on a diet containing casein, starches, salts, and fats could mature to the adult stage. However, the rats became infertile due to abnormalities of placental function post-fertilization, which resulted in embryonic resorption (Evans & Bishop, 1922). At the time, the identity of the molecule required for proper reproduction was unknown, termed as X, and was shown not to be vitamin A, B, or C, but some other substance, which reversed infertility when rat diets were supplemented with lettuce. Similar work completed by Barnett Sure corroborated these findings, and upon publishing his own findings two years after Evans and Bishop, Sure proposed this new substance be termed vitamin E following the Latin alphabetical nomenclature of vitamins at the time (Sure, 1924). Subsequent research efforts were focused on elucidating the chemical structure and biological function of vitamin E, especially to understand its necessity for reproduction.

1.1.2 Biochemistry

Later studies showed that vitamin E is not one compound, but a collection of eight naturally occurring molecules. There are two subcategories of vitamin E – tocopherols and tocotrienols – both of which consist of a chromanol ring and a 13-carbon length phytyl tail. This fatty acid chain is fully saturated for tocopherols, but contains three double bonds at positions $\Delta 3$, $\Delta 7$, and $\Delta 11$ for tocotrienols (Schneider, 2005). In addition, tocopherols and tocotrienols have further been categorized based on the number and location of methyl groups present on the benzene ring portion

of the chromanol structure. Based on the methyl substituents, four vitamers exist for both types of vitamin E – α , β , γ , and δ – resulting in eight distinct natural structures (Figure 1).

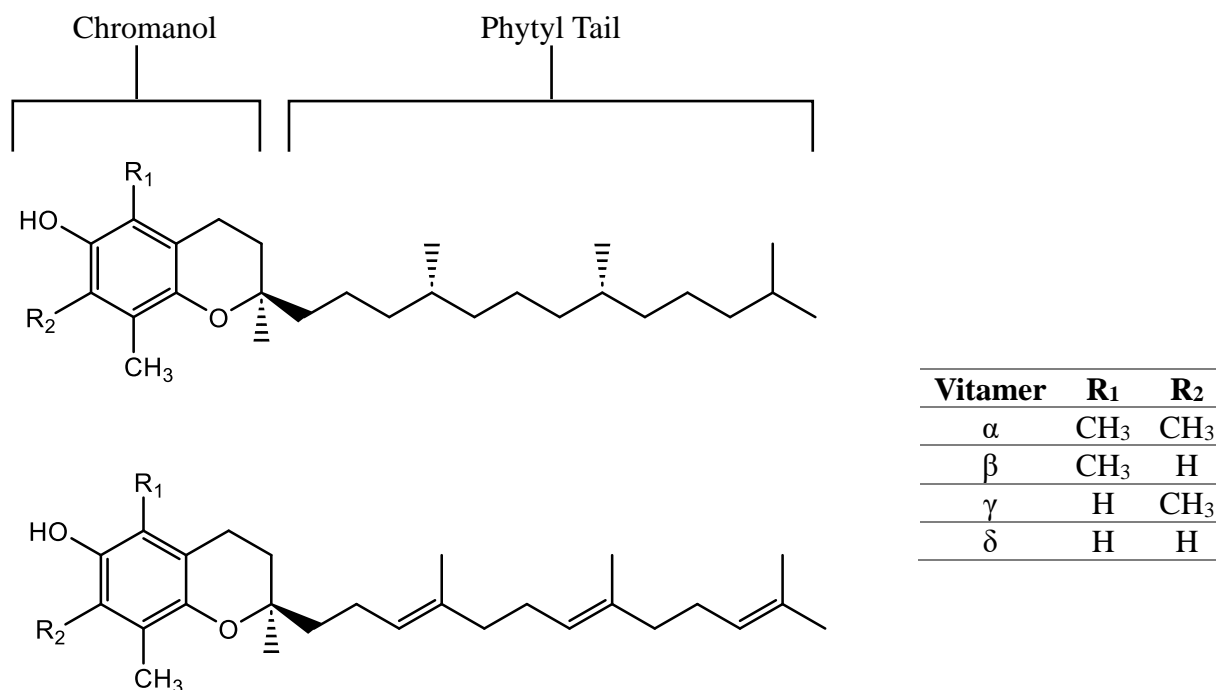
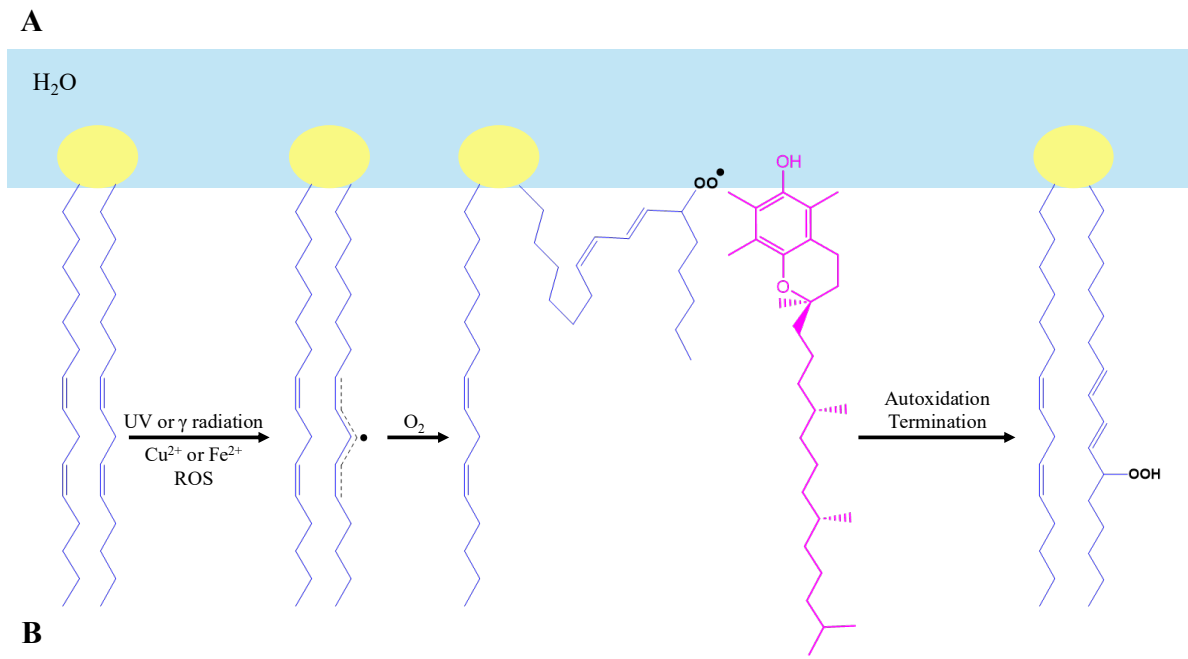
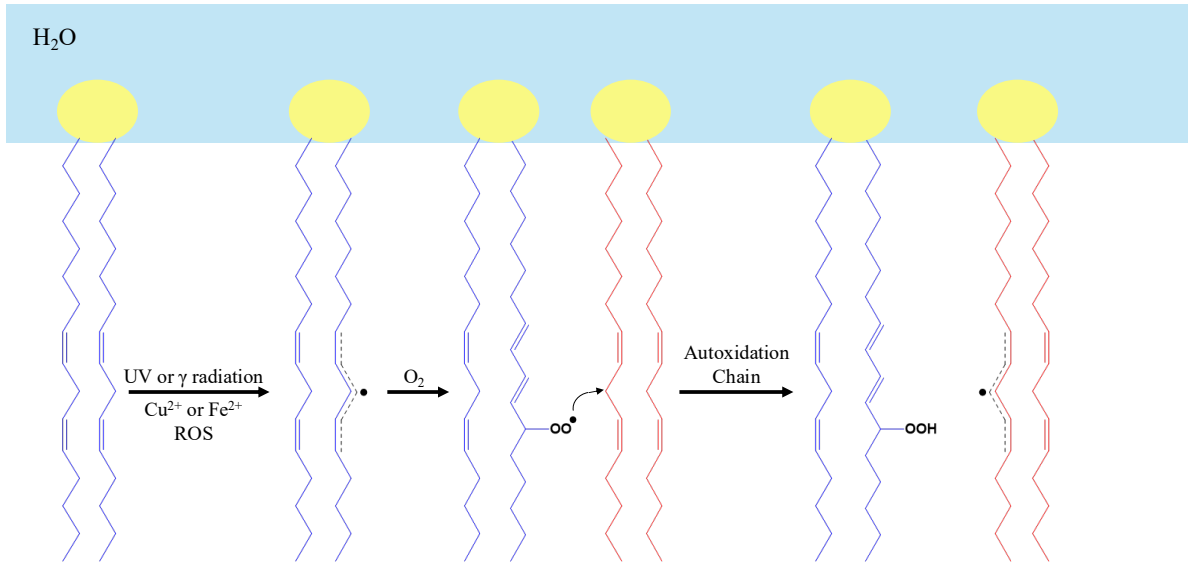


Figure 1. Natural Vitamin E Structures.

The term vitamin E encompasses two subcategories of molecules: tocopherols (top) and tocotrienols (bottom). The variation of methyl substitution at positions R₁ and R₂ on the chromanol ring yield four vitamers α , β , γ , and δ for both tocopherol and tocotrienols.

The fully saturated tocopherols have three chiral centers, giving rise to different stereochemical structures. The natural stereoisomer of α -tocopherol is 2R, 4'R, and 8'R, while tocotrienols only contain one chiral center at the C₂ position (Wang & Quinn, 1999). While all forms of vitamin E are absorbed, *RRR*- α -tocopherol is the most abundant form of vitamin E in mammalian tissues and has the highest bioactivity. In 1931, the antioxidant properties of vitamin E were shown by Henry Mattill and Harold Olcott, which showed the primary biological importance of vitamin E (Niki & Traber, 2012). The main molecular responsibility of vitamin E, predominantly α -tocopherol, is to terminate the autoxidation of polyunsaturated fatty acids (PUFAs). External factors like ultraviolet (UV) and γ -radiation, or internal factors like metal ions,

for example copper or iron, or reactive oxygen species (ROS) including hydrogen peroxide (H_2O_2) or superoxide (O_2^-) can induce autoxidation of PUFAs by extracting a hydrogen atom (Schneider, 2005). Upon this extraction, a radical is formed in the fatty acid tail, which quickly reacts with molecular oxygen to yield a fatty acid peroxy radical. Without the presence of an antioxidant, this lipid peroxidation can propagate a chain reaction of radical formation in subsequent PUFAs – ultimately leading to cell damage (Figure 2A). However, vitamin E can terminate this chain reaction by donating a hydrogen atom from its C_6 hydroxyl group to form a tocopheroxyl radical (Traber, 2007). Therefore, vitamin E is often referred to as a peroxy radical scavenger or chain breaking antioxidant because its main purpose is to stop lipid peroxidation due to radical formation (Figure 2B). To eliminate the tocopheroxyl radical of vitamin E, it can react with either another fatty acid peroxy radical and form an adduct or a second tocopheroxyl radical resulting in a dimer. In both cases, vitamin E is consumed and is no longer capable of acting as an antioxidant (Niki & Traber, 2012). However, if this were the only option, high cellular vitamin E concentrations would be required to mitigate lipid peroxidation. An alternate option is to recycle vitamin E to be used several times. In 1979, Packer and colleagues discovered that vitamin E is cellularly regenerated by ascorbate, more commonly known as vitamin C, producing the ascorbate radical, which is processed by enzyme pathways to regenerate ascorbate as well (Figure 2C). Other molecules have also been shown to regenerate vitamin E in the absence of ascorbate, including ubiquinol or thiols like glutathione (Buettner, 1993; Niki & Traber, 2012; Traber, 2007).



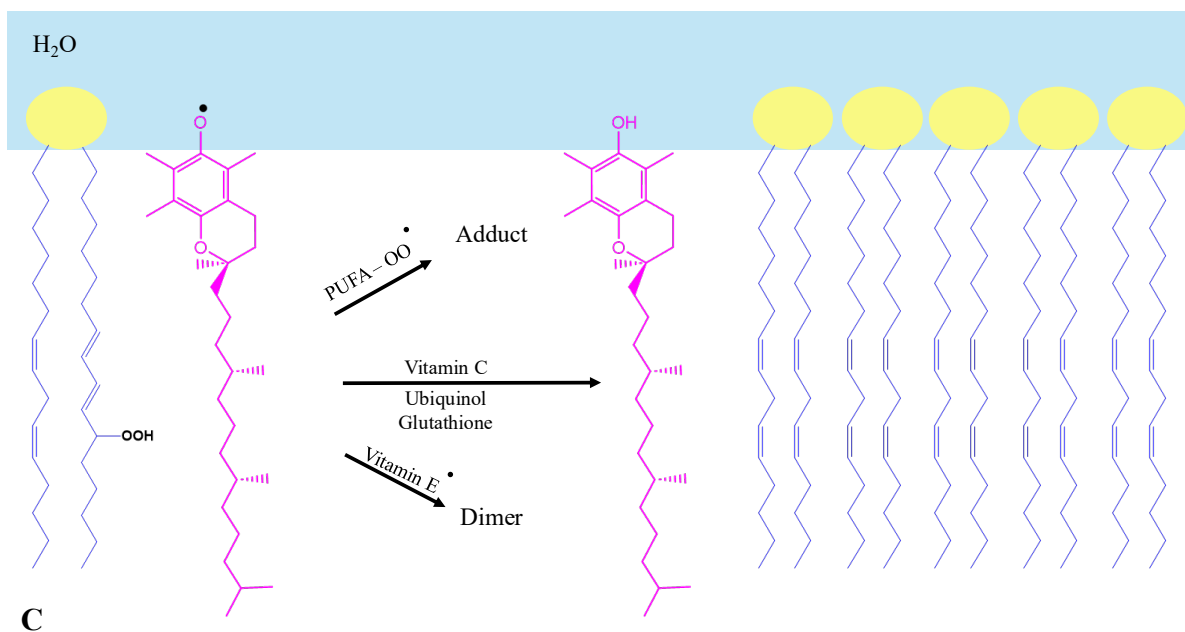


Figure 2. Schematic Diagram of the Antioxidant Bioactivity of α -Tocopherol.

Vitamin E is a cellular antioxidant that inhibits cell damage due to radical lipid peroxidation. A) Initiation and Propagation: a hydrogen atom is abstracted from a polyunsaturated lipid, producing a radical. Followed by the formation of a lipid peroxyl radical by reacting with molecular oxygen, a chain reaction of lipid autoxidation occurs in the absence of vitamin E that eventually leads to cell damage. B) Termination: once autoxidation is initiated, α -tocopherol interferes with propagation by donating the hydrogen atom from the hydroxyl group on C₆ of the chromanol ring. The lipid peroxyl radical is stabilized and the chain reaction is terminated, while a tocopheroxyl radical is produced. C) Vitamin E Regeneration: the tocopheroxyl radical is eliminated to prevent re-initiation of lipid peroxidation. Several pathways may eradicate the radical, or α -tocopherol may be recycled by ascorbate or vitamin C.

1.1.3 Dietary Sources and Transport

Vitamin E, like other vitamins, is an essential nutrient that humans cannot biosynthesize and must obtain from dietary sources. According to the National Institute of Health (NIH), adults should consume 15 mg of α -tocopherol daily – as this form of vitamin E is the primary bioactive molecule (Shahidi et al., 2021). However, natural sources of vitamin E contain varying compositions of tocopherols or tocotrienols, which can be found in different food groups – mainly vegetable and seed oils, but also certain raw vegetables, fruits and some animal products. On average, the two most abundant forms of vitamin E in many sources are α - and γ -tocopherol. α -

tocopherol makes up at least 50% of vitamin E found in coconut, olive, and peanut oils. Sunflower and wheat germ oils are especially rich in α -tocopherol, containing 88% and 75%, respectively (Shahidi et al., 2021). On the contrary, large amounts of γ -tocopherol can be found in canola, corn, cottonseed, and soybean oils. Moreover, nearly 100% of vitamin E in linseed and sesame oil is γ -tocopherol. Interestingly, the α - and γ -vitamers are also the most abundant forms of tocotrienols in seed oils and are especially abundant in palm and rice bran oils relative to other forms of tocotrienols (Niki & Abe, 2019). As per raw vegetables and fruits, α -tocopherol is the primary form of vitamin E in most, including carrot roots (99%), parsley (98%), spinach leaves (63%), and lettuce (55%) leaves, as well as in apples (90%), kiwis (90%), bananas (87%), tomatoes (78%), cranberries (76%), and strawberries (68%) (Szymańska et al, 2020). According to Shahidi and colleagues (2021), some dairy sources like milk, sour cream, cream cheese, yogurt, and egg yolks contain some amount of α -tocopherol, mostly trace amounts compared to previously mentioned sources. However, the vitamin E content in dairy products should still be considered as a nutrient source based on the amount consumed relative to seed oils.

Despite having eight forms of vitamin E that may be consumed from different nutritional sources, different types of vitamin E have varying bioavailabilities. Being a fat-soluble vitamin, vitamin E follows a similar path of absorption as other lipids. Upon ingestion, vitamin E is packaged into micelles formed from pancreatic enzymes and bile acids, which are then transported into the small intestine for absorption (Herrera & Barbas, 2001). Occurring in the duodenum, vitamin E enters enterocytes either via passive diffusion or protein-mediated transport carried out by the scavenger receptor class type B1 (SR-B1) and Niemann-Pick C1-like protein 1 (NPC1L1) transporters (Figure 3). All forms of vitamin E are then secreted from the small intestine into the lymph system by the ATP-binding cassette transporter A1 (ABCA1), where the different vitamers

are packaged into chylomicrons along with other lipids including triglycerides, cholesterol, and phospholipids (Schmölz et al, 2016). Chylomicrons then enter the bloodstream for systemic transport of vitamin E to muscle, adipose, skin, and brain tissues – which showed high concentrations of non- α -tocopherol forms. However, chylomicrons in systemic circulation are catabolized into chylomicron remnants, which carry the remaining majority of vitamin E absorbed into the liver (Jiang, 2014; Herrera & Barbas, 2001). Chylomicron remnants are then broken down in liver lysosomes and vitamin E becomes integrated into hepatic endosomes. In liver cells, the *RRR*- α -tocopherol stereoisomer is primarily bound by the α -tocopherol transfer protein (α -TTP), which secretes it from hepatocytes to be incorporated in very low-density lipoproteins (VLDLs). However, because VLDL concentrations are low in systemic circulation, some amount of α -tocopherol is also incorporated into low-density lipoproteins (LDLs) and high-density lipoproteins (HDLs) that all aid in the delivery of the main bioactive form of vitamin E to target tissues (Galli et al., 2017).

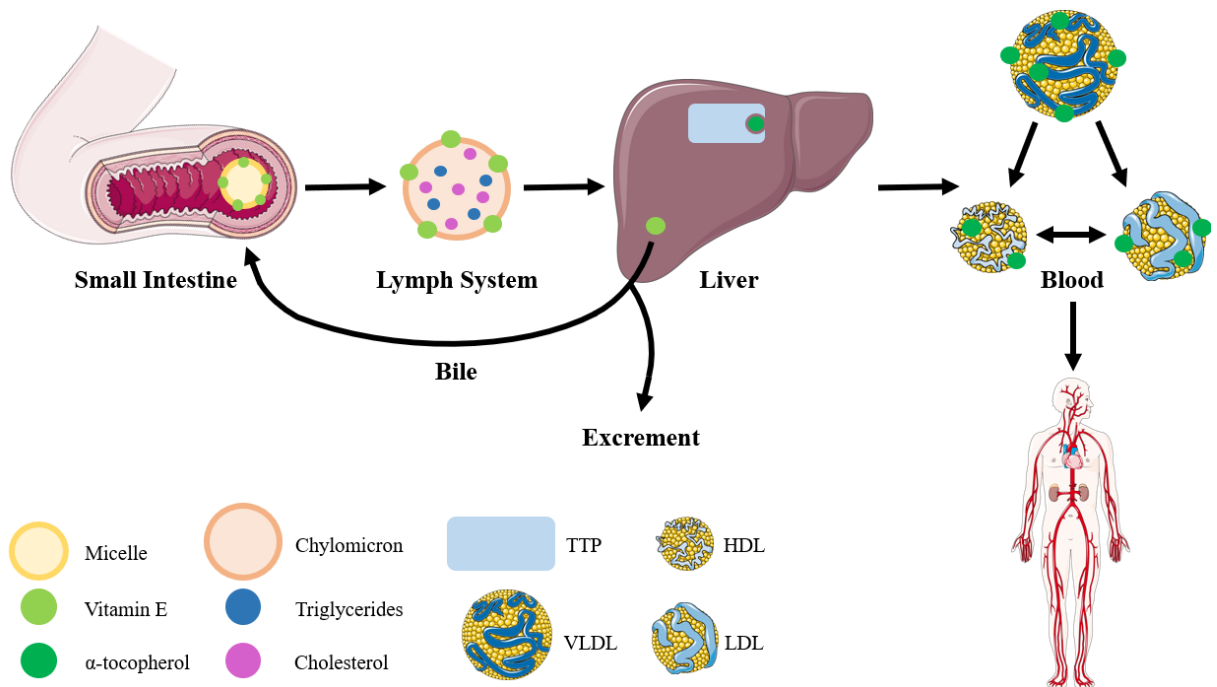


Figure 3. Digestive Transport of Vitamin E.

Vitamin E absorption occurs in the duodenum of the small intestine, where all forms of vitamin E are packaged into micelle vesicles. Vitamin E is then deposited in the liver by chylomicron remnants, where the α -tocopherol transfer protein (α -TTP) selectively binds the *RRR*- α -tocopherol stereoisomer. All other forms of vitamin E are metabolized and excreted in feces and urine. In a process that is still unknown, α -TTP helps transport *RRR*- α -tocopherol from liver cells. α -tocopherol then enters systemic circulation and is deposited in required tissues.

Contrary to other organ tissues, the *RRR*- α -tocopherol form is selected for in the liver, while all other forms are eliminated from hepatic tissue. Initially, the bioavailability discrepancies of vitamin E within the liver were explained solely by the greater binding affinity of α -TTP towards the natural stereoisomer of α -tocopherol (100%) compared to β -tocopherol (38%), γ -tocopherol (9%), and δ -tocopherol (2%) (Galli et al., 2017). However, further research showed α -TTP's preference towards α -tocopherol is not exclusively responsible for its accumulation in hepatic tissues. Unlike α -tocopherol, which is isolated in the binding site of α -TTP, the other forms of vitamin E that are not bound by α -TTP are more prone to side chain shortening (Figure 4). This metabolic pathway is initiated by ω -hydroxylation at the C_{13'} position of the phytyl tail by a cytochrome P450, either CYP4F2 or CYP3A4, followed by ω -oxidation and several rounds of β -

oxidations – producing carboxyethyl hydroxychromanol (CEHC) final metabolites (Jiang, 2014; Galli et al., 2017). Contrary to α -TTP having the highest binding affinity for α -tocopherol, CYP4F2 has greater affinity for non- α -tocopherol vitamin E. Therefore, these two activities in conjunction regulate hepatic retention of α -tocopherol and all other vitamin E metabolism and elimination.

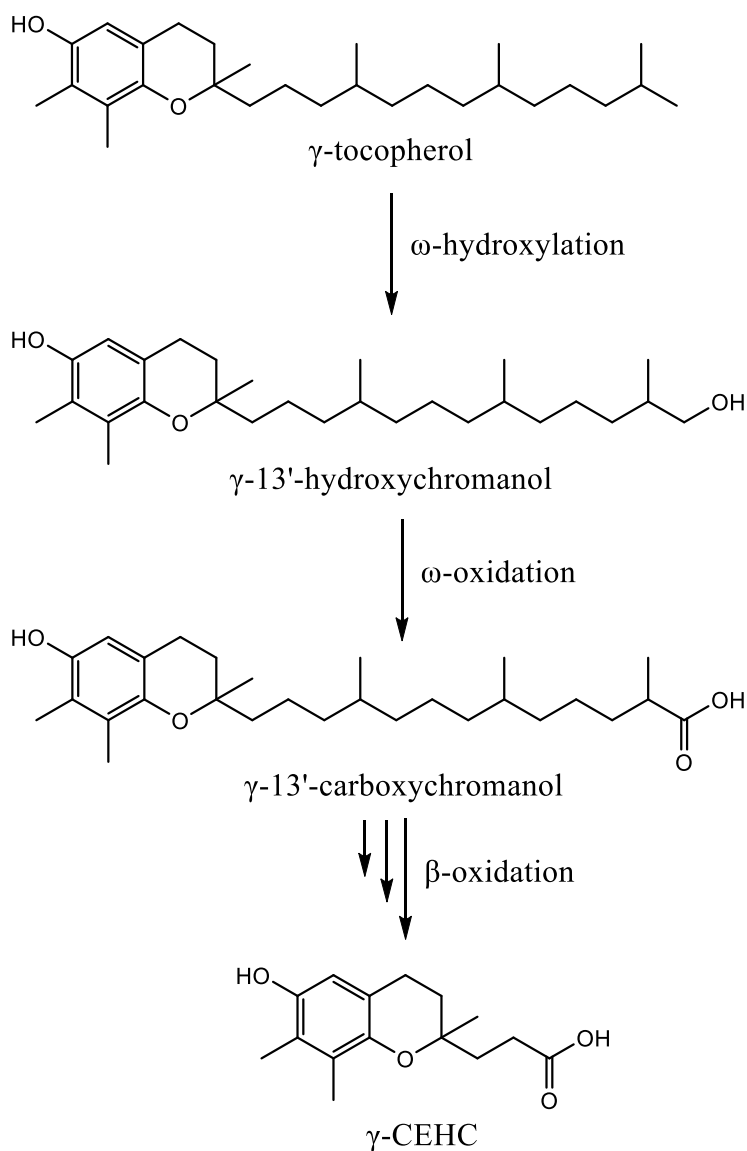


Figure 4. Schematic Example of Hepatic γ -Tocopherol Metabolism.

Apart from *RRR*- α -tocopherol, all other forms of vitamin E are metabolized in the liver and excreted. In the scheme above, γ -tocopherol is shown as an example. After several steps of metabolism, non-active forms of vitamin E are eventually eliminated as waste.

1.2 α -TTP

1.2.1 Localization and Function

Identified in 1975 by Catignani and colleagues, the α -tocopherol transfer protein (α -TTP) is responsible for secreting the *RRR*- α -tocopherol stereoisomer of vitamin E from liver cells. Localized mainly in the cytosol of hepatocytes, α -TTP is a member of the Sec14-like lipid-binding protein family, which all contain the highly conserved CRAL-TRIO binding domain (Lim & Traber, 2007). This large group of proteins include cellular retinaldehyde binding protein (CRALBP), supernatant protein factor (SPF), and the yeast protein Sec14 that is responsible for transporting phosphatidylinositol and phosphatidylcholine between membrane bilayers. Similarly, α -TTP is known to facilitate the movement of α -tocopherol from endosomal membranes to the plasma membrane of liver cells. Human α -TTP consists of 278 amino acids with a molecular weight of 31,749 Da and its gene is located at the 8q13.1-13.3 region on chromosome 8 (Arai & Kono, 2021). While α -TTP protein levels are highest in hepatocytes, there has been evidence of low levels of α -TTP expression in other tissues. Shown in rats or mice, α -TTP was detected in brain, retinal, kidney, spleen, and lung tissues, as well as the uterus and placenta in pregnant animals. Similarly, other studies have shown α -tocopherol and other vitamin E forms accumulate in non-hepatic tissues, including heart, kidney, ovaries, and adipose tissue – however, deposits of vitamin E in adipose tissue are thought to occur only for storage and not as a target area (Kiyose, 2021; Arai & Kono, 2021).

1.2.2 Structure and α -Tocopherol Binding

The structure of α -TTP and its binding of α -tocopherol were elucidated via X-ray crystallography by two separate research groups in 2003, which showed the secondary structure of α -TTP contains 14 α -helices and 5 β -sheets (Min et al., 2003; Meier et al., 2003). At its core, α -

TTP has the binding site for vitamin E, which is comprised of mainly hydrophobic residues that protect its ligand from the aqueous environment. As vitamin E enters the binding pocket, its chromanol headgroup is directed towards residues Tyr117, Ser140, Val182, and Leu189, which stabilize the C₆-OH group through hydrogen bonding with three water molecules present in the binding site (Figure 5). Meanwhile methyl groups on the chromanol show van der Waals interactions with Phe133, Ile154, Leu183, Phe187, and Ile194. The amount of stability and binding of the different vitamers is dependent on the methyl substitution of the chromanol ring – hence the binding affinity of α -TTP being much greater for α -tocopherol (100%) than the other vitamers; β -tocopherol (38%), γ -tocopherol (9%), and δ -tocopherol (2%). Despite both β - and γ -tocopherol only having two chromanol methyl substituents, it is likely that α -TTP has a higher binding affinity for the former because β -tocopherol has its methyl group at the C₅ position, which interacts with three amino acid residues, whereas γ -tocopherol has a C₇ methyl substitution that forms less van der Waals interactions (Arai & Kono, 2021; Min, 2007). Once in the binding site, α -tocopherol takes up a U-shape conformation wherein the 4' and 8' positions of the phytyl tail become kinked. This conformational arrangement likely explains the stereoselectivity of α -TTP for the *RRR*- α -tocopherol stereoisomer because the methyl groups at the 2' and 8' positions form van der Waals interactions with residues Ile179 and Ile210, respectively (Manor, 2007).

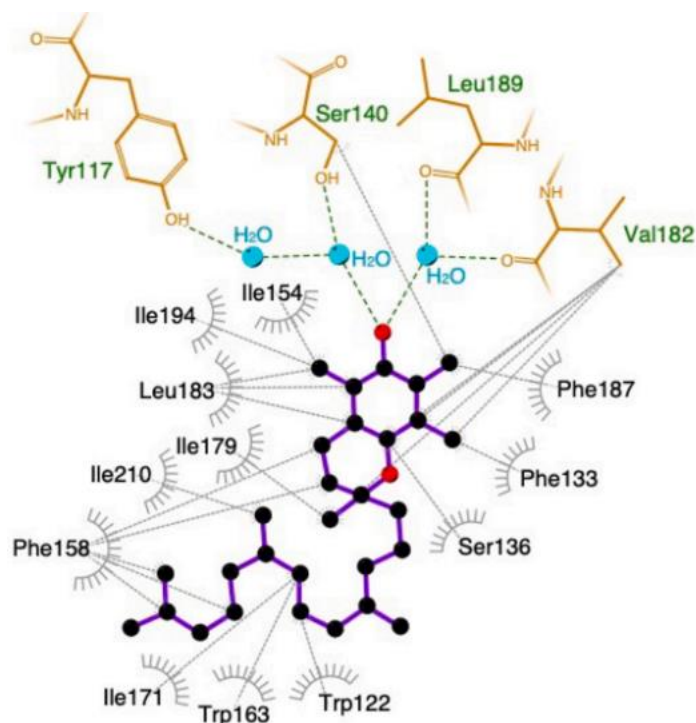


Figure 5. Interactions of α -TTP's Binding Site and α -Tocopherol.

Upon binding to the hydrophobic pocket of α -TTP, α -tocopherol takes on a U-shape that is stabilized through van der Waals interactions (gray dotted lines). The methyl substituents on the chromanol ring also form van der Waals interactions with residues Phe133, Ile154, Leu183, Phe187, and Ile194. Since α -tocopherol has all three methyl groups at these positions, the binding interactions are maximized. The presence of three water molecules in the binding site allows the hydroxyl group on the chromanol ring to form indirect hydrogen bonds (green dotted lines) with residues Tyr117, Ser140, Leu189, and Val182 – further stabilizing the chromanol portion of α -tocopherol. Figure used with permission from Arai & Kono, 2021.

During the initial structural investigations of α -TTP, it was discovered that the protein has two distinctive conformations – an open (apo) and a closed (holo) conformation. The amphipathic α -helix 10 (residues 198-221) is responsible for this conformational change upon ligand binding and is often referred to as the “lid” of α -TTP (Arai & Kono, 2021). In the open conformation, the helix is facing outwards away from the binding pocket – allowing space for α -tocopherol to enter α -TTP. Once the ligand is bound, helix 10 rotates 80° to adopt the closed conformation, in which its hydrophobic residues – Phe203, Val206, Phe207, Ile210, and Leu214 – are facing the binding site and form interactions with the phytyl tail, thereby stabilizing α -tocopherol binding. While the

polar residues of helix 10 face the aqueous environment and improve α -TTP's water solubility during ligand transport (Meier et al., 2003). There has also been evidence that α -helices 8 and 10 facilitate the docking of α -TTP on membrane bilayers during ligand uptake and release. In its open conformation, the hydrophobic residues on helix 8 (Phe165 and Phe169) and helix 10 (Val201, Ile202, Ala205, Val206, Met209, Ile210, Pro212, and Phe213) are oriented towards the outer surface of α -TTP and are thought to insert into lipid bilayers to anchor the protein (Zhang et al., 2011). However, the initial studies by Meier et al., (2003) and Min et al., (2003) also found a positively charged cleft on the surface of α -TTP, which at the time was hypothesized to allow protein binding to membranes.

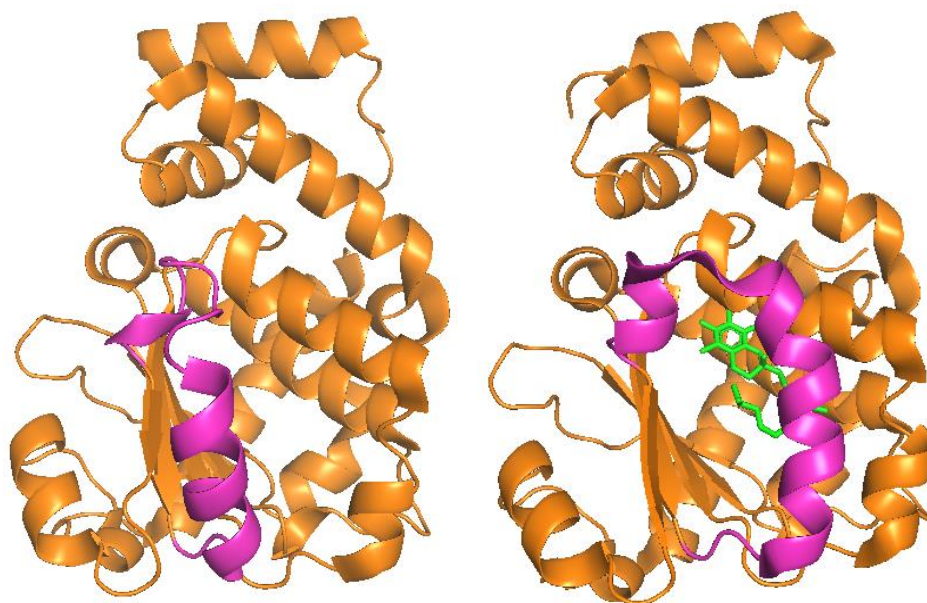
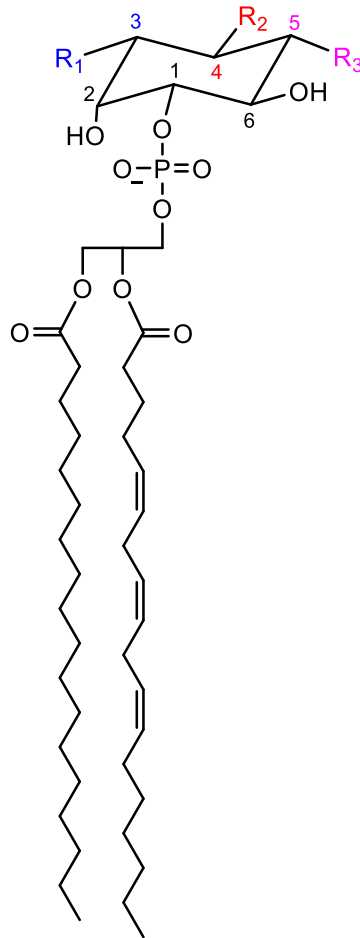


Figure 6. Closed and Open Conformations of α -TTP.

The unbound, open (apo) conformation (left) of α -TTP is thought to be present in the cytosol of liver cells when the protein is inactive in the absence of vitamin E. Once vitamin E is present, α -TTP binds α -tocopherol (green) in its hydrophobic pocket, inducing a conformational change that facilitates the rotation of α -helix 10 (pink), the lid helix, towards the binding site – shifting the protein to its closed (holo) conformation (right). The lid helix decreases its contact with the lipid membrane and α -TTP detaches to transport α -tocopherol to the hepatic plasma membrane. Figure created using PyMol and PBD files 1OIZ (left) and 1OIP (right).

1.2.3 α -TTP's Secondary Ligand

The positively charged cleft, also known as α -TTP's basic patch, is largely comprised of positively charged amino acids – namely arginine and lysine. Despite having been discovered in early X-ray crystallography of α -TTP, its true function was revealed a decade later by Kono et al., (2013) upon noting the binding of certain phosphatidylinositol phosphates (PIPs) at this site. Cellular membranes are made up of many different components, including proteins and carbohydrates, but are largely composed of lipids. Among these lipids are phosphatidylcholine (PC), phosphatidylethanolamine (PE), phosphatidylserine (PS), phosphatidic acid (PA), and phosphatidylinositol (PI). Through localization, these lipids act as signalling molecules to differentiate plasma membrane bilayers versus organelle or vesicular membranes and recruit cytosolic proteins to induce signalling cascades (Chiapparino et al., 2016). PIs are especially diverse given the variety of sites that can be phosphorylated at positions 3, 4, and 5 on the headgroup – resulting in seven different PIPs (Figure 7).



PIPs	R₁	R₂	R₃
PI	OH	OH	OH
PI(3)P	PO ₄	OH	OH
PI(4)P	OH	PO ₄	OH
PI(5)P	OH	OH	PO ₄
PI(3,4)P ₂	PO ₄	PO ₄	OH
PI(3,5)P ₂	PO ₄	OH	PO ₄
PI(4,5)P₂	OH	PO₄	PO₄
PI(3,4,5)P ₃	PO ₄	PO ₄	PO ₄

Figure 7. The Different Forms of Phosphatidylinositol.

Phosphatidylinositol (PI) has a polar headgroup that is in contact with aqueous environments, such as the cytosol, and two fatty acid chains that form a hydrophobic partition in lipid bilayers. The headgroup of PI may be phosphorylated by kinases at carbons 3, 4, and 5, giving rise to seven variations of phosphatidylinositol phosphates (PIPs). α -TTP is known to bind some PIPs, but shows greatest affinity for phosphatidylinositol bisphosphates (PIP₂) – especially PI(4,5)P₂, which is thought to be its secondary ligand.

In vitro experiments show that α -TTP preferentially binds phosphatidylinositol bisphosphates (PIP₂) PI(4,5)P₂ and PI(3,4)P₂ – both of which can be localized to plasma membranes. However, instead of binding it in a deep hydrophobic pocket like α -tocopherol, α -TTP binds PIP₂ on the surface basic patch as a secondary ligand (Figure 8). A crystal structure of α -TTP showed that it can simultaneously complex with α -tocopherol and PI(4,5)P₂, exhibiting an intermediary conformation between open and closed – suggesting that binding PI(4,5)P₂ may

induce the lid α -helix to open and release α -tocopherol (Arai & Kono, 2021). The breakthrough discovery of α -TTP's binding of PIP₂ that forms an intermediate conformation has paved the way for later research to propose a mechanistic model for the cyclic transport of α -tocopherol out of liver cells.

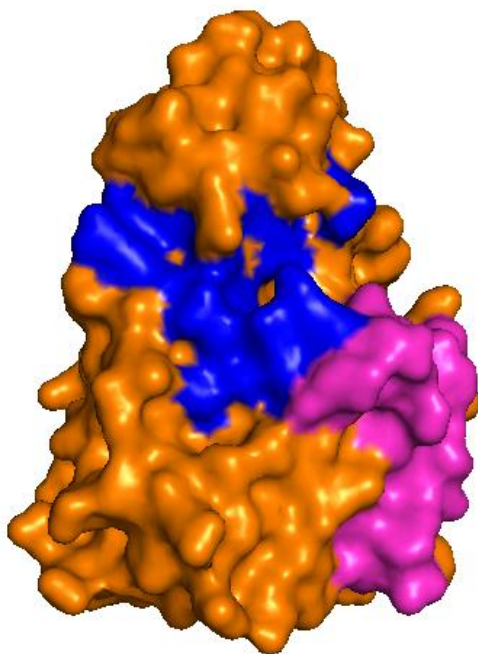


Figure 8. Surface Topology of α -TTP.

While the hydrophobic binding site for α -tocopherol resides deep within the protein and relies on the lid α -helix (pink) to facilitate vitamin E binding and release, α -TTP also has a surface binding site. This basic patch (blue) consists largely of positively charged arginine and lysine residues (Arg57, Arg59, Arg68, Arg151, Lys155, Lys190, Arg192, Lys217, Arg221) allowing the secondary ligand of PIPs to bind to α -TTP. α -TTP has been shown to preferentially bind phosphatidylinositol bisphosphates, including PI(4,5)P₂, which is thought to be involved in the α -tocopherol transfer cycle *in vivo*. Figure created using PDB file 1OIP and PyMol.

1.2.4 The α -Tocopherol Transport Cycle Model in Hepatocytes

Despite early research shedding light on the intestinal absorption and selective retention of *RRR*- α -tocopherol by α -TTP, the complete process in which α -tocopherol exits hepatocytes to enter systemic circulation remains unknown. Through *in vitro* and *in vivo* results concluded by several research groups, a model for α -tocopherol entrance into liver cells, its uptake, transport to the

plasma membrane (PM), and eventually release into the bloodstream has been constructed. The proposed transport proceeds as follows; vitamin E enters the liver cell as part of a chylomicron remnant that is then endocytosed into late endosomes or lysosomes and is catabolized, releasing vitamin E. The vitamers become incorporated into the endosomal bilayer, specifically localizing in the outer leaflet to be recognized by α -TTP (Figure 9). α -Tocopherol is then preferentially bound in the hydrophobic binding site of α -TTP, which carries α -tocopherol across the cytosol towards the hepatic PM where a ligand exchange is thought to occur. α -TTP exchanges α -tocopherol, releasing it into the PM, while simultaneously binding PI(4,5)P₂ to the positively charged cleft. Deposited α -tocopherols are then extracellularly secreted by ABCA1 and fuse into VLDLs, HDLs, and LDLs (Arai & Kono, 2021). One of the most important aspects of this process is the transport of α -tocopherol across the cytosol and insertion into the plasma membrane.

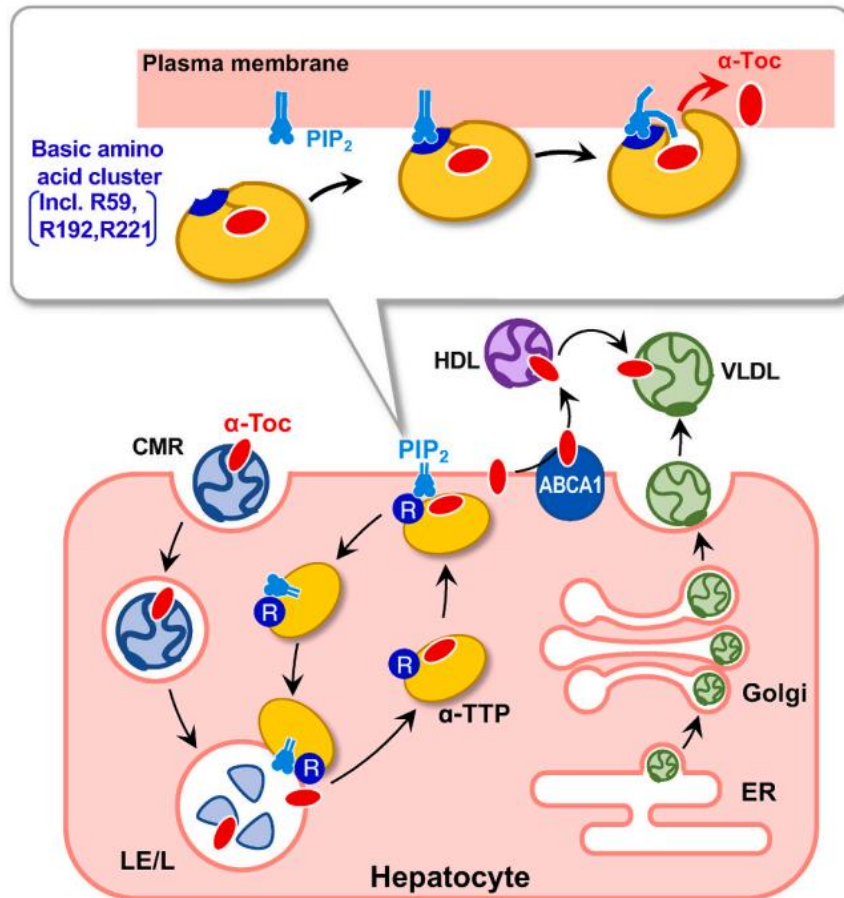


Figure 9. α -Tocopherol Transport into and out of Hepatocytes.

Once chylomicron remnants (CMR) bring α -tocopherol into liver cells, CMRs are broken down in late endosomes or lysosomes (LE/L). α -tocopherol becomes incorporated into the organelle membrane to be recognized and take up by α -TTP. α -Tocopherol is then transported across the cytosol and deposited at the plasma membrane of liver cells, where a ligand exchange is thought to occur, in which α -TTP binds PI(4,5)P₂ at the basic patch and releases α -tocopherol. However, this process is not entirely known. Figure used with permission from Arai & Kono, 2021.

A mechanistic model was proposed by Atkinson et al., (2019) that outlines, in detail, the cyclic transport of α -tocopherol from late endosomes to the PM of hepatocytes to avoid overconcentration of liver cells and sustain the progression of α -tocopherol to target tissues (Figure 10). The cycle begins once α -tocopherol inserts into the late endosomal membrane, then α -TTP binds to the membrane in an open conformation using the hydrophobic residues on α -helices 8 and 10 to pick up α -tocopherol. This binding event triggers the lid helix to rotate, inducing a conformation change to closed conformation, which in turn reduces the binding interactions of α -

TTP with the endosomal membrane – thereby releasing the α -TTP- α -tocopherol complex into the cytosol. As α -TTP transports α -tocopherol across the cytosol, the protein-ligand complex migrates toward the PM of the hepatocyte, drawn by the secondary ligand of α -TTP – PI(4,5)₂. The ligand exchange phase of the model remains the least verified but is evidenced by an intermediate conformation occurring upon the binding of PI(4,5)P₂ by α -TTP while already being bound to α -tocopherol (Kono et al., 2013). As PI(4,5)P₂ binds to the basic patch, α -TTP undergoes a conformational shift to concurrently open its hydrophobic binding site and release α -tocopherol into the PM. This event is further supported by the fact that, upon binding PI(4,5)P₂, its headgroup is nestled into the positively charged cleft, while its acyl chains are in close proximity to the lid α -helix of α -TTP (Arai & Kono, 2021). It is likely that this disturbance on the protein's surface induces its conformational change that allows the simultaneous uptake of PI(4,5)P₂ and release of α -tocopherol. Following ligand exchange, the α -TTP-PI(4,5)P₂ complex then shuttles back across the cytosol to return to the late endosome where PI(4,5)P₂ is released into the membrane and is hydrolyzed to PI(4)P. The cycle begins anew with the uptake of a second α -tocopherol molecule by α -TTP from the late endosome. Based on this model, the main driving force of the entire α -tocopherol transport cycle is the concentration gradient difference of α -tocopherol and PI(4,5)P₂ in hepatocytes (Atkinson et al., 2019). The concentration of α -tocopherol is greater in late endosomal membranes than in the PM because once α -TTP releases its primary ligand at the PM, α -tocopherol is transported out of liver cells by the ABCA1 protein. In addition, as more vitamin E is ingested, it repletes the amount of α -tocopherol in hepatic late endosomes. On the contrary, PI(4,5)P₂ is naturally more abundant in the PM and its hydrolysis to PI(4)P in the late endosomes after being released by α -TTP ensures its concentration does not accumulate there.

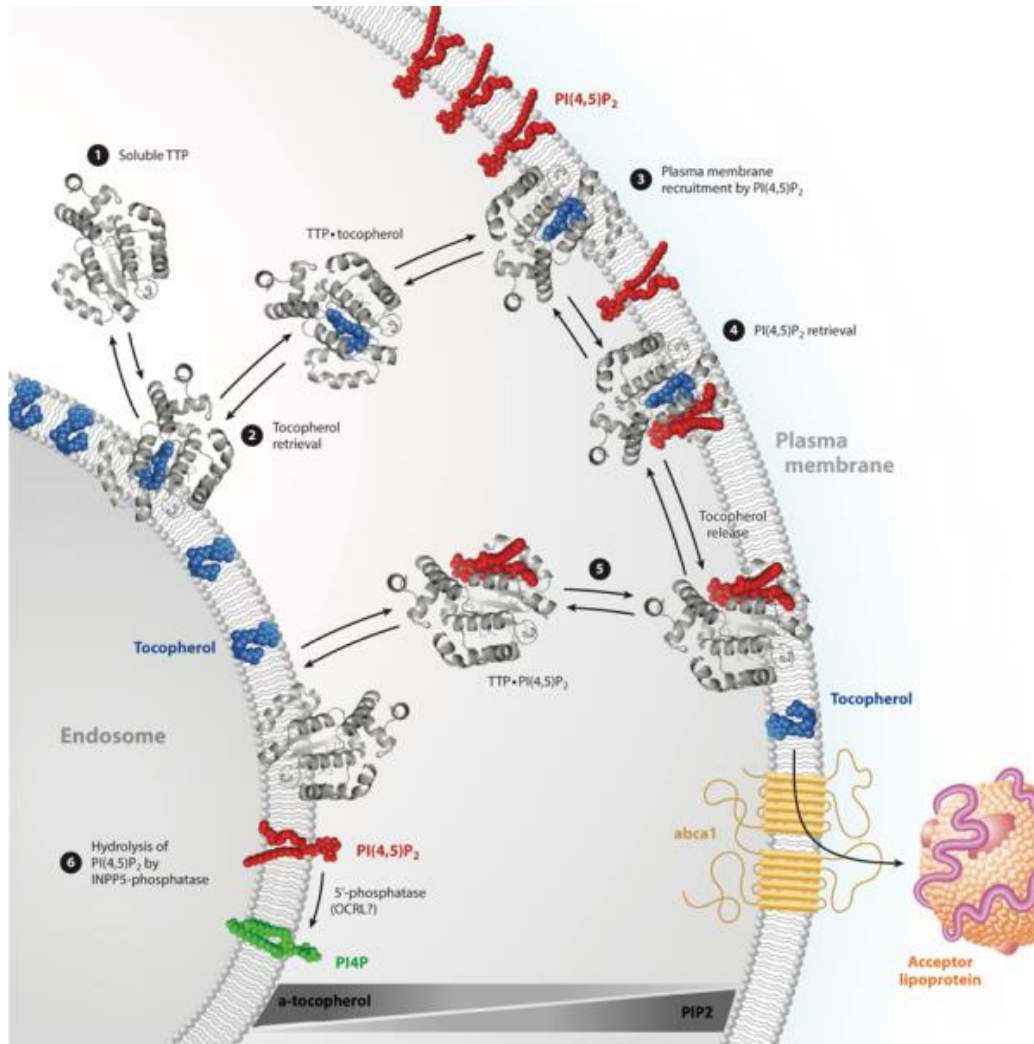


Figure 10. Proposed Mechanistic Model for the α -Tocopherol Transport Cycle via α -TTP. The cycle begins via the recognition of α -tocopherol embedded in the endosomal membrane by α -TTP floating freely in the cytosol, followed by the binding and uptake of α -tocopherol into the hydrophobic pocket. The α -TTP- α -tocopherol complex then migrates across the cytosol towards the hepatic plasma membrane, which is thought to be facilitated by the signaling of α -TTP's secondary ligand – PI(4,5)P₂. A ligand exchange is thought to occur, in which α -TTP binds PI(4,5)P₂ at the basic patch – inducing a conformational shift from closed to open conformation, resulting in the release of α -tocopherol from the hydrophobic binding site into the plasma membrane. Meanwhile the α -TTP-PI(4,5)P₂ complex travels back across the cytosol to the endosomal membrane where PI(4,5)P₂ is released and hydrolyzed to PI(4)P by a phosphatase. A new cycle then begins by α -TTP binding a second molecule of α -tocopherol. The driving force of this transport cycle is likely the opposing concentration gradients of α -tocopherol buildup in the endosome versus the presence of PI(4,5)P₂ in the plasma membrane. Both gradients are maintained by the exportation of α -tocopherol from liver cells and the hydrolysis of PI(4,5)P₂ at the endosomal membrane. Figure taken with permission from Atkinson et al., 2019.

1.3 Ataxia with Vitamin E Deficiency

Ataxia due to vitamin E deficiency (AVED), previously known as familial isolated vitamin E deficiency (FIVE), is a hereditary autosomal recessive neurodegenerative disease arising from dysfunctional α -TTP production. Unlike other diseases related to fat malabsorption or reduced lipoprotein production, AVED results in low systemic concentrations of α -tocopherol due to mutations in the *TTPA* gene responsible for producing α -TTP – resulting in detrimental defects in the protein that make it nonfunctional in transporting α -tocopherol across hepatocytes (Arai & Kono, 2021). The *TTPA* gene was found to be on chromosome 8, which consists of five exons, and was later specifically localized to regions 13.1-13.3 (Figure 11). Over twenty mutations of the *TTPA* gene across all five exons have been identified to correlate with AVED, most common are the 744delA and 513insTT mutations on exon 5 and 3, respectively (Di Donato et al, 2010). Non-conserved mutations such as these, along with others that often cause truncations or frameshifts yield misfolded, nonfunctional proteins and correlate to severe AVED that usually presents at an early age, compared to milder forms of the disease that may only present later into adulthood (Table 1). There are also many missense mutations of α -TTP that have been identified, most commonly Arg59Trp, Asp64Gly, His101Gln, Ala120Thr, Glu141Lys, Leu183Pro, Arg192His, and Arg221Trp (Kono et al., 2013). Interestingly, of these residues, only Leu183 is in the binding site for α -tocopherol – providing van der Waals interactions for the methyl group on C₅ of the chroman ring (Figure 5). All other missense mutations of the α -TTP reside on the protein surface, some of which are part of the basic patch where PI(4,5)P₂ binds. The mutations Arg59Trp and Arg221Trp both involve changing arginine to tryptophan and are known to cause severe forms of AVED with early onset symptoms (Kono et al., 2013).

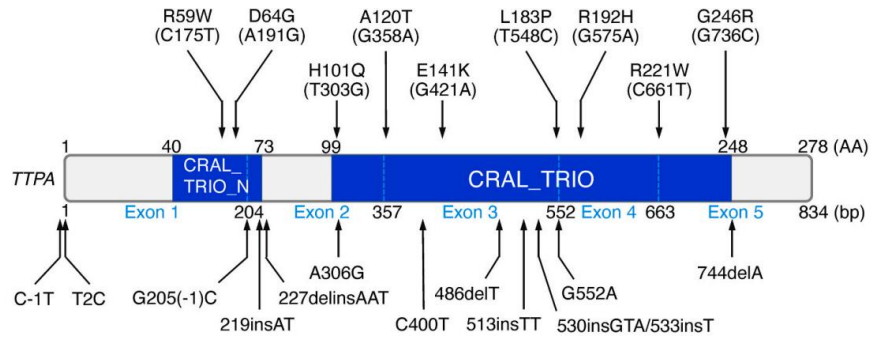


Figure 11. *TTPA* Gene.

The *TTPA* gene, present on chromosome 8q13, is transcribed to produce α -TTP and consists of five exons containing 834 base pairs (bp). Two main conserved regions are present: the CRAL_TRIO domain (shorter) and another CRAL_TRIO domain (longer), also called the Sec14 domain. There are several mutations that can occur in the *TTPA* gene that lead to AVED, such as missense mutations (top), insertions, deletions, and splicing mutations (bottom). Figure used with permission from Arai & Kono, 2021.

Table 1. Mutations Found in the *TTPA* Gene.

Most mutations of the *TTPA* gene result in severe forms of AVED, likely because many mutations result in truncations or frameshifts that lead to complete dysfunctionality of α -TTP. For example, the two most common mutations 513insTT and 744delA. However, there are also single base pair mutations that lead to missense mutations in the amino acid sequence of the protein – some of which like D64G, E141K, L183P, R221W cause severe clinical features, while others of H101Q, A120T, and R192H present with more milder symptoms. Table recreated from Di Donato et al., 2010.

	Mutation	Nucleotide Position	Location	Effect on α -TTP	Clinical Phenotype
1	C \rightarrow T	-1	5'UTR	\downarrow TTP levels	Severe
2	T \rightarrow C	2	Exon 1	Disrupts initiation	Unknown
3	T \rightarrow G	2	Exon 1	Disrupts initiation	Unknown
4	C \rightarrow T	175	Exon 1	Mis-splicing	Severe
5	A \rightarrow G	191	Exon 1	D64G	Severe
6	G \rightarrow C	IV81-1	Intron 1	Premature termination	Unknown
7	219insAT	219-220	Exon 2	Frameshift	Severe
8	delATGGAGTC	302-309	Exon 2	Frameshift	Mild
9	T \rightarrow G	303	Exon 2	H101Q	Mild
10	A \rightarrow G	306	Exon 2	Splice-site mutation	Mild
11	G \rightarrow A	358	Exon 2	A120T	Mild
12	G \rightarrow A	IV82+1	Intron 2	Splice donor	Unknown
13	C \rightarrow T	400	Exon 3	Premature termination	Unknown

14	G → T	421	Exon 3	Premature termination	Unknown
15	G → A	421	Exon 3	E141K	Severe
16	485delT	485	Exon 3	Frameshift	Severe
17	486delT	486	Exon 3	Frameshift	Severe
18	513insTT	513-514	Exon 3	Frameshift	Severe
19	AG530GTAAGT	530-531	Exon 3	Frameshift	Severe
20	G → A	552	Exon 3	Splice donor	Severe
21	T → C	548	Exon 4	L183P	Severe
22	T → C	575	Exon 4	R192H	Mild
23	C → T	661	Exon 4	R221W	Severe
24	G → C	736	Exon 5	G246R	Mild
25	744delA	744	Exon 5	Frameshift	Severe

First diagnosed in 1981 as cases of FIVE, patients presented with vitamin E deficiency symptoms but were found to have proper lipid absorption in the intestines and produced appropriate amounts of lipoproteins. Severe AVED symptoms usually present during early childhood or teenage years and range from cerebellar ataxia, dysarthria, clumsiness, loss of coordination or proprioception, areflexia, dysdiadochokinesia, and a positive Babinski sign (Thapa et al., 2022; Ulatowski & Manor, 2015). AVED is mostly misdiagnosed for Friedreich's ataxia due to many of the above symptoms overlapping between the two conditions. However, Friedreich's ataxia commonly presents with cardiomyopathy, which is usually absent in patients with AVED. On the contrary, head titubation and dystonia are specific symptoms of AVED and do not occur in Friedreich's ataxia (Di Donato et al., 2010). Therefore, diagnosis should include family history, physical symptoms and low vitamin E levels in the bloodstream, but genetic testing of the *TTPA* gene could further verify AVED diagnosis. The neurodegeneration in patients is thought to occur due to the accumulation of oxidative damage in the cerebellum and peripheral neurons in the absence of α -tocopherol. Currently, the only form of treatment is vitamin E supplementation of 800 mg per day, which has been shown to slow the progression of the disease and potentially reverse the loss of motor control in patients (Imounan et al., 2012; Di Donato et al., 2010).

1.4 Surface Plasmon Resonance

1.4.1 History

A plasmon is the oscillation of free charge in conductors such as metals, which may be confined to the surface of these materials. Upon shining light corresponding to the plasmon frequency onto the surface, resonance absorption occurs, and an electromagnetic field is produced (Hou & Cronin, 2013). This phenomenon is known as surface plasmon resonance (SPR) and was first observed by Robert W. Wood in 1902. Nearly a century later, in 1983, Liedberg, Nylander, and Lundström showed the possibility of using SPR as a technological application to biosensors for the analysis of biomolecular interactions *in vitro* (Homola & Gauglitz, 1999). The first commercially available SPR apparatus, Biacore, was developed by Pharmacia Biosensor in 1990 and set a precedent as the most advanced SPR technology for decades (Schasfoort, 2017). Unlike other biological assay techniques that rely on molecular labels and end-point data collection, SPR allows real-time detection of unlabeled samples.

1.4.2 Principles and Experimentation

While the physical and mathematical theories underlying SPR are complex, the functionality of the technique may be explained from a biological perspective. At its core, an SPR system has a sensor surface with an immobilized molecule, the ligand, and its binding counterpart, an analyte in an aqueous solution that is injected through a flow cell passing over the sensor surface. A light source is directed at the bottom of the glass sensor surface, which reflects off to a detector. Upon binding, the detector records a change of refractive index at the sensor surface and reports it as a refractive index unit (RIU) – in real-time as the interaction is occurring – generating an RIU versus time plot (Van Der Merwe, 2001). In the absence of an analyte, a running buffer solution is continuously passed through the flow cell to determine a baseline RIU, however, if the

sample and running buffers are chemically different, the SPR will detect such variation during sample analysis. Therefore, SPR apparatuses have two separate flow channels – a control and a sample channel – with the former being unoccupied by the immobilized ligand. To obtain a proper binding interaction result, the analyte is injected into both channels and the signal produced from the control channel must be subtracted from the sample channel response (Figure 12). Using proper regeneration buffers, the analyte, or both the ligand and analyte can be removed from the surface of the sensor to repeat the experiment or begin a new one.

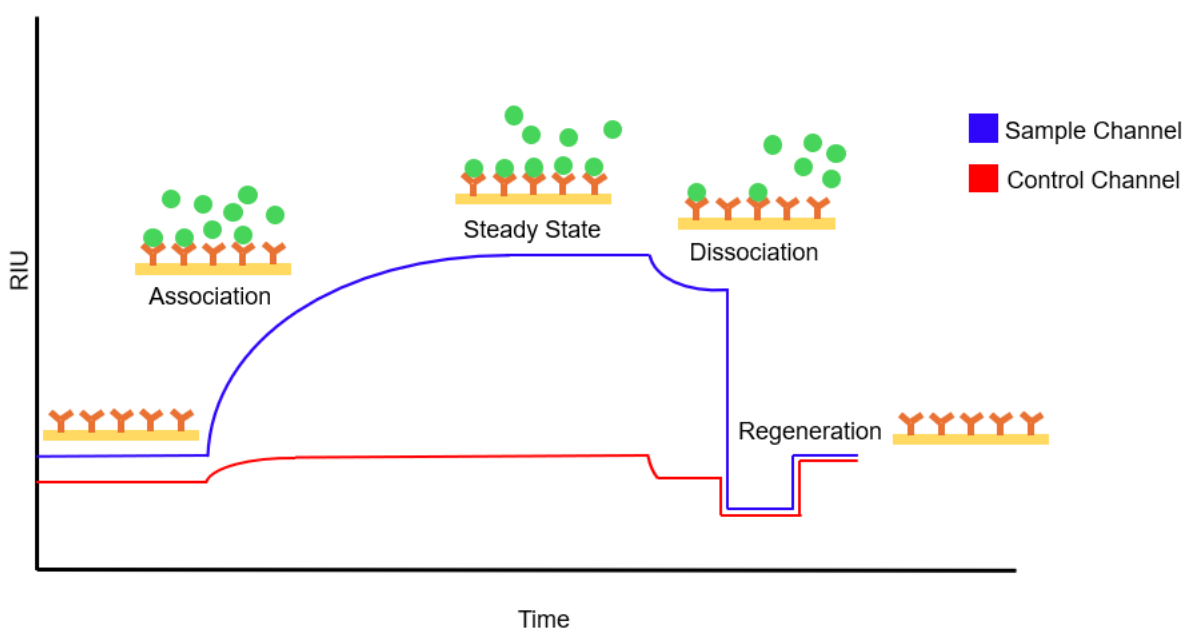


Figure 12. SPR Detector Report.

Once the ligand (orange) has been immobilized on the sensor chip surface, the analyte (green) is injected into the SPR and is applied to two separate channels. The control channel (red), without anchored ligands and the sample channel (blue) contains ligand. Once the analyte is injected, an association curve forms and eventually reaches a plateau. At the end of a cycle when no more analyte is flowing by, only running buffer, a dissociation phase occurs during which some of the weakly bound analytes separate from the ligand. Regeneration buffers are applied at the end of a cycle to remove all bound analytes and restore the sensor chip surface for a new experiment.

1.4.3 SPR Experimentation Used in this Project

SPR biosensing usually revolves around proteins – assessing protein-protein interactions, receptors and antibodies, small molecule ligands and protein binding. Experiments can be designed

to test the functionality of recombinant or mutant proteins compared to their native counterparts, test ligand binding affinities, or binding kinetics (Englebienne et al., 2003). The experiments involving SPR described herein are used specifically to monitor the binding interactions between α -TTP and lipid vesicles with varying compositions, including the incorporation of α -tocopherol or PI(4,5)P₂. The base sensor surface used in this study is similar to the one used in the Biacore instrument first developed in the 1990's – it includes a glass chip that has one side coated with a gold film – an inert conducting metal capable of producing plasmons. Attached to the golden side of the chip are long thiol chains upon which a carboxymethyl dextran layer is added. Such modifications were developed early on by Pharmacia Biosensors because it was difficult to immobilize biomolecular ligands on a surface made solely of gold (Schasfoort, 2017). Personalized modifications of the sensor chips used during this project include the addition of phytosphingosine atop the carboxymethyl dextran to be able to bind lipid vesicles to the sensor chip. Contrary to most SPR experiments, the ligand layer is made up of lipid vesicles, not proteins. The amino groups of the phytosphingosine chains insert into the lipid vesicles passed through the sample channel and immobilize them as ligands. The analyte, α -TTP, is then injected into both the control and sample channels to assess its binding to lipids (Figure 13).

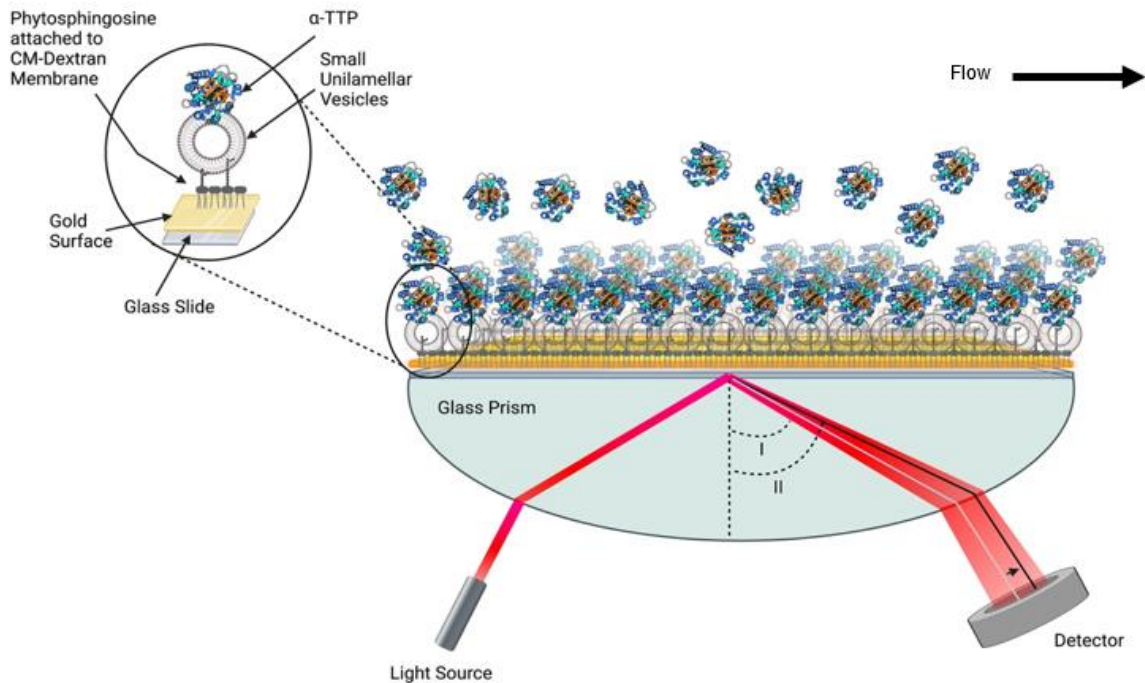


Figure 13. SPR Experiment and Sensor Chip Schematic.

SPR sensor chips produced from Reichert are used to investigate ligand binding interactions between α -TTP and lipid vesicles containing PI(4,5)P₂. The glass chip contains a gold film on top, which is further coated with a layer of carboxymethyl dextran that is derivatized with phytosphingosine – allowing the immobilization of small unilamellar lipid vesicles to the sensor chip. A light source is directed at the bottom of the glass sensor chip, it is reflected at angle I in the absence of any sample and sensed by the detector. However, as α -TTP is injected and flows over the sensor chip, some proteins bind to the lipid vesicle membranes, causing a shift in the refractive index so the reflected angle shifts to II and a different signal is recorded – showing the binding interaction between ligand and analyte in real time. Figure used from Mehta, 2023.

1.5 Project Outlines and Objectives

1.5.1 Objectives

The overall goal of this project is to elucidate the validity of the proposed mechanistic model explaining the α -tocopherol transfer cycle in hepatocytes (Figure 10). There are two main objectives for the project described herein: firstly, to determine the extent to which the addition of different PIPs to plasma membranes effects the binding of wildtype α -TTP (wtTTP) to the lipid

layer using SPR. The binding of wtTTP alone, as well as wtTTP bound to α -tocopherol will be tested on plasma membrane vesicles containing phosphatidylinositol-4,5-bisphosphate (PI(4,5)P₂), phosphatidylinositol-3,4-bisphosphate (PI(3,4)P₂), and phosphatidylinositol-3-phosphate (PI(3)P). Once those experiments are completed, the binding interactions of different mutant forms of α -TTP will be tested.

The second objective of this project analyzes ligand interactions with mutant proteins predicted to inhibit binding of either α -tocopherol or PI(4,5)P₂. The first mutant protein tested will be K217A, which has been shown by Kono et al., 2013, to be unable to bind PI(4,5)P₂. The Lys217 residue resides in the basic patch of α -TTP and has been shown to be critical for the of binding PI(4,5)P₂ because its substitution for alanine in the K217A mutant was nearly unable to bind PI(4,5)P₂. Despite being able to bind α -tocopherol, K217A mutants were unable to facilitate its release from the hydrophobic site due to having low binding affinity for PIPs (Kono et al., 2013; Atkinson et al., 2019). While the K217A mutation has not been identified with AVED, *in vitro* investigations with the K217A protein provide further insights into the ligand exchange step during the α -tocopherol transfer cycle. Table 2 provides a list of experiments that will be completed in the current project.

Table 2. Planned SPR Experiments using wtTTP and K217A.

Sixteen conditions must be run on the SPR using wtTTP or K217A. wtTTP will be injected onto lipid vesicles comprised of 1 mM PM, as well as PM vesicles containing 2%, 4%, and 6% PI(4,5)P₂. Two additional PIPs – 4% PI(3,4)P₂ and 4% PI(3)P – will also be tested. The K217A mutant experiments will largely follow the ones to be done for wtTTP regarding the PM vesicle compositions.

Experiments	
<i>wtTTP</i>	<i>K217A</i>
1 mM PM	1 mM PM
1 mM PM + 2% PI(4,5)P ₂	1 mM PM + 2% PI(4,5)P ₂
1 mM PM + 4% PI(4,5)P ₂	1 mM PM + 4% PI(4,5)P ₂
1 mM PM + 6% PI(4,5)P ₂	1 mM PM + 6% PI(4,5)P ₂
1 mM PM + 4% PI(3,5)P ₂	1 mM PM + 4% PI(3,5)P ₂
1 mM PM + 4% PI(3)P	1 mM PM + 4% PI(3)P
wtTTP + 2% toc on 1 mM PM	K217A + 2% toc on 1 mM PM + 2% PI(4,5)P ₂
	Endo + 2% toc + 10% BMP

wtTTP = wildtype α -TTP, PM = plasma membrane, toc = α -tocopherol, Endo = endosomal membrane, BMP = bis(monoacylglycerol)phosphate

In addition to K217A, other mutant forms of α -TTP will be expressed, purified, and characterized as part of the second objective of this project. The following mutants will be created – D60K, S140A, P200A, P200G, and T215H – to gain better understanding of the binding interactions required for the uptake and release of α -tocopherol in liver cells. Asp60 and Thr125 are both present in the basic patch of α -TTP where the former is thought to stabilize the overall positively charged cleft by providing a negative charge, and the latter might similarly provide stability through its polar yet uncharged hydroxyl group. The D60K mutant could potentially have an increased binding affinity for PI(4,5)P₂ via the incorporation of another positively charged lysine residue at the basic patch (Figure 14). However, without the countercharge of Asp60, the neighbouring residues may become unstable upon the addition of lysine, which could reduce the binding interaction with PI(4,5)P₂. In addition, since the D64G mutation has been associated with severe forms of AVED due to major conformational change inhibiting the transport of α -

tocopherol, it is possible a similar effect will occur with the D60K mutant (Usuki & Maruyama, 2000). Similarly, by substituting the threonine to a histidine residue at position 215, two possible outcomes are predicted based on the amphoteric nature of histidine. Since the side chain of histidine can be either uncharged or positively charged near physiological pH, the T215H mutant could increase affinity for the negatively charged headgroup of PI(4,5)P₂ if the histidine residue donates a proton and becomes positively charged. However, if the histidine residue remains uncharged it could potentially provide similar stability to nearby positively charged residues as threonine does – thereby having no net effect on the binding of PI(4,5)P₂.

The S140A mutant protein is predicted to provide one of the most informative results regarding α -tocopherol transport. Based on the structural interactions of the α -TTP-tocopherol complex, the hydroxyl side chain of the Ser140 residue is hydrogen bonded to a water molecule in the hydrophobic binding site, and this same water molecule is also hydrogen bonded to the hydroxyl group of the chromanol ring of α -tocopherol (Figure 5). Therefore, serine 140 is a key residue that indirectly stabilizes α -tocopherol and allows α -TTP to transport it across the cytosol. It is hypothesized that by substituting serine with alanine – an amino acid similar in size but lacking the hydroxyl group – at this position, the S140A protein will have reduced binding affinity for α -tocopherol compared to the native protein. Since the methyl side chain of alanine does not form a hydrogen bond with the water molecule, thus cannot stabilize the chromanol ring, the S140A mutant could potentially be a non-functional protein.

The final two mutant proteins to be created are P200A and P200G, which both revolve around the proline residue at the 200th position in the lid α -helix 10 (Figure 14). P200 is located at the C terminus of the lid helix and is thought to play a major role in allowing it to rotate and change the protein conformation between open and closed during α -tocopherol uptake and release. By

exchanging a structurally rigid amino acid like proline for a much smaller and more flexible residue – either alanine or glycine – it is predicted that the α -helix lid could alternate between open and closed conformations easily, allowing further insight into how the α -tocopherol and PI(4,5)P₂ ligands are exchanged.

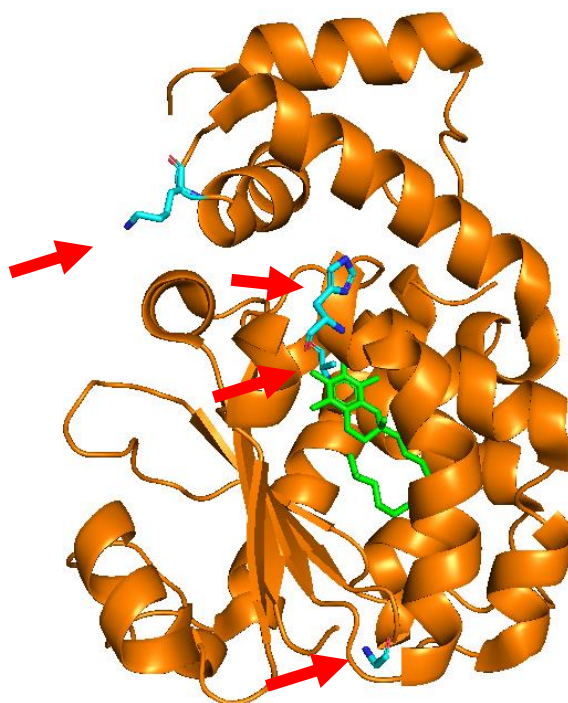


Figure 14. Single Point Mutations of α -TTP.

Five new mutant proteins will be created via single point mutagenesis, including D60K, S140A, P200A, P200G, and T215H (red arrows). D60K and T215H reside in the basic patch of α -TTP and could potentially influence the binding of PI(4,5)P₂, while S140A is present in the hydrophobic binding site for α -tocopherol and the mutation will likely reduce α -TTP's binding affinity for its primary ligand. Lastly, the two mutant proteins where P200 is exchanged for alanine or glycine will affect the rotation of the lid helix, resulting in faster rates of conformation changes between open and closed conformations. Figure created via PyMol and PDB file 1OIP.

1.5.2 Project Outlines

The initial stages of this project will consist of the expression, purification and use of wtTTP and the K217A mutant on the SPR to complete the experiments listed in Table 2. Once those results are verified, focus will shift to expressing and purifying the new mutant forms of α -

TTP, after which their characterizations will be completed. For instance, binding assays between all mutants and a fluorescent derivative of α -tocopherol will be completed in comparison to wtTTP to determine if any of the mutations influence the binding of the primary ligand. Subsequently, SPR injections onto various lipid vesicles, primarily consisting of plasma membrane compositions, and containing either α -tocopherol or PI(4,5)P₂. Based on these experiments, the proposed mechanistic model of the α -tocopherol transport cycle by α -TTP in hepatocytes can be attested and will be used to better understand the underlying causes of AVED.

2 Experimental

2.1 Instruments

- Adventurer™ Pro Analytical Balance (Ohaus Corp., Parsippany, NJ, United States)
- Allegra X-30R Centrifuge (Beckman Coulter Inc., Brea, CA, United States)
- Fisherbrand™ Variable Speed Nutator (Thermo Fisher Scientific, Waltham, MA, United States)
- Gel Doc™ EZ Imager (Bio-Rad, Mississauga, ON, Canada)
- Laboratory Autoclave MLS-3751L (Panasonic Healthcare Co. Ltd., Wood Dale, IL, United States)
- Magnetic heating stir plate: Fisherbrand™ Isotemp™ Hot Plate Stirrer (Thermo Fisher Scientific, Waltham, MA, United States)
- Micromax Centrifuge (Thermo IEC, Needham Heights, MA, United States)
- New Brunswick™ Incubator Shakers I26 (Eppendorf, Hamburg, Germany)
- pH probe & meter: Orion™ Dual Start™ Benchtop pH/ISE Meter (Thermo Scientific, Waltham, MA, United States)
- Photon Technology International QuantaMaster Steady-state Fluorometer (Wisconsin Institute for Medical Research, Madison, WI, United States)
- PS 500XT DC Power Supply (Hofer Scientific Instruments, San Francisco, CA, United States)
- PURELAB® Flex Water Dispenser (ELGA LabWater, High Wycombe, United Kingdom)
- Q500 Sonicator (QSonica, Newtown, CT, United States)
- Series 25 Controlled Environment Incubator Shaker (New Brunswick Scientific Co., Edison, NJ, United States)

- Sorvall RC 6+ Centrifuge (Thermo Fisher Scientific, Waltham, MA, United States)
- SR7500DC 2 Channel Surface Plasmon Resonance Spectrophotometer (Ametek Reichert Technologies, Depew, NY, United States)
- SpectraMax® i3x (Molecular Devices, San Jose, CA, United States)
- Thermal Rocker (Thermo Scientific, Waltham, MA, United States)
- Genesys 10S UV-Vis Spectrophotometer (Thermo Fisher Scientific, Waltham, MA, United States)
- VWR® Analog Vortex Mixer (Avantor™, West Chester, PA, United States)
- Water Bath 6L EX-111 (Neslab Instruments Inc., Newington, NH, United States)

2.2 Software

- ChemDraw (PerkinElmer, Waltham, MA, United States)
- Felix32 Spectroscopy Software, Version 1.2 (Wisconsin Institute for Medical Research, Madison, WI, United States)
- GraphPad Prism, version 10.1.2 (GraphPad Software, CA, United States)
- Image Lab, version 6.1 (Bio-Rad, Mississauga, ON, Canada)
- Integrated SPR Autolink, version 1.1.14-T (Depew, NY, United States)
- Microsoft 365 Excel 2019 MSO, version 2302 (Microsoft, Redmond, WA, United States)
- PyMol (Schrödinger, Inc, New York, New York, United States)
- SoftMax® Pro Software version 6.5.1 (Molecular Devices, San Jose, CA, United States)
- TraceDrawer, version 1.6.1 (Ridgeview Instruments AB, Vänge, Sweden)

2.3 Materials

- Avanti Lipid Mini-Extruder (Avanti, Alabaster, AL, United States)
- BD Precision Glide™ Needle (Becton Dickinson, Franklin Lakes, NJ, United States)
- Disposable Pasteur Pipets (Chem Science Inc., Saint-Laurent, QC, Canada)
- Econo-Column® Chromatography Columns, 1.0 x 10 cm (Bio-Rad, Mississauga, ON, Canada)
- Fisherbrand™ Gel Loading Pipet Tips 200 µL (Fisher Scientific, Waltham, MA, United States)
- Fisherbrand™ Premium Microcentrifuge Tubes: 1.5 and 2 mL (Fisher Scientific, Waltham, MA, United States)
- Fisherbrand™ SureOne™ Pipet Tips: 10 µL, 200 µL, 1000 µL, and 5000 µL (Fisher Scientific, Waltham, MA, United States)
- Hellma® Quartz Glass Cuvettes (Hellma (Canada) Limited, Concord, ON, Canada)
- Kimtech® Low-Lint Precision Wipers (ULINE, Toronto, ON, Canada)
- Luer-Lok™ 3 mL Syringe (Becton Dickinson, Franklin Lakes, NJ, United States)
- Luer-Lok™ 10 mL Syringe (Becton Dickinson, Franklin Lakes, NJ, United States)
- Microflex® Midnight Powder-Free Nitrile Examination Gloves (Ansell Healthcare Products LLC, Reno, NV, United States)
- Microplate, PS, 96 well, F-bottom (Chimney Well), Black, Fluotrac, Med Binding (Greiner Bio-One, Monroe, NC, United States)
- Mini-PROTEAN® Tetra Cell System (Bio-Rad, Mississauga, ON, Canada)
- Mini-PROTEAN® TGX (12% acrylamide) Precast Gel (Bio-Rad, Mississauga, ON, Canada)
- Model 1001 Gastight RN SYR 1 mL Hamilton Syringes (Hamilton, Reno, NV, United States)

- Polycarbonate membranes, 100 nm (Avestin, Ottawa, ON, Canada)
- SR7000 SPR Device (Ametek Reichert Technologies, Depew, NY, United States)
- Supor[®] 450 membrane filter (Pall Corp., Ann Arbor, MI, United States)

2.4 Bacterial Strains and Plasmids

- Wildtype α -TTP was expressed in BL21 (DE3) strain of *Escherichia coli*
- K217A α -TTP was expressed in BL21 (plain) strain of *E. coli*
- D60K, S140A, P200A, P200G, and T215H α -TTP mutants were expressed in Rosetta (DE3) strain of *E. coli*
- pGEX-4T3 plasmid from GE Lifesciences was used to clone the human α -TTP gene into the vector using SaII and NotI by a previous student. The mutant proteins were also produced using the pGEX-4T3 plasmid.

2.5 Chemicals, Reagents, Buffers, and Solutions

2.5.1 Protein Expression, Purification, and Quantification Reagents

- Albumin from bovine serum (Sigma-Aldrich, Oakville, ON, Canada)
- Ampicillin (BioShop, Burlington, ON, Canada)
- Bio-Tryptone (BioShop, Burlington, ON, Canada)
- Bradford Reagent (Sigma-Aldrich, Oakville, Canada)
- DL-Dithiothreitol (DTT) (Bio Basic Inc, Markham, ON, Canada)
- DNase (Invitrogen by Thermo Fisher Scientific, Waltham, MA, United States)
- Ethylenediaminetetraacetic acid (EDTA) (BioShop, Burlington, ON, Canada)
- Glutathione-agarose lyophilized powder (Sigma-Aldrich, St. Louis, Missouri, United States)
- Glutathione-agarose Resin (BioShop, Burlington, ON, Canada)
- Glycerol (ACP, Montreal, QC, Canada)

- Isopropyl- β -D-Thiogalactopyranoside (IPTG) (BioShop, Burlington, ON, Canada)
- Lysozyme (BioShop, Burlington, ON, Canada)
- Magnesium chloride hexahydrate (BioShop, Burlington, ON, Canada)
- Phenylmethylsulfonyl fluoride (PMSF) (Sigma-Aldrich, Oakville, Canada)
- Potassium phosphate dibasic (BioShop, Burlington, ON, Canada)
- RNase A (BioShop, Burlington, ON, Canada)
- Sodium chloride (BioShop, Burlington, ON, Canada)
- Tris (hydroxymethyl) aminomethane (Tris) (BioShop, Burlington, ON, Canada)
- TritonTM X-100 (Sigma-Aldrich, Oakville, Canada)
- Yeast Extract (Sigma-Aldrich, Oakville, Canada)

2.5.2 Protein Expression Solutions

- Luria Bertani Plus (LB+) Cell Preculture Medium: 15 g/L yeast extract, 5 g/L NaCl, 10 g/L bio-tryptone, and 100 μ g/mL ampicillin
- Terrific Broth (TB) Cell Culture Medium: 24 g/L yeast extract, 12 g/L bio-tryptone, 5 mL/L glycerol, and 100 μ g/mL ampicillin
- 10X TB Buffer: 170 mM KH_2PO_4 and 720 mM K_2HPO_4

2.5.3 Protein Purification Buffers

- 1X Phosphate Buffered Saline (PBS) (pH 7.4): 137 mM NaCl, 2.7 mM KCl, 4.3 mM $\text{Na}_2\text{HPO}_4 \cdot 7 \text{H}_2\text{O}$, and 1.4 mM KH_2PO_4
- Wash Buffer A: 150 mM Tris (pH 8.0), 10% glycerol, 150 mM NaCl, 1 mM EDTA, 0.1 mM DTT, and 0.1 mM PMSF
- Wash Buffer B: 0.5% Triton X and 10 mM MgCl_2 in Buffer A

- Chaperone Wash Buffer: 0.1 mg/mL *E. coli* lysate supernatant, 10 mM ATP, and 20 mM MgCl₂
- 1X SPR Protein Elution Buffer: 1.9 mM KH₂PO₄, 8.1 mM K₂HPO₄, and 137 mM NaCl
- Glutathione Elution Buffer (pH 9.0): 3 mg/mL glutathione in 1X PBS
- Cleansing Buffer #1 (pH 8.5): 100 mM H₃BO₃ and 500 mM NaCl
- Cleansing Buffer #2 (pH 4.5): 100 mM sodium acetate and 500 mM NaCl
- Storage Solution: 2.5 M NaCl

2.5.4 SDS-PAGE Chemicals

- Bromophenol blue (Bio Basic Inc., Markham, ON, Canada)
- BLUeye Prestained Protein Ladder (Sigma-Aldrich, Oakville, ON, Canada)
- Colloidal Coomassie G-250 Stain (National Diagnostics, Atlanta, GA, United States)
- DL-Dithiothreitol (DTT) (Bio Basic Inc., Markham, ON, Canada)
- Glycerol (ACP, Montreal, QC, Canada)
- Sodium dodecyl sulfate (SDS) (BioShop, Burlington, ON, Canada)
- Tris(hydroxymethyl) aminomethane (Tris) (BioShop, Burlington, ON, Canada)
- Trichloroethylene (TCE) (Sigma-Aldrich, Oakville, ON, Canada)

2.5.5 SDS-PAGE Solutions

- Resolving Gel Buffer (pH 8.8): 1.5 M Tris
- Stacking Gel Buffer (pH 6.8): 0.5 M Tris
- 1X SDS Running Buffer (pH 8.3): 25 mM Tris-HCl, 192 mM glycine, and 0.1% SDS
- 5X Loading Dye: 0.5-1 mg/mL bromophenol blue, 1.54 mg/mL DTT, 0.1 g/mL SDS, 250 mM Tris-HCl (pH 6.8), and 4-5 mL 100% glycerol

- Gel Stain: 1.2 mM Colloidal Coomassie G-250 stain

2.5.6 Protein Binding Assay Buffer

- 1X TKE Buffer (pH 7.4): 50 mM Tris, 100 mM KCl, 1 mM EDTA

2.5.7 Lipid Membrane Vesicle Reagents

All lipids, except cholesterol, were sourced from Avanti Polar Lipids, Alabaster, AL, United States.

- Cholesterol (Sigma-Aldrich, Oakville, ON, Canada)
- 1,2-dioleoyl-sn-glycero-3-phosphate (sodium salt) (DOPA)
- 1,2-dioleoyl-sn-glycero-2-phosphocholine (DOPC)
- 1,2-dioleoyl-sn-glycero-3-phosphoethanolamine (DOPE)
- 1,2-dioleoyl-sn-glycero-3-phospho-L-serine (DOPS)
- L- α -phosphatidylinositol-4,5-bisphosphate (porcine brain) (ammonium salt) (PI(4,5)P₂)
- Sphingomyelin (SM) (porcine brain)

2.5.8 SPR Reagents

- Anhydrous ethyl alcohol (Commercial Alcohols, Brampton, ON, Canada)
- Glycine (BioShop, Burlington, ON, Canada)
- Monopotassium phosphate (BioShop, Burlington, ON, Canada)
- Dipotassium phosphate (BioShop, Burlington, ON, Canada)
- Sodium chloride (BioShop, Burlington, ON, Canada)
- Sodium dodecyl sulfate (SDS) (BioShop, Burlington, ON, Canada)
- Sodium hydroxide (British Drug Houses by VWR, Mississauga, ON, Canada)

2.5.9 SPR Buffers

- 1X SPR Running Buffer (pH ~ 7.0): 1.9 mM KH₂PO₄, 8.1 mM K₂HPO₄, and 137 mM NaCl
- Regeneration Solutions:
 - 50 mM NaOH
 - 0.5% SDS
 - 50 mM Glycine (pH 9.0)
 - 80% Ethanol (EtOH)

2.5.10 SPR Chip Derivatization Reagents

- Dimethyl sulfoxide (DMSO) (Fisher Chemicals, Ottawa, ON, Canada)
- Ethanolamine (British Drug Houses by VWR, Mississauga, ON, Canada)
- N-Hydroxysuccinimide (NHS) (Aldrich Chemical Company, Milwaukee, WI, United States)
- N-(3-Dimethylaminopropyl)-N'-ethylcarbodiimide hydrochloride (EDC) (Sigma-Aldrich, Oakville, ON, Canada)
- Phytosphingosine (Matreya LLC, States College, PA, United States)
- Sodium acetate (ACP, St. Leonard, QC, Canada)

2.5.11 SPR Chip Derivatization Solutions

- 1:1 phytosphingosine:DMSO
- 20 mM sodium acetate (pH 5.2)
- 1 M ethanolamine HCl (pH 8.5)

2.6 Methods

2.6.1 α -TTP Transformations

The transformation procedure described herein applies to both wildtype and mutant forms of α -TTP, only the bacterial cell strains were varied as outlined in section 2.6. All surfaces were cleaned with 70% ethanol to create a disinfected area, and a Bunsen burner was used to flame all vessel openings and tools during cell transformations. The DNA and competent cells were removed from storage at -20°C and -80°C , respectively, and placed on ice to thaw. Once thawed, 5 μL of 100 ng/mL DNA for the desired α -TTP was added to a sterile 1.5 mL Eppendorf tube, then 50 μL of the competent cells were added to the DNA while the tube remained on ice. The mixture was incubated on ice for 30 minutes, then the cells were heat shocked at 42°C for 30 seconds, followed by incubation on ice for 5 minutes. After incubation, 900 μL of super optimal growth medium with catabolic repressor (SOC) was added to the cell mixtures, and the Eppendorf tubes were placed in the incubator at 37°C and 266 rpm for 60 minutes. Next, 200 μL of the cell mixture was pipetted onto agar plates containing ampicillin or ampicillin and chloramphenicol for BL21 and Rosetta strains, respectively. The growth plates were incubated at 37°C overnight, and once colonies were visible, placed at 4°C until used for protein expression.

2.6.2 Protein Expression

Wildtype α -TTP and the K217A mutant were expressed using the transformed cells described above, as well as frozen BL21 *E. coli* cell cultures that were transformed by previous members of the Atkinson group. The new α -TTP mutants were expressed using colonies grown on agar plates after the transformation described above. All surfaces were cleaned with 70% ethanol to create a disinfected area, and a Bunsen burner was used to flame all vessel openings and tools during protein expression. The expression procedure was initiated by adding 100 $\mu\text{g/mL}$ of

ampicillin to 5 mL of LB+ media precultures that were then inoculated with the frozen cell cultures or bacterial colonies from plates for each respective α -TTP. These precultures were then incubated at 30°C and shaken at 266 rpm overnight. The following day, 1 L inoculation medium was prepared by adding 100 μ g/mL of ampicillin and 100 mL of 10X TB buffer to 900 mL of TB medium. From this solution, 1 mL was removed and used as a blank when determining cell growth, while the remaining culture medium was aliquoted into three or four 1 L Erlenmeyer flasks. The overnight precultures were then added to each flask and the cultures were incubated at 37°C and 266 rpm until the optical density (OD) at 600 nm measured was between 0.4 to 0.8. Once the optimal OD₆₀₀ measurements were obtained, each culture was induced with 0.4 mM isopropyl β -D-1-thiogalactopyranoside (IPTG) and incubated overnight at 28°C and 266 rpm. On day three, the cells were harvested via centrifugation using the Sorvall RC 6+ centrifuge and rotor F12S6X500LEX at 8,000 rpm for 20 minutes at 4°C. Cell pellets were then transferred to 15 mL Falcon tubes and stored at -80°C until protein purification.

2.6.3 Protein Purification via Glutathione S-Transferase Affinity Chromatography

The Falcon tube containing the cell pellet was thawed in a beaker of water at room temperature while buffer A was prepared. After thawing, the cell pellet was transferred to a centrifuge tube, diluted with 5 mL of wash buffer A per gram of pellet, and the mixture was passed through an 18-gauge needle attached to a 10 mL syringe multiple times to reduce its viscosity. Once transferred, 400 μ L of 200 mg/mL of lysozyme was added to the mixture and then incubated on ice for 30 minutes, followed by sonication for cell lysis. The centrifuge tube was placed in an ice water bath and held under the sonicator for one-minute intervals three times – each one-minute cycle consisted of one second pulsing sonication at 500 W, 20 kHz, and 35% amp, then incubation on ice for one minute. After sonication, the following reagents were added to the mixture: 1000

units of DNase, 50 µg/mL RNase, 10 mM MgCl₂, and 0.1% Triton X-100. The mixture was syringed again to combine these reagents throughout the cell mixture, then incubated on ice for 15 minutes, during which time wash buffer B was prepared. After incubation, the cell debris and supernatant were separated via centrifugation at 18,000 rpm for 25 minutes at 4°C using the Sorvall RC 6+ centrifuge with the F21-S8X50Y rotor.

While centrifuging the mixture, the glutathione *S*-transferase (GST) agarose column was prepared by draining the storage solution and washing once with a column full of 1X PBS buffer. Followed by the addition of any remaining buffer A solution to the column that was then drained. Finally, around 10 mL of buffer B was added to the column and drained until approximately 2 cm remained to ensure the agarose resin was submerged until it was ready to be used for protein purification. Once centrifugation was complete, the centrifuge tube was retrieved and 1 mL of the supernatant was saved for protein quantification, while the remaining supernatant was decanted onto the GST column and the cell pellet was discarded. The supernatant on the column was oscillated at room temperature for 10 minutes to allow protein binding to the resin, after which the supernatant was drained through the column and the resin was rinsed with 15 mL of buffer B to wash off non-binding proteins. A column-volume of 1X SPR was added twice to the column to remove any residual proteins and detergent from the resin prior to the addition of 100 µL of thrombin (50 units) and 1,900 µL 1X SPR to the column. The thrombin digestion in the column was incubated overnight at 4°C while oscillating to provide adequate mixing of the resin and the thrombin.

The next day, the GST elution buffer was prepared by adding 15 mg of glutathione to a 15 mL Falcon tube, dissolving it in 4 mL of 1X PBS and 1 mL of distilled water, and bringing it to a pH of 9.0 ± 0.15 using a solution of NaOH. Once the GST elution buffer was prepared, the entire

flow through from the column was collected as eluted fraction E1, then between 4 to 5 mL of 1X SPR elution buffer was added to the column to collect the remaining protein as fractions E2 to E6. After collecting the elution fractions, the GST elution buffer was added to the column to remove the GST tags bound to the resin and collected as fractions GST1 to GST3. The column resin was then regenerated by washing the column with Cleansing Buffer #1, two column-volumes of autoclaved MilliQ water, Cleansing Buffer #2, and a final wash with autoclaved MilliQ water. Approximately 2.5 mL of 2.5 M NaCl was added to the column to cover the resin as a storage solution and the column was stored at 4°C until the next use. The agarose affinity resin was used for fourteen consecutive purifications, after which new resin was prepared by hydrating 250 mg of glutathione-agarose in 50 mL of MilliQ water overnight at 4°C. The resin mixture was then transferred to the 1.5 x 20 cm column, the water was drained for resin packing and stored in 2.5 M NaCl until next use.

2.6.4 Protein Concentration Quantification

Bradford assays were carried out immediately after protein purification to quantify the concentrations in each elution fraction. A standard curve with a concentration range of 0 to 0.8 mg/mL was created by diluting a stock solution of 1 mg/mL BSA with 1X PBS to a total volume of 50 µL. The protein elution fractions from purification were also diluted with 1X PBS to the same volume with the following additions from each fraction – 5 µL of E1, 10 µL of E2, 10-20 µL of E3, 30-50 µL of E4, and 50 µL of E5 and the GST fractions. Once diluted, 1 mL of Bradford reagent was added to all samples and after incubation for 10 minutes at room temperature, the absorbance values were measured at 595 nm. The protein concentrations of the elution fractions were then calculated based on a standard curve generated from the known concentrations and absorbance values of the standard samples.

2.6.5 SDS-PAGE

2.6.5.1 *13% Acrylamide Gel Casting*

The gel casts were cleaned with 70% ethanol and thoroughly dried prior to mixing reagents and setting up the gel molds. The resolving gel (final volume 70.32 mL) was created first by combining 32 mL distilled water with 26 mL 40% acrylamide, 10 mL resolving buffer, 800 μ L of 10% SDS, 400 μ L trichloroethylene (TCE), and 240 μ L of 50% glycerol. The final two reagents – 800 μ L of 10% ammonium persulfate (APS) and 80 μ L tetramethylethylenediamine (TEMED) – were added immediately before pipetting the resolving gel into the gel casts to fill each one approximately $\frac{3}{4}$ of the way. A small amount of butanol was pipetted on top of each gel cast to remove any bubbles in the resolving gel prior to it solidifying at room temperature. Once the resolving gel had set and the butanol was removed, the stacking gel (final volume 24.74 mL) was mixed, consisting of 15.6 mL distilled water, 2.5 mL of 40% acrylamide, 6 mL stacking buffer, 250 μ L of 10% SDS, and 116 μ L of 50% glycerol. Immediately before pipetting, 250 μ L of 10% APS and 25 μ L TEMED were added to the mixture. After the addition of the stacking gel, gel combs were added in the gel molds, and the gels were left at room temperature to solidify. The gel molds were then wrapped in moistened paper towels and stored at 4°C until used.

2.6.5.2 *Gel Electrophoresis*

A 13% precast acrylamide gel described in the above protocol was obtained to determine if the purification was successful. If no in-house gels were available, a 12% precast gel from Bio-Rad was used. The gel and a buffer dam were inserted into the Mini-PROTEAN® Tetra Cell System, which was then filled with 1X SDS running buffer. All samples contained 5 μ L of 5X loading dye and protein samples from the supernatant and elution fractions ranging between 5 μ L and 30 μ L, with the total volume not exceeding 40 μ L. Samples were vortexed and pulse

centrifuged to ensure adequate mixing of the loading dye and protein samples prior to loading into each gel well. 7 μL of the BLUeye protein ladder was loaded into one well as a molecular weight standard. The gel was electrophoresed at 125 V until the samples had entered the gel, then the voltage was increased to 140 V and the electrophoresis continued until the dye front had run off the gel. Once complete, the gel was removed from the cast, stained with Colloidal Coomassie G-250, and incubated on a rocker overnight. The following day the stain was removed, the gel was rinsed with distilled water and destained with 25% methanol, after which the gel was imaged using the Gel DocTM EZ Imager and the Image Lab software.

2.6.6 α -TTP and NBD- α -Tocopherol Binding Assays

2.6.6.1 *NBD- α -Tocopherol Quantification*

Prior to performing the binding assays, a stock solution of α -tocopherol fluorescently labelled with nitrobenzoxadiazole (NBD) prepared by another member of the Atkinson group (Phil Nava, 2007) was quantified to determine its concentration. 500 μL of absolute ethanol was added to a Hellma[®] quartz glass cuvette 10 x 4 mm, which was used as a blank solution during quantification. A second quartz glass cuvette was also filled with 500 μL absolute ethanol, and 0.5 μL of stock NBD- α -tocopherol was added, then its absorbance was measured at 466 nm. Two additional measurements were taken by adding 0.5 μL of NBD- α -tocopherol to the same cuvette after each measurement. An average absorbance value was then calculated based on the example provided in Scheme 1. The concentration (C) was then calculated using equation 1 where the extinction coefficient (ϵ) was $17,852 \text{ cm}^{-1} \text{ M}^{-1}$, the light path length (l) was 1 cm, and the dilution factor (DF) was 1,000. The newly quantified NBD- α -tocopherol stock solution was used to prepare a working stock solution of 500 μM NBD- α -tocopherol in ethanol for preparing the secondary

working stock solutions – 7 μM , 21 μM , 42 μM , 84 μM , 147 μM , and 210 μM – used during the binding assays.

Absorbance Values (466 nm)

Blank (500 μL) – 0.000

#1: Blank + 0.5 μL NBD- α -tocopherol – 0.031 Δ 0.031

#2: #1 + 0.5 μL NBD- α -tocopherol – 0.065 Δ 0.034

#3: #2 + 0.5 μL NBD- α -tocopherol – 0.091 Δ 0.026

$$\text{Average abs.} = \frac{0.031+0.034+0.026}{3} = 0.0303_3$$

$$\text{Equation 1: } C = \frac{A}{\epsilon \cdot l} \times \text{DF} = \frac{0.03033}{17,852 \text{ M}^{-1}\text{cm}^{-1} \cdot 1 \text{ cm}} \times 1,000 = 1.70 \text{ mM}$$

Scheme 1. NBD- α -Tocopherol Quantification Calculation. The absorbance values are measured at 466 nm and the absorbance differences are calculated to obtain an average absorbance value that is then used to determine the concentration of the NBD- α -tocopherol stock solution using equation 1.

2.6.6.2 *Microplate Reader Binding Assay*

2.6.6.2.1 Experimental Procedure

Black bottom 96-well plates from Greiner Bio-One were used to conduct binding assays, with each well containing a total volume of 200 μL . Wells B2 to B12 contained control solutions consisting of 1X TKE buffer and NBD- α -tocopherol, with concentrations ranging from 0 to 800 nM. Wells C1, D1, and E1 were also controls containing 1X TKE buffer and 0.4 μM α -TTP, while the sample wells C2 to E12 contained replicates of 1X TKE buffer, 0.4 μM protein, and 0 to 800 nM NBD- α -tocopherol (Figure 15). Master mixes for all wells were prepared in 1.5 mL Eppendorf tubes to ensure proper mixing of components prior to pipetting into singular wells. The order of addition was 1X TKE buffer, protein, then NBD- α -tocopherol. The mixtures were then incubated at room temperature for approximately 2 minutes, after which each tube was vortexed and centrifuged. 200 μL of each solution was pipetted into the corresponding wells and the plate was incubated at room temperature for approximately 5 minutes while the microplate reader and the

software were initialized. Once complete, the plate was placed in the microplate reader, and the fluorescence spectrum was measured with an excitation wavelength of 466 nm and an emission wavelength range of 510 to 550 nm. The plate was shaken for five seconds before taking the first read.

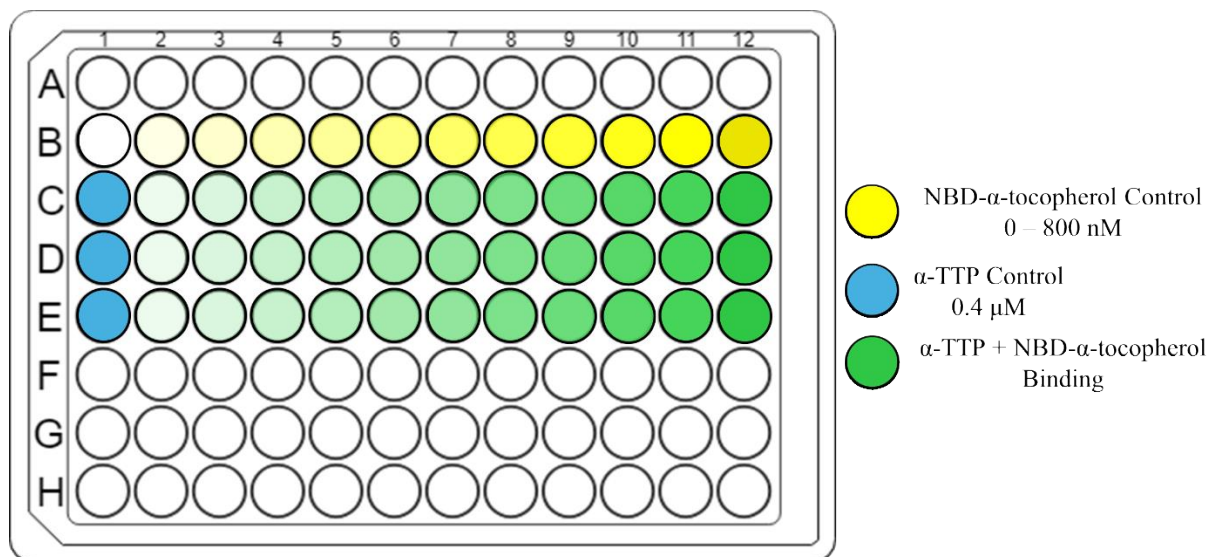


Figure 15. Binding Assay Plate Configuration.

Each well was brought to a total volume of 200 μL using 1X TKE buffer. Wells B2 to B12 were the ligand control samples with a concentration range of 0 to 800 nM. The protein control set, only containing 0.4 μM $\alpha\text{-TTP}$, was in wells C1, D1, and E1. Three replicate experiments – C2 to C12, D2 to D12, and E2 to E12 – were conducted on each assay plate to analyze the protein-ligand binding interactions. Each sample well contained the same concentration of NBD- α -tocopherol as the corresponding B control well and all sample wells had a constant protein concentration of 0.4 μM .

2.6.6.2.2 Data Analysis

Once the binding assay reading was complete, the values were copied to an Excel sheet to be transferred to GraphPad Prism 10.1.2 for analysis. A table containing one x-value column and three column y-values was used to analyze the data. The concentrations of NBD- α -tocopherol were used as the x-values, while the fluorescence values obtained at 530 nm for replicates C1-C12, D1-D12, and E1-E12 were placed in three separate y-columns. A binding curve was generated by clicking “Analyze” \rightarrow “Regression and Curves” \rightarrow “Nonlinear Regression (Curve Fit)” \rightarrow “XY

Analyses” → “Nonlinear regression (curve fit)” → “Binding – Saturation” → “One site -- Specific binding”.

2.6.6.3 *Fluorometer Binding Assay*

2.6.6.3.1 Experimental Procedure

Two working stocks of 100 μM and 500 μM NBD- α -tocopherol were prepared by diluting a quantified original stock of NBD- α -tocopherol with absolute ethanol. The circulating cooling water bath was turned on approximately 30 minutes prior to beginning the experiment as it had to cool from room temperature to 8°C. Once the water bath was ready, the fluorometer light source was turned on and allowed to warm up for approximately 5 minutes. The fluorometer and operating system were then also powered on, and the Felix software was opened to begin the experiment. The experimental conditions were setup using the software controls “New Acquisition” → “Emission Scan” → “QM Configuration”. The emission wavelength range was set between 510 to 550 nm and the excitation wavelength was 466 nm. The emission wavelength was collected in increments of 0.5 nm selected under the “Step size” bar. “Integration” and “Average” were set to 0.1 seconds and 1, respectively. While the fluorometer chamber was empty, the “Background” acquisition was completed to determine if the system was prepared for operation.

Four Hellma® quartz glass cuvettes (10 mm x 10 mm) were cleaned using 70% ethanol and thoroughly dried using air prior to filling each with 3 mL of 1X TKE buffer. 0.4 μM of α -TTP was added to three cuvettes – representing three replicates during each binding assay, while the fourth cuvette only contained buffer and remained the blank control sample. The experiment was initiated by measuring the baseline fluorescence of the blank control sample by clicking “Acquisition” → “Start” after the cuvette was placed into the sample holder. The baseline

fluorescence of the three replicate samples containing protein was then determined by consecutively placing each cuvette one at a time into the sample holder and acquiring traces for each. The working stocks of NBD- α -tocopherol prepared were used to add the ligand to each cuvette, with concentration increasing from 0 to 700 nM (Table 3). After the addition of NBD- α -tocopherol to each cuvette, samples were incubated and inverted by hand at room temperature for five minutes, followed by fluorescence measurements carried out in the same cuvette order as was done for the baseline measurements. All subsequent measurements were carried out in the same manner of ligand addition, incubation, and measurement.

Table 3. Concentration of NBD- α -Tocopherol During Fluorometer Binding Assays.

Consecutive additions of NBD- α -tocopherol from either a 100 μ M or 500 μ M primary stock was used to gradually increase the concentration of ligand from 0 to 700 nM in each sample cuvette. Samples were incubated and mixed by hand at room temperature for two minutes before measuring fluorescence after each addition.

Addition	NBD-α-Tocopherol Stock Used and Volume Added	Concentration (nM)
1 st	0.5 μ L of 100 μ M	16.67
2 nd	0.5 μ L of 100 μ M	33.34
3 rd	1.0 μ L of 100 μ M	66.67
4 th	0.5 μ L of 100 μ M	83.34
5 th	0.5 μ L of 100 μ M	100.0
6 th	0.6 μ L of 500 μ M	200.0
7 th	0.5 μ L of 500 μ M	283.3
8 th	0.5 μ L of 500 μ M	366.6
9 th	1.0 μ L of 500 μ M	533.3
10 th	1.0 μ L of 500 μ M	700.0

Once the binding assay measurements were completed, data was exported from the Felix data sheet by clicking “Display” \rightarrow “Grid view” that displayed the fluorescence spectra values, which were copied to an Excel spreadsheet. The original data was then saved using the Felix software. All components of the fluorometer were then shut down in a backwards order as they were powered on. The water bath was left to operate approximately 10 minutes after turning off the light source to prevent overheating of the lamp while it cooled back to room temperature.

2.6.6.3.2 Data Analysis

Data analysis was conducted using GraphPad Prism 10.1.2 – a new file was created having x-values in one column and y-values in three replicate side-by-side columns. The concentration gradient of NBD- α -tocopherol was entered into the x-value column and the fluorescence measurement values at 530 nm were copied from the Excel spreadsheet into the y-value columns. The column A:Y1 contained the fluorescence values measured for the blank control sample, while columns B:Y1, B:Y2, and B:Y3 contained the fluorescence values of each replicate sample, respectively. Once the data was entered, a binding curve was generated by selecting “Analyze” → “Regression and Curves” → “Nonlinear Regression (Curve Fit)” → “XY Analyses” → “Nonlinear regression (curve fit)” → “Binding – Saturation” → “One site -- Specific binding”.

2.6.7 Lipid Membrane Vesicle Preparation

Plasma membrane lipid vesicles contained six different lipid types, with the addition of PI(4,5)P₂, PI(3,4)P₂, or PI(3)P for different experimental conditions. Table 4 describes the mole percent composition of the plasma membrane lipid vesicles with a final 1 mM concentration.

Table 4. Plasma Membrane Lipid Composition.

Plasma membrane lipid vesicles contained mole percentages of each lipid below to mimic *in vivo* compositions. For samples containing either of the three PIPs, with amounts ranging between 2-6%, the mole percent of DOPC was reduced to accommodate the addition of the ligands.

Lipid Type	Mole Percent Composition (%)
Cholesterol	19
1,2-dioleoyl-sn-glycero-3-phosphate (DOPA)	2
1,2-dioleoyl-sn-glycero-2-phosphocholine (DOPC)	44
1,2-dioleoyl-sn-glycero-3-phosphoethanolamine (DOPE)	20
1,2-dioleoyl-sn-glycero-3-phospho-L-serine (DOPS)	5
Sphingomyelin (SM)	10

The lipid vesicles were prepared by adding the required volumes of each lipid type to a glass vial and evaporating the chloroform solvent using N₂ (g) until none remained. The glass vial was then placed on a high vacuum for one hour to ensure all the solvent had completely evaporated.

The lipid mixture was then resuspended in 1X SPR and placed at 4°C to rehydrate overnight. The lipids were extruded the next day using the Avanti lipid mini-extruder and a 100 nm polycarbonate membrane filter to produce unilamellar vesicles and placed in a new glass vial. All extruded lipid mixtures were used within a month before the lipids precipitated out of solution.

2.6.8 Wildtype α -TTP Preincubations with α -Tocopherol

Prior to incubating wtTTP with α -tocopherol the Eppendorf tubes used to store the protein-ligand mixture was coated with BSA to prevent the adsorption of α -tocopherol to the test tubes. Each sample tube was coated with 1 mL of 0.5 mg/mL BSA and incubated at room temperature overnight to ensure proper coverage. The BSA solution was decanted the next day, dried with N₂ (g), rinsed three times with distilled water, and dried again before using it during ligand preincubation.

In separate Eppendorf tubes from the ones coated with BSA, 50 μ M of α -tocopherol was added, brought to 100 μ L final volume with absolute ethanol that was then evaporated with N₂ (g). Then, 1 mL of 0.5 μ M wtTTP was added to these test tubes and vortexed for approximately 30 seconds to ensure proper mixing. The protein-ligand solution was then transferred to the BSA-coated Eppendorf tubes and incubated at 4°C overnight. The preincubation solutions were then used for SPR injections the following day.

2.6.9 Gold SPR Sensor Slide Derivatization

All buffers and reagents were obtained prior to beginning the chip derivatization. Two large glass petri dishes were used as a platform to hold the chip and cover it during incubation times. A gold sensor slide coated with 500 kDa carboxymethyl dextran was obtained from storage at 4°C and placed in a petri dish containing a KimWipe. A solution containing 40 mg of *N*-(3-dimethylaminopropyl)-*N*'-ethylcarbodiimide hydrochloride (EDC) and 10 mg of *N*-

hydroxysuccinimide (NHS) dissolved in 1 mL of autoclaved MilliQ water was added to a glass vial. Immediately after dissolving, the EDC/NHS solution was added dropwise to the surface of the chip using a glass Pasteur pipet. The chip was covered with the second petri dish and incubated at room temperature for 12 minutes. Once complete, the excess EDC/NHS was washed off using MilliQ water and the chip surface was completely dried with $N_2(g)$. Once the chip was dry, 500 μ L of a 1:1 stock solution of phytosphingosine/DMSO was pipetted into a sterile 1.5 mL microcentrifuge tube, then 500 μ L of 20 mM sodium acetate (pH 5.2) was added dropwise to the same tube. Immediately after making up this solution, it was added dropwise to the sensor slide surface, which was incubated for 1.5 hours. After incubation, the excess phytosphingosine:DMSO solution was washed off and the chip was dried as previously described, followed by the addition of 1 M ethanolamine HCl (pH 8.5) to the surface. The chip was incubated for 10 minutes then washed and dried, while the previous sensor slide was removed from the SPR apparatus, and the chip holding site was washed with 70% ethanol and wiped clean with a KimWipe. One drop of SPR immersion oil ($\sim 0.5 \mu$ L) was added to the site prior to placing the new chip into placement, which was then allowed to equilibrate in 1X SPR running buffer for at least one night prior to performing injections.

2.6.10 SPR Injection Procedure

2.6.10.1 SPR Injection Protocol

The α -TTP-ligand interaction experiments were conducted with a two channel SR7500DC surface plasmon resonance (SPR) apparatus and a gold sensor slide derivatized with phytosphingosine as described in 2.7.8. Upon beginning a new experiment, a new SPR Autolink file was created by clicking 'Start' on the SPR instrument direct control, and once the system

initiation was complete, the detector scan data was examined to confirm proper function of the SPR by showing the proper trace (Figure 16).

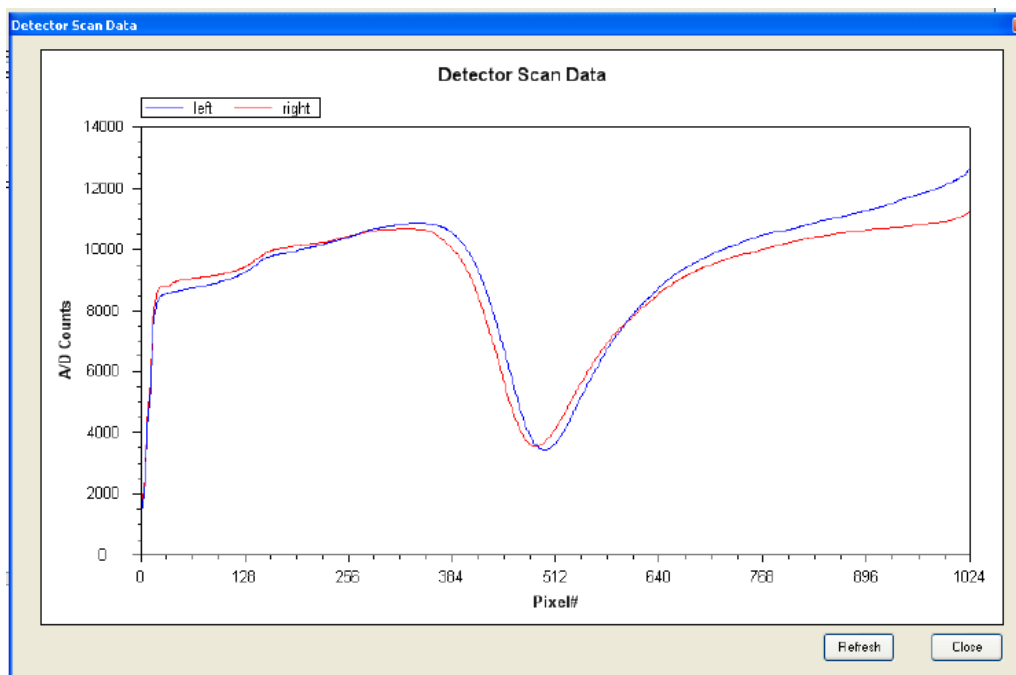


Figure 16. Detector Scan Data Trace.

The following trace was expected when checking the detector scan data prior to beginning a new experiment on the SPR to ensure proper working conditions of the machine. Both the left (blue) and right (red) channels must depict the above pattern showing a steep rise followed by a gradual increase before plunging to a valley but not reaching zero A/D counts and ending in a gradual rise. The two channels may not be entirely superimposed on top of each other but must trace one another closely.

Once the detector scan data was confirmed, the experiment was initiated via priming the sensor slide by selecting the following from the drop-down menu: 'Form' → 'Run Table Editor' → 'Prime with Semi-Automatic Wizard' → 'Run'. The data trace was then viewed in real-time by selecting 'Data Plot' under the 'Form' tab to view as the machine detected a baseline value, which was recorded in the SPR logbook each day to monitor the sensor slides viability over time. While the priming was in progress, the regeneration, lipid, and protein injection syringes were cleaned before use according to the procedure outlined in Table 5. After cleaning each syringe, the regeneration syringes (50 mM NaOH, 0.5% SDS, 50 mM glycine, and 80% EtOH) were filled

with approximately 2 mL of their respective solutions and degassed. Syringe degassing consisted of placing a parafilm ball at the needle tip of a syringe to create an airtight seal, then pulling the plunger down and quickly releasing it, which was repeated until no bubbles remained in the syringe.

Table 5. SPR Injection Syringe Cleaning Protocol.

Each syringe was cleaned before and after a new experiment each day via the specific protocols listed here. The lipid and protein syringes were also cleaned between experiments if different lipid vesicles or proteins were used on the same day.

Syringe Type	Cleaning Protocol
1X SPR Buffer	3 x 1X SPR buffer
50 mM NaOH	3 x autoclaved MilliQ water
0.5% SDS	
50 mM glycine	2 x 80% EtOH
80% EtOH	
Lipid	1 x 80% EtOH
Protein	3 x 1X SPR buffer

Once the priming protocol was complete, the SPR sample injection loop (100 μ L) was cleaned via the general cleaning method of one full 10 mL syringe filled with air, excess 1X SPR buffer, and another push of air until no more liquid exited the loop. The general loop cleaning procedure was carried out after every injection throughout an experiment. Following sensor slide priming and sample loop cleaning, the regeneration protocol was completed at the start of each new experiment. The order of regeneration buffers injected was 50 mM NaOH, 0.5% SDS, 50 mM glycine, and 80% EtOH – to ensure proper cleaning of the chip surface. Enough of each regeneration buffer is injected into the sample loop until at least a single solution drop exits the loop – noting the loop contained excess solution and was full for the injection. The syringe was left attached to the injection port throughout the run. To initiate sample injection the following were selected: ‘Form’ \rightarrow ‘Run Table Editor’ \rightarrow ‘Regeneration’ and the ‘Index’ was set to the desired regeneration buffer being injected – 3, 4, 5, or 6 for 50 mM NaOH, 0.5% SDS, 50 mM

glycine, and 80% EtOH, respectively. After the final regeneration buffer injection was complete, the sample loop was cleaned three times via the general cleaning procedure prior to starting the experiment via the lipid solution injection.

During the regeneration protocol, the extruded lipid solution used for the specific experiment was taken up via syringe and degassed as described above. After the final general loop cleaning, the lipid solution was injected into the sample loop, once again until at least a single drop exited, and the syringe remained in the injection port. The lipid injection was initiated by selecting 'Form' → 'Run Table Editor' → 'Vesicle Capture' → 'Run', then the injection was monitored in real-time by selecting 'Form' → 'Data Plot'. The protein injection solution was prepared while the lipid vesicle capture injection was running by diluting a stock solution of α -TTP with 1X SPR buffer to the desired concentration. The protein solution was then taken up into the designated syringe and degassed before use. Once the lipid injection was complete, the syringe was removed, and any remaining lipid solution was replaced into its glass vial. The sample loop was cleaned twice using the general cleaning method to ensure no lipids remained in the injection loop before the protein sample was injected. After filling the sample loop with the protein solution, the injection occurred by clicking 'Form' → 'Run Table Editor' → 'Protein Injection' → 'Run'. The injection of a lipid layer then a protein layer on top constituted as a single experiment. The lipid and protein layers were removed from the chip surface between consecutive experiments by injecting 50 mM NaOH and 80% EtOH as described during the regeneration process. After the final experiment, the complete regeneration protocol was carried out prior to ending the session by clicking 'Stop' on the SPR instrument direct control. When not in use, the sensor slide remained hydrated with a continuous flow of 1X SPR running buffer at a flow rate of 15 μ L/min.

2.6.10.2 SPR Injection Conditions

Priming

Infused the flow rate at 250 $\mu\text{L}/\text{min}$ for 8 minutes, then directed the diverter valve to only the left channel for 1 minute. The diverter valve was then directed to both the right and left channels for one minute, and the flow rate was infused at 25 $\mu\text{L}/\text{min}$.

Regenerations

The flow rate was infused at 25 $\mu\text{L}/\text{min}$ and the pump refilled with 25,000 $\mu\text{L}/\text{min}$. After 10 seconds, the regeneration buffer was injected into the SAV valve for 1 minute, followed by SAV loading for another minute.

Vesicle Capture

The flow rate was reduced to 8 $\mu\text{L}/\text{min}$ for 10 seconds and the diverter valve was directed only towards the left channel for 10 seconds. Then the lipid vesicles were injected for 11 minutes, then loaded for 1 minute, then the diverter valve directs the running buffer to both channels for 10 seconds.

Protein Injection

The flow rate was infused at 10 $\mu\text{L}/\text{min}$, waited 10 seconds, then the protein injection was applied to the SAV valve for 9 minutes and loaded for 5 minutes.

2.6.11 SPR Data Analysis

2.6.11.1 SPR Data Extraction

The required SPR file was opened using the SPR Autolink software, clicking “File” then “Open” and choosing the desired run. Once open, “Form” \rightarrow “Post-Processing” was chosen, which generated two μRIU versus time plots – the source data and segment overlays. Double clicking the

protein-binding curve from the source data plot and clicking “Add” in the bottom right corner transferred the binding curve to the segment overlay plot. Both the right and left channel data were automatically transferred, therefore, the right control channel showing only the buffer injection was removed by clicking on the “Right” in the bottom right corner and hitting “Delete” once the curve was highlighted. The above steps were repeated for each replicate, and once all three curves have been added to the segment overlay plot, “TraceDrawer” was selected at the top control panel, which automatically added the selected curves into the Trace Drawer software and a binding curve was generated. The curve was extracted from Trace Drawer by right clicking on the curve plot, choosing “Export curves”, and the file was named then saved. The Trace Drawer file was also saved and converted to a text file for further analysis.

2.6.11.2 SPR Data Analysis

The required binding curve text files were opened in an Excel spreadsheet, with the “X” columns containing the time values and the “Y” columns reporting the μ RIU binding signal values. A new Prism file was opened with single y-columns, the three replicate signal values were copied to three separate y-columns, and the single x-column contained the time values. Binding curves were generated by clicking “Analyze” → “Regression and Curves” → “Nonlinear Regression (Curve Fit)” → “XY Analyses” → “Nonlinear regression (Curve Fit)” → “Exponential” → “One phase association”. A μ RIU versus time (s) plot was generated that showed the complete run of the SPR data. Protein binding curve results only required the association segment of the generated plots, therefore, the data was trimmed – removing the time and signal values outside the binding association section of the graph.

3 Results and Discussion

3.1 α -TTP Expression and Purification

After culturing a batch of *E. coli* containing recombinant α -TTP plasmids, protein expression was confirmed via sodium dodecyl sulfate polyacrylamide gel electrophoresis (SDS-PAGE). Each SDS-PAGE gel was loaded with a prestained protein ladder, a sample of uninduced cell culture, and samples from each overnight culture. α -TTP expression was verified on the gel if the induced sample lanes contained a protein band at approximately 58 kDa, which was the expected molecular weight of the glutathione *S*-transferase (GST) tagged α -TTP fusion protein, while the uninduced sample lane did not contain such band (Figure 17). Once protein expression was confirmed on a gel, cell pellets were decanted into 15 mL Falcon tubes and stored at -80°C until used for protein purification.

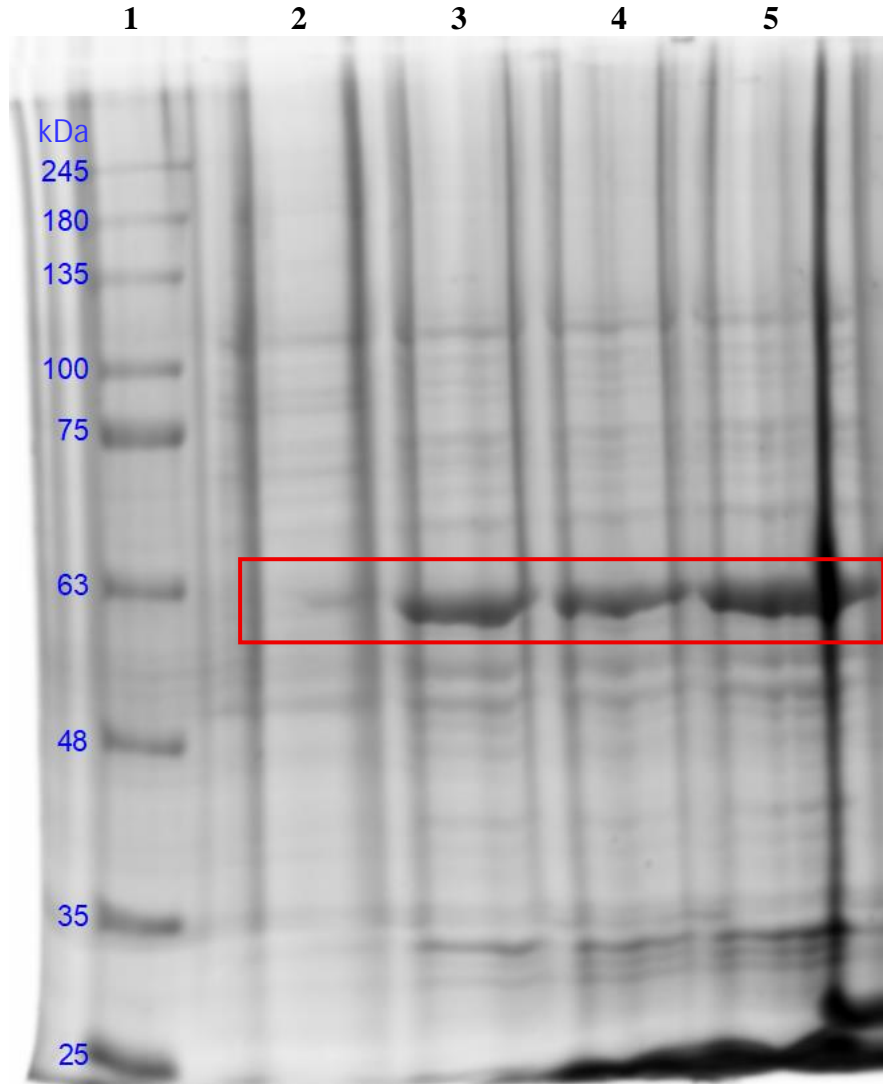


Figure 17. wtTTP Expression Using Different Cell Lines.

Wildtype α -TTP (wtTTP) with a GST tag was expressed using Rosetta and BL21 *E. coli* cell lines, and a frozen cell culture prepared by a previous member of the Atkinson group. The presence of prominent bands at approximately 58 kDa in lanes three through five containing induced cell samples confirmed proper expression of the α -TTP-GST fusion protein after induction compared to the absence of this band in the uninduced sample in lane two. Lane 1: BLUeye prestained protein ladder, lane 2: uninduced cell sample, lane 3: Rosetta *E. coli*, lane 4: BL21 *E. coli*, lane 5: colony F freeze culture. Figure created via Image Lab, version 6.1.

α -TTP, both wildtype and the mutant forms, were expressed with a GST tag protein (~ 27 kDa) to allow for protein purification via affinity chromatography using a glutathione-agarose resin. Upon the addition of the cell culture supernatant to the chromatograph column the GST

portion of the GST fusion protein binds to the immobilized glutathione (GSH) and the target protein, for instance α -TTP, is retained while non-specific proteins are washed out (Schäfer et al., 2015). The pGEX plasmid vector used in this project included a cleavage recognition site for the thrombin protease that cleaved α -TTP from the GST tag, which allowed α -TTP to be eluted separate from GST and prevented contamination. Following enzymatic cleavage and α -TTP elution, the GST tagged proteins retained on the resin were then removed from the column via the addition of excess solution of reduced GSH. The GST tagged proteins then bind to the newly added GSH and elute from the resin to recondition the column for reuse (Figure 18).

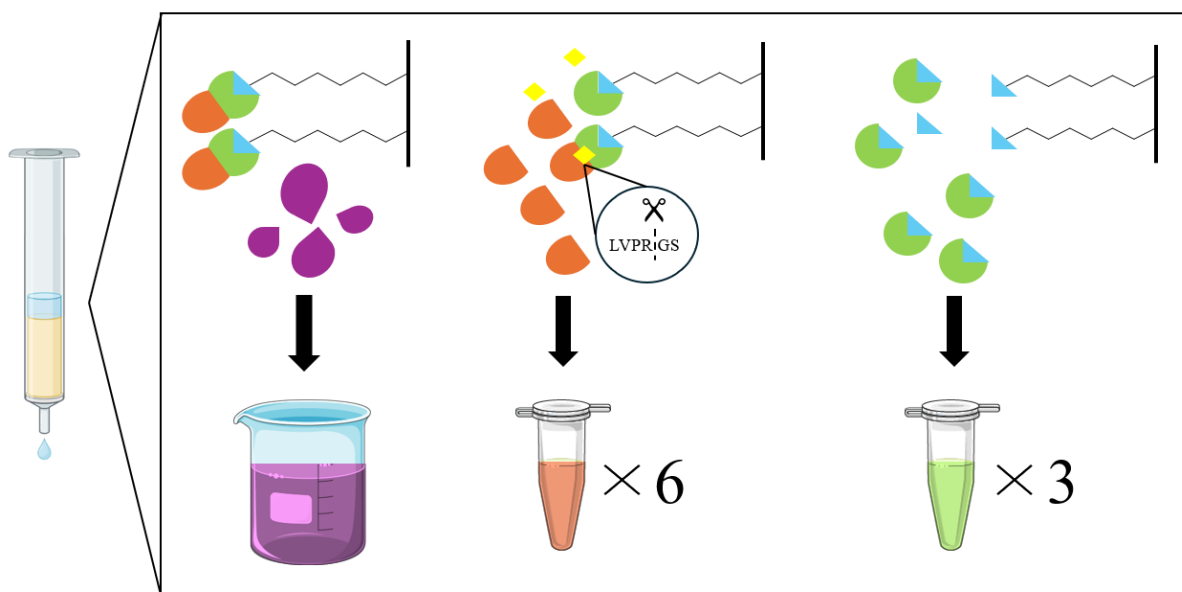


Figure 18. Schematic Diagram of GST Affinity Purification.

Upon the addition of the cell lysate supernatant to the GST affinity chromatography column, the α -TTP-GST fusion protein (orange and green) binds to the immobilized glutathione (blue) on the resin, while non-specific proteins (purple) were washed out of the column using Buffer B and 1X SPR running buffer. Following these wash steps, thrombin protease (yellow) was added to the column and incubated at 4°C overnight to cleave α -TTP from the GST tag. The thrombin recognition site of LVPRGS is present at the N-terminus of α -TTP, thus when thrombin cleaves between the arginine and glycine residues, a sequence of four amino acids remains attached to α -TTP (Waugh, 2011). These α -TTP flow through samples were collected as elution fractions E1-E6, after which a glutathione elution buffer, pH 9.0, was added to the column to remove the GST bound to the resin, thereby recycling the column for another purification.

An SDS-PAGE gel was performed after each purification to verify proper cleavage from GST tags and elution of α -TTP from the column. These gels were also loaded with a prestained protein ladder, a sample of the supernatant (prior to its addition to the column) to ensure α -TTP was present after cell lysis and to approximate the amount of target protein lost throughout purification. α -TTP elution fractions (E1-E6), which typically should only contain decreasing amounts of α -TTP, were also loaded into gel lanes to determine their purity, along with some of the GST elution fractions that indicated if the cleavage and purification was successful. However, during the initial purification attempts based on a previously established protocol, the SDS-PAGE gel showed E1-E6 had multiple high molecular weight contaminants of approximately 10% relative quantities compared to α -TTP when the gel image was analyzed via BioRad Image Lab software. In addition, the GST elution fraction not only contained large amounts of free GST at approximately 27 kDa, but also showed the presence of cleaved α -TTP (~ 32 kDa), as well as high concentrations of fusion protein (~ 58 kDa) that remained on the column after cleavage by thrombin (Figure 19).

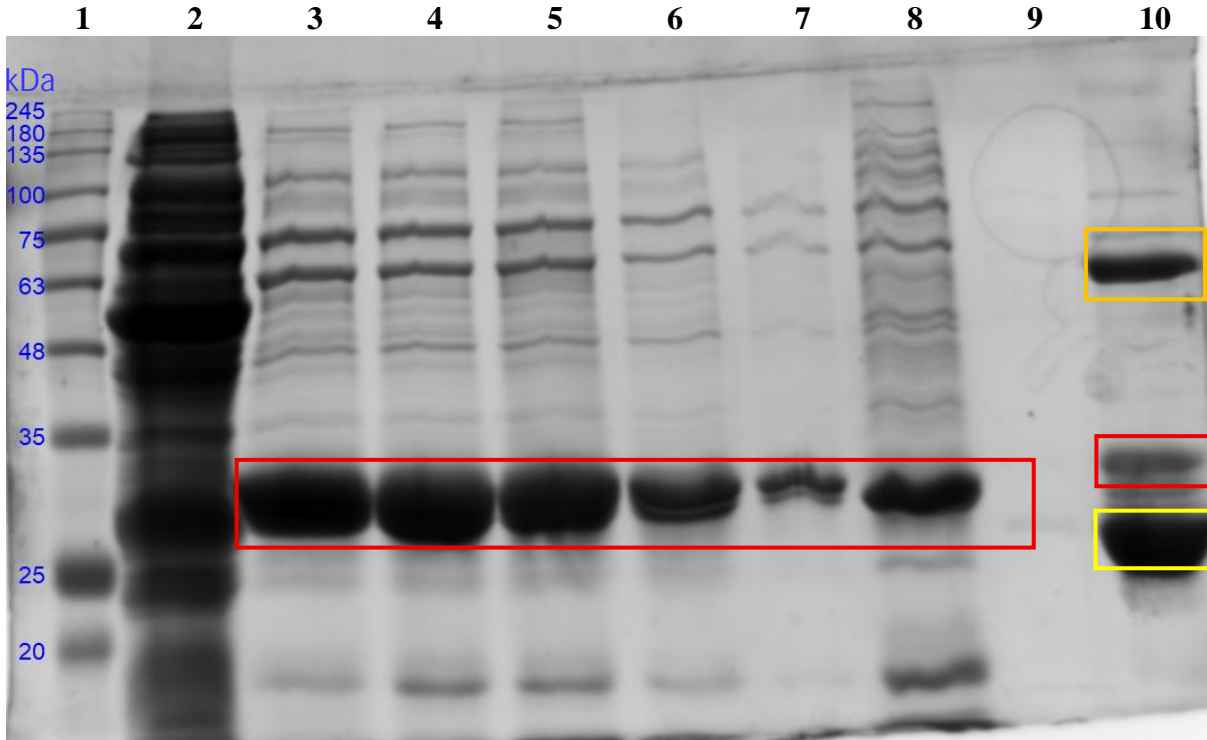


Figure 19. α -TTP Purification via GST Affinity Chromatography Pre-Optimization. Prominent, thick bands of approximately 32 kDa in elution fractions one through six (E1-E6) confirmed the cleavage and elution of α -TTP from the GST affinity resin. Several high molecular weight bands were also present in relatively high concentration in each of the elution fractions. The glutathione elution fraction in lane ten contained prominent fusion and free α -TTP protein bands at approximately 58 and 32 kDa, respectively, in addition to the thicker band around 27 kDa representing the GST tag protein. Lane 1: BLUeye prestained protein ladder, lane 2: cell lysate supernatant, lane 3: E1, lane 4: E2, lane 5: E3, lane 6: E5, lane 7: E6, lane 8: E4, lane 9: GST1, lane 10: GST2. Red box = wtTTP, orange box = fusion protein, yellow box = GST protein. Figure imaged and annotated via Image Lab, version 6.1.

Furthermore, upon protein quantification of E1-E6 and GST1-3 via Bradford assay, all elution fractions contained high concentrations of α -TTP, between 60 to 70 μ M. The Bradford protein quantification method relies on the binding of Coomassie Brilliant Blue G-250 dye to mainly positively charged amino acids such as arginine, lysine, and histidine. In the presence of proteins, the dye has a visible colour change from reddish brown to blue, and the dye's absorbance shifts from 465 nm to 595 nm, which allows the amount of protein to be estimated by measuring the absorbance at 595 nm (Bonjoch & Tamayo, 2001). The presence of 41 total arginine, lysine,

and histidine residues in α -TTP allows the dye to bind to many sites of the target protein. However, if the high molecular weight contaminating proteins present in E1-E6 also contain many of these positively charged amino acids, the Bradford quantification would overestimate the amount of α -TTP present in the elution fractions as reported during the purification in Figure 19.

Numerous experimental strategies were trialed to improve α -TTP purity in the elution fractions and reduce the amount of fusion protein and free α -TTP in the GST elution fractions. Initially, GST resins from three different suppliers were available to test which one yielded optimal purification conditions. Resins from Cytiva and BioShop had comparable amounts of target protein retention and elution fractions of similar purities. The third resin from Sigma-Aldrich, which was used in the preliminary purification attempts, resulted in higher amounts of α -TTP loss during purification and more contamination present in E1-E6 compared to the two other resins (Table 6). Therefore, subsequent purifications were carried out using the glutathione-agarose resin from BioShop. A second optimization strategy was to include a chaperone protein removal wash step after the first Buffer B wash of the column prior to the addition of thrombin to the column (2.6.3). This chaperone removal wash was attempted based on its success reported by another member of the Atkinson group during the purification of several proteins, including phosphatidylinositol 4-kinase type III beta protein (PI4K-III β), phosphatidylinositol/phosphatidylcholine transfer proteins (PITPs), and frequenin (Frq1). During the purification of PI4K-III β , PITPs, and Frq1, the presence of ATP-binding protein contaminants in the elution fractions required the addition of a chaperone removal wash, which increased the purity of samples (Muniz Correa, 2023). Other studies have also found that chaperone molecules present during bacterial recombinant protein expression often include contaminated protein elution fractions during purification. Specifically, heat shock protein 70 (Hsp70), is a common chaperone molecule found in *E. coli* that recognizes and binds to exposed

polypeptide regions in many different proteins to facilitate proper folding (Morales et al., 2019). It has been shown that Hsp70 can bind to the connector peptide region between target proteins and a thrombin cleavage site and remains attached to the target protein even after extensive purification steps are taken to remove it. Hsp70 is known to have ATPase activity, and a study by Rial and Ceccarelli, (2002), showed that adding a combination of adenosine triphosphate (ATP) with magnesium and *E. coli* lysate during protein purification could remove Hsp70 contaminants from protein elution fractions. A similar chaperone removal wash was utilized to determine if any of the high molecular weight contaminants observed in E1-E6 were Hsp70 or other chaperone molecules capable of binding ATP. A solution of 5 mL Buffer B, 0.1 mg/mL by volume of *E. coli* lysate, 20 mM MgCl₂, and 10 mM adenosine triphosphate (ATP) was prepared prior to protein purification and decanted onto the column after the first Buffer B wash outlined in 2.6.3. The column containing the chaperone removal wash was then incubated at 37°C for 10 minutes before the solution was drained and a sample of the flow through was collected. However, when assessed on an SDS-PAGE gel, it showed no difference compared to the Buffer B wash prior to the removal wash. The high molecular weight contaminants persisted in E1-E6 after the inclusion of the chaperone removal wash, therefore, this step was not implemented in the optimized purification protocol (Table 6). The remaining optimization strategies did not include new methods but instead increased the amounts of reagent added at certain steps of the purification. For instance, the initial dilution of a protein pellet with Buffer A was increased from 2 mL/g to 5 mL/g to reduce the viscosity of the solution. An additional wash with 1X SPR running buffer was added to the column prior to pipetting thrombin onto the resin to ensure all non-bound proteins were removed from the column. Lastly, the amount of thrombin added to the column was increased from 50 to 100 units to ensure adequate cleavage of the α -TTP-GST fusion protein (Table 6). The combined use of the

BioShop resin, increased pellet dilution, additional 1X SPR wash, and increased thrombin use all demonstrated greater purity during consecutive α -TTP purification trials.

Table 6. α -TTP Purification Optimization Strategies.

Several purification optimization strategies were trialed, including trying glutathione-agarose affinity resins from three different suppliers – Cytiva, BioShop, and Sigma Aldrich. The two former resins yielded equal purity results, while the resin from Sigma Aldrich produced more contaminated protein elution fractions. A chaperone protein wash was also tried to reduce non-specific protein retention, but did not reduce contamination. The final three modifications all improved α -TTP purification.

Optimization Method	Result
Different GST-agarose affinity resins	
Cytiva	=
BioShop	=
Sigma Aldrich	X
Chaperone wash	X
Additional 1XSPR washes before thrombin application	✓
Increased thrombin aliquot addition	✓
Increased pellet dilution with Buffer A	✓

An SDS-PAGE gel (Figure 20) showed that the successful optimization methods from Table 6 increased protein purification. The absence of any protein flow through in lane three, which contained a sample from the second 1X SPR wash, demonstrated that no unbound proteins were left on the column. The α -TTP elution fractions E1-E5 from lanes four to eight only showed prominent protein bands at approximately 32 kDa and no high molecular weight contaminants. Furthermore, the two GST elution fractions, GST1 and GST3 contained high amounts of free GST at 27 kDa, with only minimal amounts of free α -TTP. No fusion protein was present in any of the purification samples evident based on a band of about 58 kDa present in the supernatant that was absent in all other lanes of the gel (Figure 20).

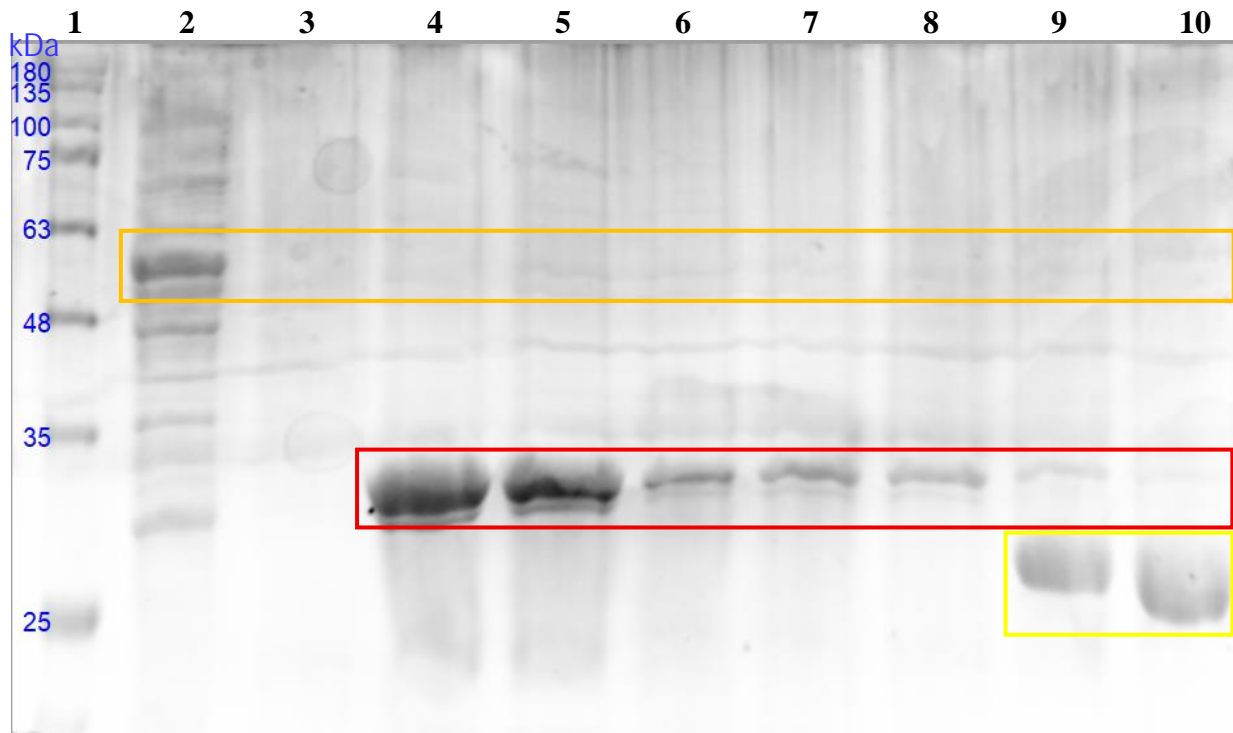


Figure 20. α -TTP Purification via GST Affinity Chromatography Post-Optimization.

Less contaminants were visible in all α -TTP elution fractions after implementing all the successful optimization methods from Table 6 *Error! Reference source not found.* that resulted in purer α -TTP elution fractions. In addition, only low amounts of α -TTP were present and no fusion protein remained uncleaved in the GST elution fractions. Lane 1: BLUeye prestained protein ladder, lane 2: cell lysate supernatant, lane 3: 1X SPR wash, lane 4: E1, lane 5: E2, lane 6: E3, lane 7: E4, lane 8: E5, lane 9: GST1, lane 10: GST3. Red box = wtTTP, orange box = fusion protein, yellow box = GST protein. Figure imaged and annotated via Image Lab, version 6.1.

A new protein purification protocol was developed for α -TTP based on the successful purities shown in Figure 20 that included the effective strategies outlined in Table 6. All subsequent α -TTP purifications for wtTTP were performed utilizing the updated protocol, and it should also be implemented when purifying the mutant proteins in the future.

3.2 SPR Concentration Binding Curve Using Wildtype α -TTP

The first experimental stage using the surface plasmon resonance (SPR) apparatus (henceforth referred to as ‘the SPR’) was to generate a concentration binding curve to determine if the α -TTP concentration used by previous members of the Atkinson group was appropriate to

investigate the binding interactions between α -TTP and its ligands. Binding assays can be used to determine important kinetic parameters when analyzing the protein-ligand binding reaction as it approaches equilibrium, such as the adsorption and desorption rate constants (k_{on} and k_{off} , respectively) and the dissociation constant (K_d) (De Jong et al., 2005). However, during such experiments, the concentration of ligand or protein is usually fixed and must not exceed that of K_d or else the equilibrium will be affected by titration and may lead to false estimation of binding affinities between ligand and protein (Du, 2024; Pollard, 2010).

Most binding assays assess binding interactions between receptor proteins and small molecule ligands or protein-protein interactions – with typical experimental setups revolving around non-dynamic conditions where fixed amounts of both the receptor protein and the binding partner are introduced at the start of an experiment. The results produced usually only convey the final binding interactions observed at the end of the experiment. The basis of the SPR technique differs from such binding assays given its principal use is via immobilization of a receptor to the detection surface and then continuously flowing an analyte over it. This method allows for the detection of binding interactions in real-time, however, the dynamic nature of SPR also increases the complexity of data analysis and interpretation.

The binding assay configuration on the SPR in this project also varies greatly from most other experiments using the SPR. Typically, signal responses are a result of protein flowing over the sensor surface that has been immobilized with another target protein. However, the use of the SPR in this project was inverted by incorporating the ligand(s) of α -TTP in lipid vesicles that were immobilized on the sensor chip of the SPR and then injecting α -TTP to flow over the immobilized lipid layer containing the ligand. Earliest experiments of the Atkinson group were performed using 1 μ M α -TTP but have since been conducted at half that concentration after having observed that

adequate signal responses could also be reached at 0.5 μM concentrations (Mehta, 2023). However, despite witnessing sufficient signal responses using 0.5 μM α -TTP, a concentration binding curve has not yet been established before this work. Therefore, the main objective of generating a concentration binding curve at the beginning of this project was to verify whether continuing SPR experiments using 0.5 μM protein was indeed suitable for data analysis or if it exceeded the dissociation constant concentration.

The concentration binding curve depicted in Figure 21 was generated by injecting wtTTP of increasing concentrations from 0.25 to 6 μM onto 1 mM plasma membrane (PM) lipid vesicles that were approximately 100 nm in diameter (Appendix, Figure 31). Each concentration injection was completed in three replicates, after which the average of the three B_{max} values at each concentration were plotted against wtTTP concentration. The concentration binding curve produced a K_d value of $1.11 \pm 0.08 \mu\text{M}$, thus the previous use of 0.5 μM α -TTP was below the dissociation constant and could therefore be used in subsequent SPR experiments.

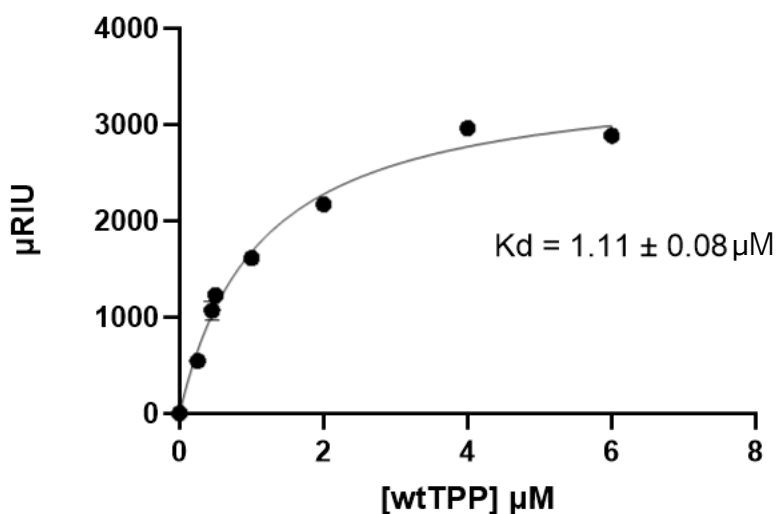


Figure 21. wtTTP Concentration Binding Curve.

wtTTP concentrations ranged between 0.25 to 6 μM and were injected onto 1 mM PM lipid vesicles. Three replicate SPR injections were conducted for each wtTTP concentration sample to generate the binding curve above with a B_{max} of 3539 μRIU and a K_d of 1.11 μM . All

subsequent α -TTP-lipid SPR injections were carried out using 0.5 μ M protein. Image created using GraphPad Prism, version 10.1.2.

3.3 SPR Injections Using Wildtype α -TTP, α -Tocopherol, and Lipid Vesicles with PIPs

3.3.1 Wildtype α -TTP Injections

According to the initial project goals, the first stage of experiments was to determine if wtTTP with or without α -tocopherol produces different binding responses when injected onto the SPR lipid layer consisting of either plain PM lipid vesicles or ones containing various phosphatidylinositol phosphates (PIPs). These PIPs included phosphatidylinositol-4,5-bisphosphate (PI(4,5)P₂), as well as phosphatidylinositol-3,4-bisphosphate (PI(3,4)P₂), and phosphatidylinositol-3-phosphate (PI(3)P) to determine the binding specificity of α -TTP. While previous experiments have been conducted using 4% PI(4,5)P₂ components in PM lipid vesicles, current experiments included 2%, 4%, and 6% PI(4,5)P₂ to determine if a concentration-dependent response could be observed during SPR injections. It was hypothesized that as the amount of PI(4,5)P₂ in lipid vesicles increased, the rate of wtTTP binding would also increase since α -TTP has been shown to preferentially bind to it (Atkinson et al., 2019). Similarly, it was predicted that the binding of wtTTP to 4% PI(3,4)P₂ would show comparable signal response to that of 4% PI(4,5)P₂ because it has also been shown to bind to α -TTP (Arai & Kono, 2021). On the contrary, it was hypothesized that wtTTP injected onto lipid vesicles containing PI(3)P would produce binding responses below that of the PI(4,5)P₂ and PI(3,4)P₂ based on the lack of a second phosphate group on the headgroup.

The order of the six lipid vesicle condition injections was randomly conducted to mitigate experimental bias. Three consecutive replicate injections were conducted for each condition at a time and after all six experiments were completed, the data was analyzed as outlined in 2.6.11. The values of each replicate were averaged at every time point to generate binding curves where the

association of protein to the lipid vesicles were plotted (Appendix Figure 33). Curves were then normalized based on the average B_{\max} value of wtTTP on PM (516.2 μ RIU) to generate Figure 22. All PIP injections except 4% PI(3,4)P₂ produced binding curves that plateaued above PM, with 4% PI(4,5)P₂ and 4% PI(3)P having the highest normalized plateaus at 1.195 and 1.183 μ RIU, respectively (Appendix, Table 8). Statistical analysis of the non-normalized B_{\max} values depicted in Figure 23 (right) showed that the plateaus of 4% PI(4,5)P₂, 4% PI(3,4)P₂, and 4% PI(3)P were significantly different in comparison to that of PM. In addition, the comparison of B_{\max} values between each PIP also showed statistical differences, 4% PI(3,4)P₂ having the greatest difference from all other conditions. Therefore, the final phase of wtTTP binding on the SPR was altered by the addition of different amounts of PI(4,5)P₂ and different types of PIPs.

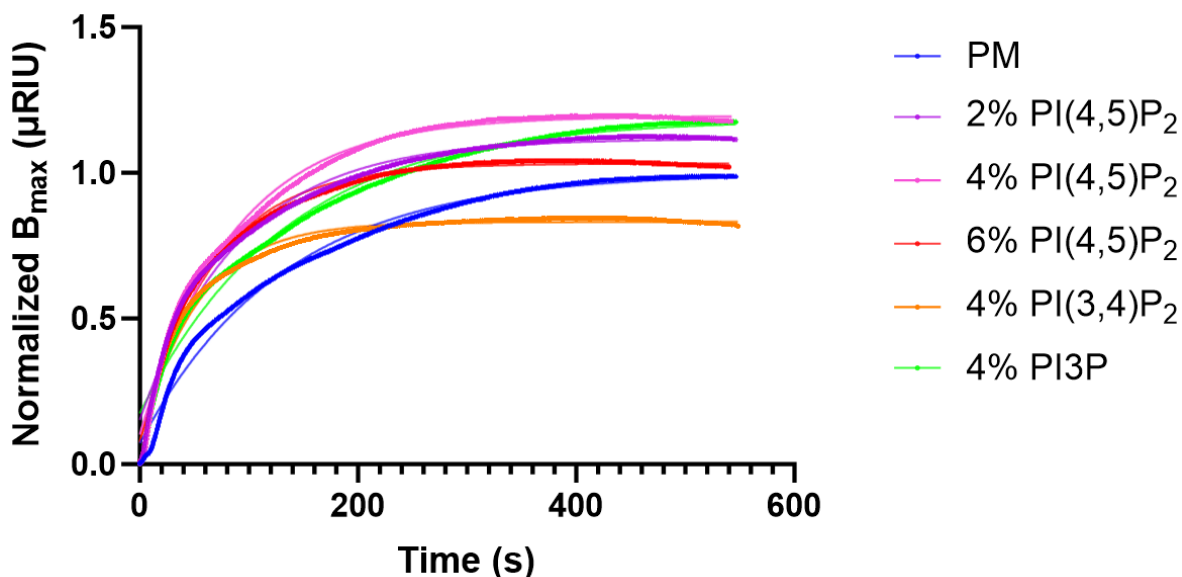


Figure 22. Injections of wtTTP onto PM with PIPs.

Three replicate injections were conducted for each experiment during which 0.5 μ M wtTTP was injected onto lipid layers consisting of plasma membrane (PM) vesicles alone or PM vesicles containing various types of PIPs with concentrations ranging between 2% to 6%. The triplicate values for each condition were averaged then normalized to wtTTP on PM to generate the binding curves. Image created using GraphPad Prism, version 10.1.2.

Based on previous protein-ligand binding assays, it was estimated that the binding interactions depicted at the beginning of the curves, approximately 0 to 200 seconds, could roughly indicate the rate of wtTTP binding to each PIP-containing membrane – which was interpreted as binding attraction. When compared to the PM curve, the curves of all PIPs had a steeper initial binding profile (k_{on}), except for 4% PI(3)P which behaved more similarly to the curve of PM (Figure 22). Therefore, despite 4% PI(3)P having plateaued above the PM curve, results showed wtTTP seemingly had greater attraction for PI(4,5)P₂ and PI(3,4)P₂ than PI(3)P. Once the rate constants (k_{on} , s⁻¹) for each condition were determined and statistically analyzed, the results corroborated these preliminary observations. The average rate constants for wtTTP binding to membranes containing 2%, 4%, 6% PI(4,5)P₂ and 4% PI(3,4)P₂ were all greater than the average rate constant of PM, while the average rate constant of 4% PI(3)P remained almost the same as that of PM (Figure 23). Therefore, wtTTP was attracted more to PIP₂ compared to the monophosphate used, which aligned with the observations reported by Kono et al., 2013 when using PI(3,4)P₂ to pull-down wtTTP. Statistical analysis of the rate constants showed that only two conditions were significantly different from PM – 6% PI(4,5)P₂ and 4% PI(3,4)P₂ – with the latter having the greatest statistical difference and highest average k_{on} . These results suggested that wtTTP had higher attraction for PI(3,4)P₂ than PI(4,5)P₂. However, it should be noted that the three rate constant values of PI(3,4)P₂ experienced more variation from the average than the replicates of other conditions, which could have contributed to this discrepancy. Nonetheless, there appeared to be a concentration-dependent increase in rate constants for the three PI(4,5)P₂ conditions since the average k_{on} increased from the 2% to 4% to 6% injections, thus, showing that the binding attractions of wtTTP increased as the amount of PI(4,5)P₂ increased.

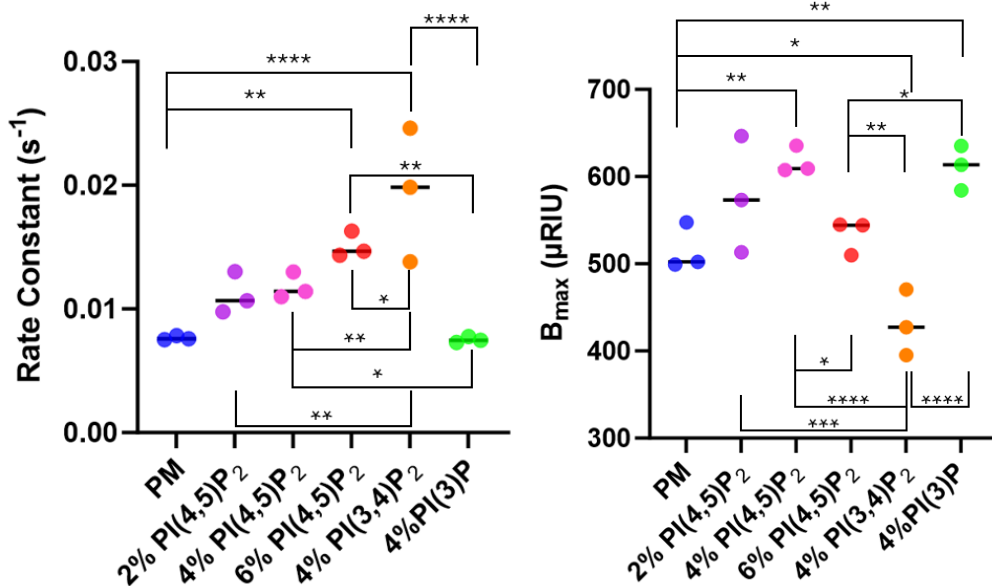


Figure 23. One-Way ANOVA Test of Rate Constants and B_{\max} Values of wtTTP Injections.

The three replicate values of rate constants (k_{on}) and B_{\max} for all wtTTP injections on lipid vesicle conditions containing PIPs were plotted and statistically compared to that of plain plasma membrane. The rate constant plot (left) showed that 4% PI(3,4)P₂ had the greatest deviation between triplicates compared to the other injections. It was also one of the experiments with significant variation compared to PM, in addition to 6% PI(4,5)P₂ that also showed significant difference of rate constants. The B_{\max} plot (right) showed that 4% PI(3,4)P₂ had less deviation compared to the rate constants, instead 2% PI(4,5)P₂ had the greatest deviation from the mean value. Statistical analysis revealed that the B_{\max} values of PM were significantly different from those of 4% PI(4,5)P₂, 4% PI(3,4)P₂, and 4% PI(3)P. Image created using GraphPad Prism, version 10.1.2.

* = $p < 0.05$, ** = $p < 0.01$, *** = $p < 0.001$, **** = $p < 0.0001$

PM (blue), 2% PI(4,5)P₂ (purple), 4% PI(4,5)P₂ (pink), 6% PI(4,5)P₂ (red), 4% PI(3,4)P₂ (orange), 4% PI(3)P (green)

3.3.2 Wildtype α -TTP Preincubated with α -Tocopherol Injections

After completing the injections using wtTTP, the same six lipid condition experiments were conducted using wtTTP preincubated with its primary ligand – α -tocopherol. The night prior to each injection, 0.5 μ M wtTTP was preincubated with 50 μ M α -tocopherol at 4°C. Samples were then allowed to come to room temperature before being injected onto lipid vesicles on the SPR. Similar binding results to that of non-incubated samples were expected for the preincubation experiments, as it was hypothesized that the rate of wtTTP binding for PI(3,4)P₂ would be less

than that of PI(4,5)P₂, and the ligand bound protein would bind poorly or not at all to vesicles only containing PI(3)P. In addition, the binding attraction of wtTTP to PI(4,5)P₂ would increase as the ligand concentration in the lipid vesicles was increased. According to the proposed mechanism of α -tocopherol transport within hepatocytes (Figure 10), once α -TTP binds α -tocopherol from the endosomal membrane, the presence of much higher concentrations of PI(4,5)P₂ within the plasma membrane attracts the ligand bound protein towards the cell membrane. Based on this hypothesis, the *in vitro* experiments conducted on the SPR where wtTTP was bound to α -tocopherol prior to injection onto the lipid layer should show faster binding rates compared to wtTTP without bound α -tocopherol. However, the B_{max} plateau values reached were thought to potentially decrease as less wtTTP would remain bound to the lipid layer once it had deposited α -tocopherol in the membrane and potentially exchanged it for a PIP ligand.

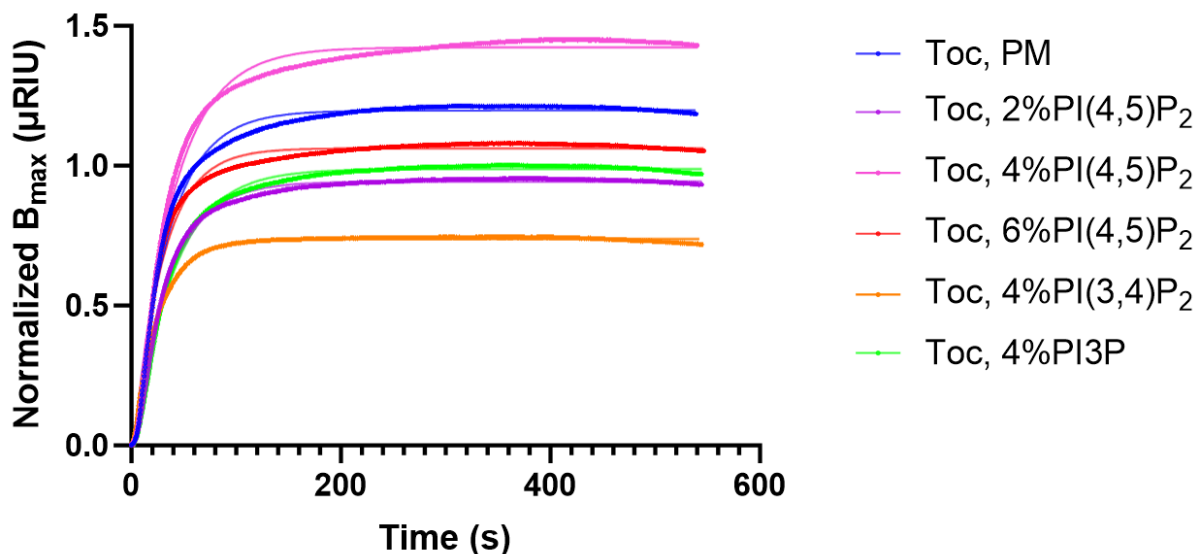


Figure 24. Injections of wtTTP Preincubated with α -Tocopherol onto PM with PIPs.

Three replicate injections were conducted for each experiment during which 0.5 μ M wtTTP preincubated with 50 μ M α -tocopherol overnight was injected onto lipid layers consisting of PM vesicles alone or PM vesicles containing various types of PIPs with concentrations ranging between 2% to 6%. The triplicate values for each condition were averaged then normalized to wtTTP on PM (blue, Figure 22) to generate the binding curves. Image created using GraphPad Prism, version 10.1.2.

Once again, the order of conditions injected was randomized, and three replicate injections were conducted for each experiment – the values of which were then averaged and normalized using the average B_{\max} value of wtTTP on PM (Appendix Figure 36 and Table 11). The B_{\max} value of wtTTP- α -tocopherol on plain PM vesicles was slightly higher than its non-preincubated counterpart, but similar to the first set of conditions in Figure 22, and the 4% PI(4,5)P₂ curve reached the highest plateau during these experiments. With the exception of this curve, all other curves plateaued below the wtTTP- α -tocopherol on PM curve, and 4% PI(3,4)P₂ reached the lowest plateau of approximately 75% of wtTTP on PM (Figure 24). Furthermore, the B_{\max} values of all PIP conditions were statistically different from that of wtTTP- α -tocopherol on PM, with all conditions being lower except for that of 4% PI(4,5)P₂ (Figure 25 right). Similarly, there was statistical difference between each concentration of PI(4,5)P₂, as well as between each of the PIPs compared to the B_{\max} of 4% PI(3,4)P₂. These results suggest that increasing the concentration of PI(4,5)P₂ and the use of different types of PIPs alter the final stage of protein-membrane interactions. Whilst the end-stage of binding (B_{\max}) did not change drastically between preincubated versus non-incubated samples, the values of k_{on} showed greater differences between these conditions. The rate constant for wtTTP- α -tocopherol on PM was more than three times that of unbound wtTTP on PM, which was a trend observed for all other conditions – the rate constants were all at least double that of their non-incubated counterparts (Figure 25 left). Compared to the rate constants observed in Figure 23, the rate constant of PI(3)P for preincubated wtTTP was statistically lower than that of wtTTP- α -tocopherol on PM – giving further credence to the fact that α -TTP has greater binding attraction for lipids with dual phosphate groups. However, when analyzing the data set of preincubations, there were some inconsistencies. Firstly, there appeared to be no concentration-dependent binding rate response based on the increased concentration of

PI(4,5)P₂. The average rate constant of 2% PI(4,5)P₂ was not significantly different from that of PM but was still slightly lower, while the rate constant of 4% PI(4,5)P₂ was significantly lower than both that of PM and 2% PI(4,5)P₂. However, k_{on} of 6% PI(4,5)P₂ was higher than the lower concentrations of PI(4,5)P₂ (Figure 25 left). Nonetheless, the rate constant of 4% PI(3,4)P₂ was the highest of these conditions, which was similar to the trend observed for plain wtTTP binding to 4% PI(3,4)P₂ – suggesting that wtTTP preincubated with α -tocopherol has greater binding attraction for it than PI(4,5)P₂.

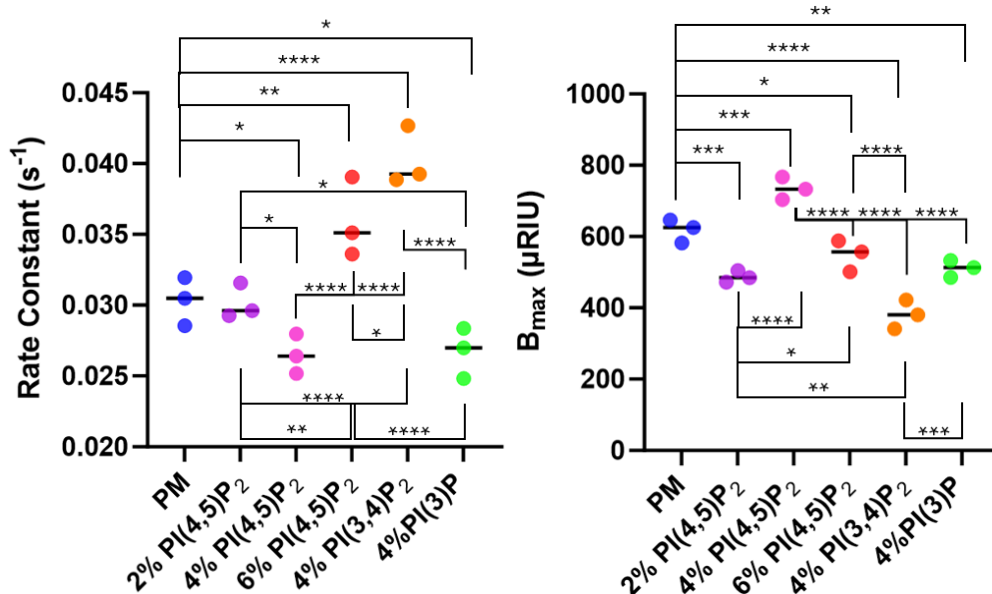


Figure 25. One-Way ANOVA Test of Rate Constants and B_{max} Values of wtTTP Preincubation Injections.

The three replicate values of rate constants (k_{on}) and B_{max} for all wtTTP preincubated with α -tocopherol injections on lipid vesicle conditions containing PIPs were plotted and statistically compared to that of plain plasma membrane. The rate constant plot (left) showed that there was significant difference between PM and all other PIP conditions, except for 2% PI(4,5)P₂, with the greatest variation fitting 4% PI(3,4)P₂. Similarly, the B_{max} plot (right) showed that all PIP conditions were statistically different from PM, with the greatest difference being between PM and 4% PI(3,4)P₂. However, it also showed significant differences when comparing PM to 2% PI(4,5)P₂ and 4% PI(4,5)P₂, respectively. Image created using GraphPad Prism, version 10.1.2.

* p = < 0.05, ** p = < 0.01, *** p = < 0.001, **** p = < 0.0001

PM (blue), 2% PI(4,5)P₂ (purple), 4% PI(4,5)P₂ (pink), 6% PI(4,5)P₂ (red), 4% PI(3,4)P₂ (orange), 4% PI(3)P (green)

Therefore, the absence of a concentration-dependent response of PI(4,5)P₂ and the rate constant of 4% PI(3,4)P₂ having been higher than that of 4% and 6% PI(4,5)P₂, suggested that the secondary ligand of α -TTP might be PI(3,4)P₂ instead of PI(4,5)P₂. While this result is a possibility because both PIPs are predominantly present on the inner leaflet of plasma membranes in eukaryotic cells, it is estimated that PI(4,5)P₂ is naturally present at approximately 40 times greater amounts than PI(3,4)P₂ (Van Meer et al., 2008; Ray et al., 2024). Therefore, while wtTTP showed greater preference for PI(3,4)P₂ *in vitro*, the *in vivo* secondary ligand of α -TTP in hepatocytes likely remains PI(4,5)P₂ based on its overabundance in cell membranes compared to PI(3,4)P₂. However, upon reattempting some of the wtTTP injections to test their reproducibility, abnormal binding patterns were noted on the SPR.

3.4 SPR Troubleshooting

When attempts were made to reproduce the result for the standard wtTTP injected on PM vesicles from Figure 22 prior to conducting injections using the K217A mutant, the injections on the SPR showed atypical characteristics for both the lipid vesicle layer and the protein layer. Typical injections of lipid vesicles produced a binding curve depicted in Figure 26A, with a rapid increase in signal response in the first 100 seconds and reaching a plateau of around 10,000 μ RIU before 200 seconds. When 0.5 μ M wtTTP was injected on such a lipid layer, the protein binding curve produced reached a plateau of approximately 500 μ RIU at around 400 seconds and had a typical binding curve shape (Figure 26B). However, when reattempting the wtTTP on PM standard to test result reproducibility, both the lipid layer and protein binding curves changed drastically. The 1 mM PM lipid layer produced a curve that had a gradual rise, it did not plateau until about 600 seconds and reached a maximum that was less than 1,500 μ RIU – almost a 90% drop in signal intensity (Figure 26C). In addition, when 0.5 μ M wtTTP was injected onto the abnormal lipid

layer, the protein layer depicted in Figure 26D also had greatly reduced signal intensity – having dropped to around 80 μ RIU, a reduction of approximately 85% compared to the regular protein curve. Furthermore, this protein curve was not a proper binding curve, because it did not actually reach a maximum at the end of the injection time but continued to increase and produced jagged signals responses.

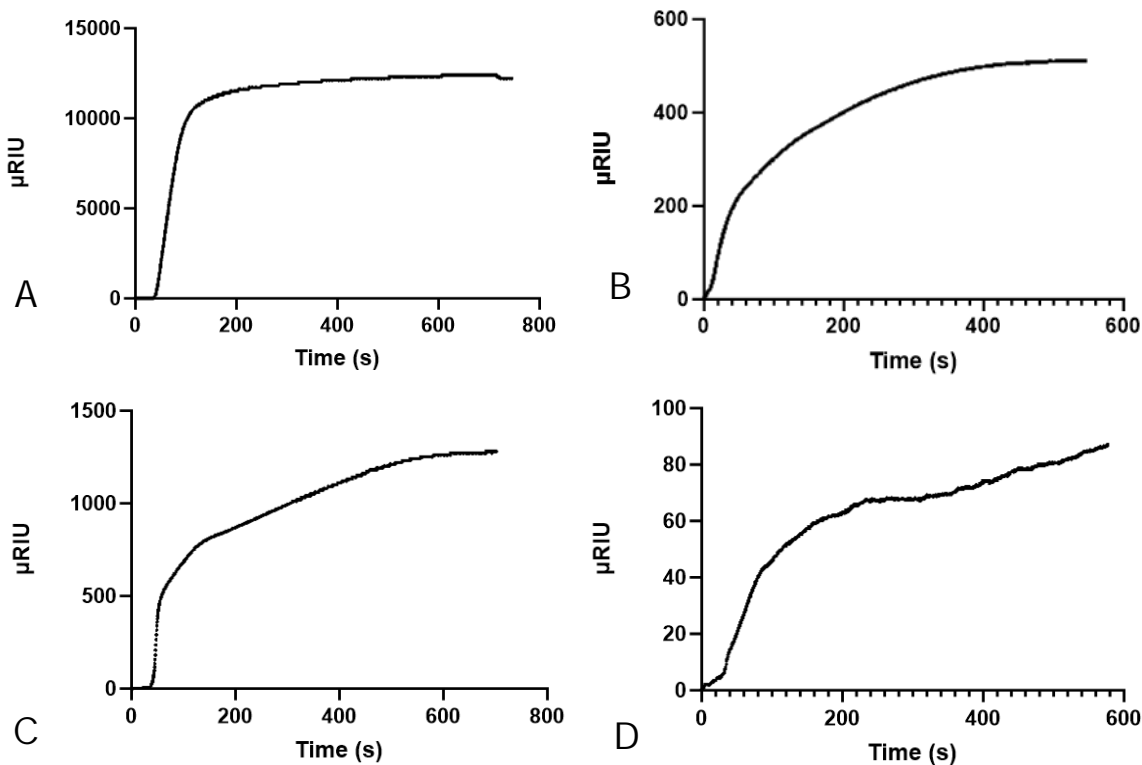


Figure 26. Lipid and Protein Injection Issues.

A) Regular lipid binding curve produced upon injection of 1 mM PM vesicles onto the derivatized sensor slide. B) Regular protein binding curve produced upon injection of 0.5 μ M wtTTP onto the 1 mM PM lipid layer depicted in A. C) Abnormal lipid binding curve produced upon injection of 1 mM PM vesicles onto the derivatized sensor slide. D) Abnormal protein binding curve produced upon injection of 0.5 μ M wtTTP onto the 1 mM PM lipid layer depicted in C. Image created using GraphPad Prism, version 10.1.2.

The injections were performed numerous times, with several different lipid membranes, including PM, 2% PI(4,5)P₂, and 4% PI(3)P, however, the results remained irregular. Therefore, some troubleshooting methods were devised to elucidate what experimental component could be the cause of the anomalies. Initial troubleshooting efforts revolved around the SPR, namely its

buffer systems (Table 7). All the regeneration buffers – 50 mM NaOH, 0.5% SDS, 50 mM glycine (pH 9.5), and 80% ethanol – as well as the 1X SPR running buffer were all freshly prepared, filtered, and autoclaved as described in 2.5.9. However, no change was observed when using the newly prepared running buffer and regeneration buffers during 1 mM PM lipid vesicle injections. Next, a new preparation method was developed to make up 10X SPR running buffer to reduce the ionic strength and pH variation that could potentially cause the change in signal response. Ionic strength has been known to reduce protein binding activity, and buffer pH has been shown to play a major role in maintaining the proper hydrogel structure of SPR sensor slides (Stoll & Blanchard, 2009; Jeenanong & Kawaguchi, 2008). Therefore, instead of combining dry sodium chloride, monobasic (KH_2PO_4) and dibasic (K_2HPO_4) potassium phosphates at once, stock solutions were prepared separately for each component, which were then combined to create a solution of 10X SPR running buffer. However, this new buffer preparation method also did not yield any difference in lipid or protein binding. The last buffer troubleshooting attempt was to trial other buffer systems that have been reported when using the SPR. Based on literature, phosphate buffers are most commonly used for SPR binding assays, however, it has been shown that Tris and *N*-2-hydroxyethylpiperazine-*N*-2-ethanesulfonic acid (HEPES) based buffers are also commonly used (Frostell et al., 2013; Acevedo & Pauron, 2014). Therefore, two new running buffers were prepared – 10 mM HEPES and 10 mM Tris-HCl – with both containing 137 mM NaCl. When the HEPES-based running buffer was used for injections, no difference was observed compared to the phosphate buffer system normally used. On the contrary, when using Tris buffer for protein injection tests, it was noted that signal responses were greater than normal, and upon injection of Tris buffer alone, a signal was produced, which suggested that this new buffer system was not better suited than the regular phosphate buffer. Thus, since neither new buffer system proved

useful, consecutive experiments were carried out with the original phosphate buffer system to minimize signal variations.

Due to the lack of success with various buffer alterations, efforts were then targeted to the only other variable component of the SPR – the sensor slides. Several new gold chips from stored orders were derivatized and tried with fresh lipids and wtTTP, but the protein binding issues persisted regardless of how many new chips were trialed. The manufacturer of the SPR was then contacted to determine if any mechanistic component of the apparatus could potentially be malfunctioning. However, all machine parameters such as current, light source viability, calibrations, etc. were in proper order. In addition, the standard injection of 1 M NaCl upon the instruction of the manufacturer gave the expected response signal of around 9,000 μ RIU. Therefore, it appeared that all the components of the SPR were functional, and some other experimental variable was the cause of the binding issues.

Table 7. SPR Troubleshooting Methods.

Several troubleshooting techniques were implemented to resolve the lipid and protein binding issues depicted in Figure 26. Fresh regeneration and running buffers were prepared and tried without showing any change to lipid injections. A new preparation method was developed to make up 10X SPR running buffer. Other running buffer systems were also tried but either no difference was observed, or the buffer system produced a binding signal when injected on the chip. Several new sensor slides were derivatized and tried without change to lipid or protein binding.

Troubleshooting Method	Result
Fresh regeneration buffers	X
Fresh 1X SPR running buffer	X
New 10X SPR running buffer preparation method	X
Different running buffers	
HEPES	X
Tris-HCl	X
New sensor chip derivatizations	X

The next point of troubleshooting was α -TTP – to determine its proper functionality via binding assays. Two types of binding assays were performed using wtTTP and a fluorescently labelled α -tocopherol derivative, NBD- α -tocopherol. Nitrobenzoxadiazole (NBD) is a hydrophobic fluorophore group that has been widely used in lipid-based fluorescence studies, both *in vitro* and *in vivo*. It has an approximate excitation and emission maxima of 466 nm and 530 nm, respectively, and is quenched to near non-fluorescence in aqueous environments (Chattopadhyay, 1990). Therefore, binding assays have been designed by previous members of the Atkinson group in which NBD- α -tocopherol is gradually titrated into a solution of aqueous buffer containing a fixed concentration of α -TTP. Once NBD- α -tocopherol binds to α -TTP, it is no longer quenched by the aqueous buffer system and becomes fluorescently active as it occupies the hydrophobic binding site of α -TTP. Since α -TTP only has one α -tocopherol binding site, the fluorescence signal is directly proportional to the concentration of NBD- α -tocopherol bound to α -TTP. Such fluorescence binding assays were conducted to investigate the functionality of wtTTP and determine if it could be the cause of the problems observed during protein binding on the SPR.

3.5 Wildtype α -TTP Binding Assays

Fluorescence binding assays were carried out using two methods – a microplate reader and a fluorometer – the experiments for each involved using 0.4 μ M wtTTP and NBD- α -tocopherol concentrations ranging between 0 to 800 nM. For specifics about experimental setup on the plate reader and fluorometer refer to 2.6.6.2 and 2.6.6.3, respectively. Initial binding assays on both instruments produced uncharacteristic binding curves. The ones obtained from the microplate reader did not produce a curve at all but yielded increasing linear trends between fluorescence signal and NBD- α -tocopherol concentrations, with the protein-containing sample values only

producing slightly higher fluorescence signals compared to the blank samples without protein (Figure 27A). Even when the concentration maximum of NBD- α -tocopherol was increased above 1 μ M, the microplate binding assays remained linear and never plateaued, which indicated that wtTTP was not saturated even at 2.5 times excess NBD- α -tocopherol amounts. Equally unusual results were produced when performing binding assays on the fluorometer – despite generating a more proper binding curve that was non-linear, a maximum was reached at approximately 100 nM NBD- α -tocopherol that only reached 5,000 relative fluorescence units (RFU). Previous fluorometer binding assays have produced binding curves with proper shape and maxima exceeding 100,000 RFU. In addition, the binding curve containing wtTTP was only approximately 2,000 RFU greater than the values produced by the blank samples, which further indicated that something was awry with the binding assays (Figure 27B).

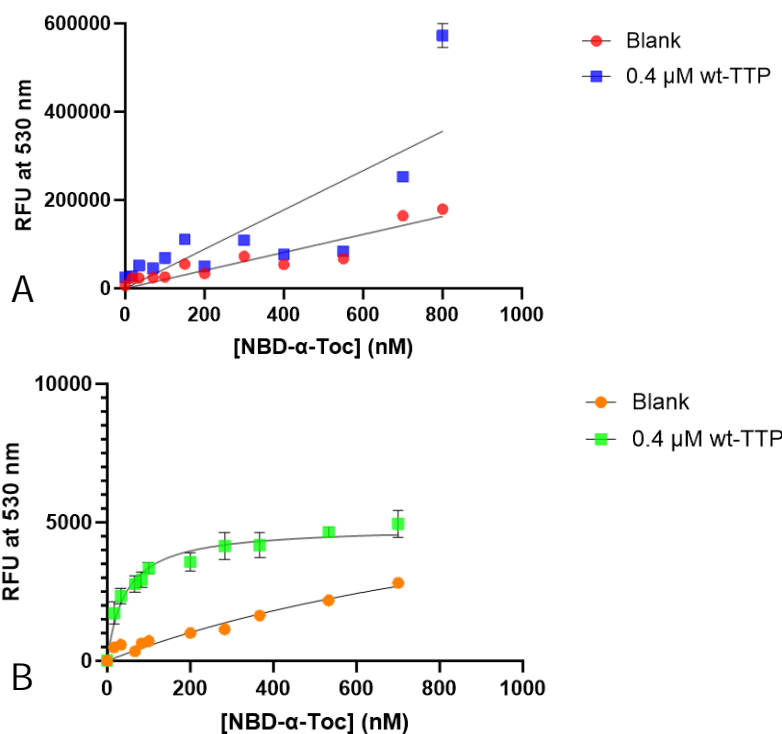


Figure 27. Binding Assays Performed Using wtTTP Purified with Triton X-100.

A) Microplate reader binding assay. No saturation was observed upon increased addition of NBD- α -tocopherol. Protein-containing samples produced similar results compared to blank

samples. B) Fluorometer binding assay. Binding curve produced was only slightly above blank samples without protein. Figure created via GraphPad Prism, version 10.1.2.

With only three variable components of the experiments, both on the microplate and the fluorometer – wtTTP, NBD- α -tocopherol, and 1X TKE buffer – troubleshooting systematically progressed through all three variables. First, the 1X TKE buffer was refiltered to remove any potential particulates that could inhibit fluorescence detection during the binding assays. When refiltration proved ineffective, new 1X TKE buffer was freshly prepared, but binding assay signals remained unaffected. Troubleshooting then targeted wtTTP, which included performing another Bradford assay and SDS-PAGE on the elution fraction samples to verify that α -TTP was still present in the fractions at the concentrations measured immediately after purification. Once that had been confirmed, binding assays were repeated with the new 1X TKE buffer, but no change was observed. A new pellet of wtTTP was then purified in an attempt to perform the binding assays with fresh protein, but that also proved ineffective. Therefore, the last component of the binding assays, NBD- α -tocopherol, was analyzed. The working stock solutions used to perform binding assays were re-quantified and their concentrations had not changed from initial preparation. Next, the original stock solution of NBD- α -tocopherol was analyzed via mass spectroscopy (MS) to determine if the ligand had potentially decomposed, despite remaining a bright yellow solution, or had been contaminated. The MS data however showed the highest peak of 509.2 g/mol that corresponded to the expected molecular weight of NBD- α -tocopherol at 510.64 g/mol (Appendix Figure 38**Error! Reference source not found.**). Therefore, the original NBD- α -tocopherol stock was viable and mainly contained a single ion associated with the expected compound. In addition, the solution was analyzed multiple times via thin layer chromatography, with only a single compound shown in the sample. None of the troubleshooting results showed any evidence that

either of the three components of the binding assays were the cause of the issue and without any clear indication as to what else could be the underlying problem, further research was conducted in the literature.

After noting the use of Triton X-100 in the elucidation of the structure of α -TTP in early X-ray crystallography experiments, it was evident that α -TTP could bind Triton X-100 in the binding site of α -tocopherol (Meier et al., 2003). Therefore, it was hypothesized that, during the purification of wtTTP, the Triton X-100 added to the pellet after sonication, as well as the Triton X-100 component in Buffer B used to perform washes on the column once the fusion protein was already bound could occupy the binding site of α -TTP and thus interfere with the binding of NBD- α -tocopherol during binding assays. Another new wtTTP expression pellet was purified via the optimized purification method described in section 3.1 but with the modification that all Triton X-100 was removed from the protocol. No difference was observed during protein quantification or on SDS-PAGE, which indicated that excluding Triton X-100 during purification did not compromise the purity of the samples or the amount of wtTTP recovered. On the contrary, the microplate reader and fluorometer binding assays both improved when utilizing wtTTP from the no Triton X-100 purification. The binding assay on the microplate reader generated a proper binding curve that approached a plateau around 500,000 RFU instead of a linear correlation (Figure 28A). Similarly, upon using wtTTP without Triton X-100 on the fluorometer, the fluorescence signal responses greatly increased – having approached a plateau slightly above 30,000 RFU and producing a typical binding curve shape, while the blank control samples remained at much lower signal values below 2,000 RFU (Figure 28B). Based on the binding assay results, it was evident that Triton X-100 contaminated the protein samples and prevented protein-ligand binding. Therefore, future experiments involving α -TTP should avoid Triton X-100 completely. Since the

absence of Triton X-100 during protein purification did not affect wtTTP retention and recovery, the removal of Triton X-100 was included in the optimized purification protocol. It should be noted that the binding assays without Triton X-100 were only conducted once due to time constraints, thus should be repeated to verify results and reproducibility.

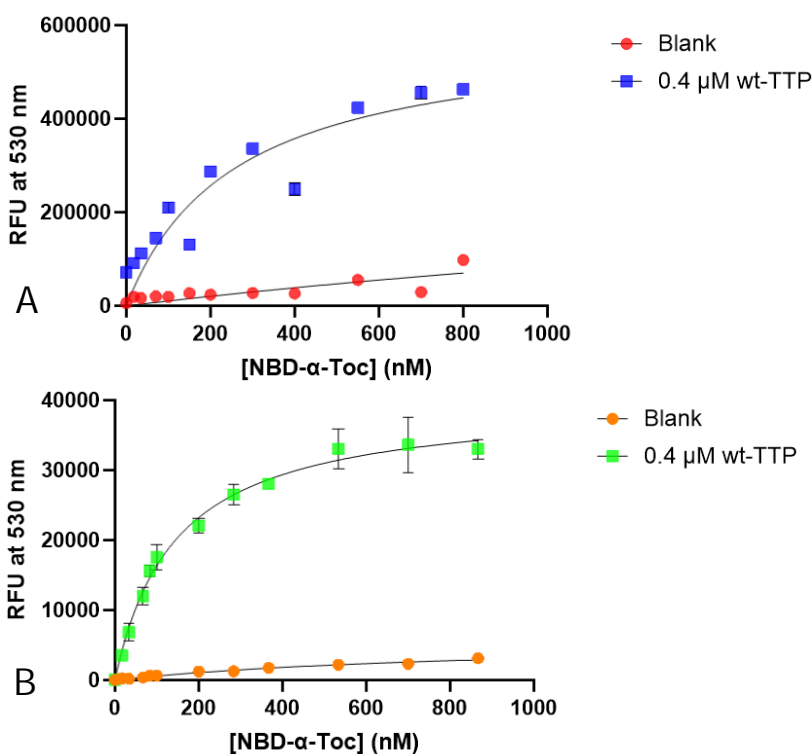


Figure 28. Binding Assays Performed Using wtTTP Purified without Triton X-100.

A) Microplate reader binding assay. Proper protein-ligand binding curve was produced with a plateau around 400,000 RFU, while the blank sample remained linear. B) Fluorometer binding assay. Binding curve plateaued above 30,000 RFU while the blank sample remained linear. Figure created via GraphPad Prism, version 10.1.2.

3.6 Remaining SPR Issues

Once the functionality of wtTTP without Triton X-100 was verified via binding assays it was hypothesized that the lack of protein binding observed during the latest SPR injections (Figure 26D) could have also been a result of wtTTP already containing Triton X-100 within its binding site. The injection of wtTTP newly purified without Triton X-100 on 1 mM PM lipid vesicles was

needed to test this hypothesis. Even though the Triton X-100 contamination would not explain the issues also observed with the lipid layer binding, if a greater protein binding signal response was produced upon the injection of new wtTTP, it could further validate the need for Triton X-100 free purifications. When preparing fresh PM lipids, it was noted that majority of the lipid stocks required for its composition had been depleted, thus fresh lipids were obtained but from different suppliers. In addition, due to the amount of time passed from the last SPR use, a new sensor chip was derivatized prior to any new injections. Upon the injection of fresh 1 mM PM lipids prepared from the new lipid stocks onto the new sensor slide, the signal response produced was characteristic of a proper lipid layer (Figure 26A) both in shape and signal intensity which reached approximately 9,000 μ RIU. Whether this change was due to the lipids having been prepared with entirely new lipid stocks from different suppliers or the use of a new sensor chip remains unknown. The signal response remained consistent upon numerous lipid layer injections, thus the lipid layer issues seemed to have been resolved.

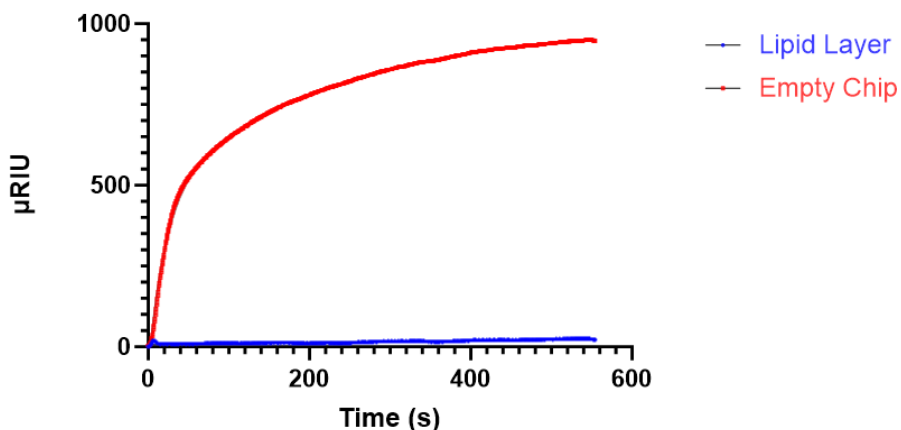


Figure 29. BSA Standard Injection.

Proper coverage by the lipid layer upon the injection of 1 mM PM vesicles onto the SPR sensor slide was tested to determine if it was the cause of deficient wtTTP binding. After the lipid injection, 0.5 μ M BSA protein was injected and low, almost negligible response signal was produced on the lipid layer (blue) compared to a much higher response approximating 1,000 μ RIU when introduced onto the bare chip exposing the derivatized dextran layer (red). Figure produced via GraphPad Prism, version 10.1.2.

However, upon the injection of the newly purified wtTTP without Triton X-100, the protein signal response produced remained unchanged from that depicted in Figure 26D, with signal intensities only reaching around 100 μ RIU maxima. It was hypothesized that the lipid coverage on the sensor chip could be insufficient for protein binding and some of the dextran layer remained exposed after lipid injection. Del Vecchio and Stahelin, (2016), have shown that it is possible to test the extent of lipid coverage by injecting a non-lipid binding protein such as bovine serum albumin (BSA) on the SPR. According to their research, under proper lipid surface coverage the signal produced upon BSA injection should be minimal and not exceed 100 μ RIU, but a signal response of 1,000 μ RIU or greater indicates minimal to no coverage (Del Vecchio & Stahelin, 2016). Based on the responses depicted in Figure 29, the lipid coverage was adequate on the sensor slide because the BSA signal response did not exceed 50 μ RIU on the lipid layer, in comparison to the signal response produced when BSA was injected onto the uncovered chip, which resulted in a binding curve plateauing around 1,000 μ RIU. Therefore, the low protein binding observed when wtTTP was injected onto the new PM lipid layer was not due to a lack of proper lipid coverage of the sensor slide. The cause of improper protein binding on the SPR currently remains unknown and requires further investigation.

4 Conclusion and Future Directions

Whilst much of this project deviated from the original project goals set out at the beginning and instead revolved around troubleshooting efforts, it was not without success. Optimization methods were uncovered to improve protein purity and recovery during affinity purification. It was found that the best resins for glutathione *S*-transferase affinity chromatography were from Cytiva and BioShop. Increasing protein pellet dilution at the start of purification, including an extra wash step with 1X SPR, and increasing the amount of thrombin used to cleave the fusion protein all improved wtTTP recovery. The concentration binding curve using wtTTP showed that the concentration of protein used during past and present experiments was below the dissociation constant, and thus did not exceed equilibrium conditions. The SPR injections conducted using wtTTP on plasma membrane vesicles containing various PIPs showed that wtTTP prefers to bind to phosphatidylinositol bisphosphates instead of the monophosphate tested. In addition, the k_{on} of each injection condition when using plain wtTTP showed a concentration-dependent attraction for PI(4,5)P₂, but had an even greater preference for PI(3,4)P₂. wtTTP preincubated with α -tocopherol had higher rate constants than non-incubated wtTTP for all conditions, however, the concentration-dependence of PI(4,5)P₂ was not present, which was attributed to numerous issues that arose during repeats of SPR experiments when testing reproducibility.

Anomalies of both lipid and protein injections occurred which led to the extensive analysis of experimental components – namely buffer systems, sensor slides, lipid stocks, and protein binding capabilities. After preparing fresh buffers, trying new buffer preparation techniques, other buffer system compositions, and the derivatization of several sensor slides all proved to be unsuccessful, the functionality of wtTTP was tested via fluorescence binding assays. Initial attempts using both a microplate reader and a fluorometer yielded insufficient binding results that

showed that even micromolar concentrations of NBD- α -tocopherol could not saturate wtTTP. Once the purity of the protein and ligand were verified, it was found that wtTTP was likely contaminated by Triton X-100 used during the purification process which prevented the binding of NBD- α -tocopherol to wtTTP during the binding assays. Protein purification was then performed in the absence of Triton X-100 which did not interfere with wtTTP recovery. The newly purified wtTTP without Triton X-100 produced proper binding curves on both the fluorometer and microplate reader with samples reaching saturation – confirming wtTTP was functioning suitably. However, when injected on a correctly formed lipid layer, this freshly purified wtTTP continued to present poor binding on the SPR.

Short-term future experiments should focus on reproducibility, after performing the fluorescence binding assays again, solving the protein binding issues that persisted on the SPR after all the troubleshooting attempts will become most pertinent. If those problems can be overcome, the wtTTP injections on plasma membrane vesicles containing different PIPs should be repeated for reproducibility. Especially because Triton X-100 has been shown to greatly reduce the binding of NBD- α -tocopherol to wtTTP during the binding assays, it could potentially also have similar effects on the binding of wtTTP to lipid vesicles on the SPR. Therefore, it may be necessary to replicate the wtTTP injections reported in this project.

Future directions in the long-term would revolve around the mutant forms of α -TTP, with initial experiments being carried out with K217A, a mutant that has been shown to have poor binding to PI(4,5)P₂ (Arai & Kono, 2021). However, future protein purifications, including for K217A should include the method optimizations outlined in 3.1 to improve protein yield. In addition to K217A, the expression of other mutant forms of α -TTP including D60K, S140A, P200A, P200G, and T215H should be confirmed, after which the optimized purification protocol

should be used to purify each mutant. While all the mutants listed would produce valuable information about the binding interactions of α -TTP, it must be emphasized that future investigations with S140A will likely yield the most definitive results to support the mechanistic model proposed for the transport of α -tocopherol in hepatocytes. Since S140A is predicted to have poor or no binding capacity of α -tocopherol, its use in binding assays on the SPR, microplate, and fluorometer would provide further insight into the binding characteristics of α -TTP and the exchange of α -tocopherol for PI(4,5)P₂. Therefore, the expression, purification, characterization, and SPR experimentation using S140A should take precedence over the other mutant forms of α -TTP in future studies.

5 References

- Arai, H., & Kono, N. (2021). α -Tocopherol transfer protein (α -TTP). *Free Radical Biology and Medicine*, *176*, 162-175.
- Atkinson, J., Thakur, V., & Manor, D. (2019). The tocopherol transfer protein: regulator of vitamin E status. *Vitamin E in human health*, 111-124.
- Acevedo, O. L. B., & Pauron, D. (2014). Protein-lipid interaction analysis by surface plasmon resonance (SPR). *Bio-protocol*, *4*(18), 1-8.
- Bonjoch, N. P., & Tamayo, P. R. (2001). Protein content quantification by Bradford method. In *Handbook of plant ecophysiology techniques* (pp. 283-295). Dordrecht: Springer Netherlands.
- Buettner, G. R. (1993). The pecking order of free radicals and antioxidants: lipid peroxidation, α -tocopherol, and ascorbate. *Archives of biochemistry and biophysics*, *300*(2), 535-543.
- Chattopadhyay, A. (1990). Chemistry and biology of N-(7-nitrobenz-2-oxa-1, 3-diazol-4-yl)-labeled lipids: fluorescent probes of biological and model membranes. *Chemistry and physics of lipids*, *53*(1), 1-15.
- Chiapparino, A., Maeda, K., Turei, D., Saez-Rodriguez, J., & Gavin, A. C. (2016). The orchestra of lipid-transfer proteins at the crossroads between metabolism and signaling. *Progress in lipid research*, *61*, 30-39.
- De Jong, L. A., Uges, D. R., Franke, J. P., & Bischoff, R. (2005). Receptor–ligand binding assays: technologies and applications. *Journal of chromatography B*, *829*(1-2), 1-25.
- Del Vecchio, K., & Stahelin, R. V. (2016). Using surface plasmon resonance to quantitatively assess lipid–protein interactions. *Lipid Signaling Protocols*, 141-153.
- Di Donato, I., Bianchi, S., & Federico, A. (2010). Ataxia with vitamin E deficiency: update of molecular diagnosis. *Neurological sciences*, *31*, 511-515.
- Du, Y. (2024). Binding Curve Viewer: Visualizing the Equilibrium and Kinetics of Protein–Ligand Binding and Competitive Binding. *Journal of Chemical Information and Modeling*, *64*(10), 4180-4192.
- Englebienne, P., Hoonacker, A. V., & Verhas, M. (2003). Surface plasmon resonance: principles, methods and applications in biomedical sciences. *Journal of Spectroscopy*, *17*(2-3), 255-273.
- Evans, H. M., & Bishop, K. S. (1922). On the existence of a hitherto unrecognized dietary factor essential for reproduction. *Science*, *56*(1458), 650-651.
- Frostell, Å., Vinterbäck, L., & Sjöbom, H. (2013). Protein–ligand interactions using SPR systems. *Protein-Ligand Interactions: Methods and Applications*, 139-165.
- Galli, F., Azzi, A., Birringer, M., Cook-Mills, J. M., Eggersdorfer, M., Frank, J., ... & Özer, N. K. (2017). Vitamin E: Emerging aspects and new directions. *Free Radical Biology and Medicine*, *102*, 16-36.

- Herrera, E., & Barbas, C. (2001). Vitamin E: action, metabolism and perspectives. *Journal of physiology and biochemistry*, 57, 43-56.
- Homola, J., Yee, S. S., & Gauglitz, G. (1999). Surface plasmon resonance sensors. *Sensors and actuators B: Chemical*, 54(1-2), 3-15.
- Hou, W., & Cronin, S. B. (2013). A review of surface plasmon resonance-enhanced photocatalysis. *Advanced Functional Materials*, 23(13), 1612-1619.
- Imounan, F., Bouslam, N., Aasfara, J., Regragui, W., Benhaddou, E. H. A., Bouhouche, A., ... & Yahyaoui, M. (2012). Vitamin E in ataxia and neurodegenerative diseases: a review.
- Jeenanong, A., & Kawaguchi, H. (2008). Effect of pH and temperature on the behavior of microgel in SPR sensor. *Colloids and Surfaces A: Physicochemical and Engineering Aspects*, 315(1-3), 232-240.
- Jiang, Q. (2014). Natural forms of vitamin E: metabolism, antioxidant, and anti-inflammatory activities and their role in disease prevention and therapy. *Free Radical Biology and Medicine*, 72, 76-90.
- Kiyose, C. (2021). Absorption, transportation, and distribution of vitamin E homologs. *Free Radical Biology and Medicine*, 177, 226-237.
- Kono, N., Ohto, U., Hiramatsu, T., Urabe, M., Uchida, Y., Satow, Y., & Arai, H. (2013). Impaired α -TTP-PIPs interaction underlies familial vitamin E deficiency. *Science*, 340(6136), 1106-1110.
- Manor, D.. (2007). [Vitamins & Hormones] *Vitamin E Volume 76 || The α -Tocopherol Transfer Protein*. , (), 45–65. doi:10.1016/S0083-6729(07)76003-X
- Mehta, V. A. (2023). A surface plasmon resonance investigation of the role of bilayer phospholipids in the binding and ligand interactions of the α -tocopherol transfer protein.
- Meier, R., Tomizaki, T., Schulze-Briese, C., Baumann, U., & Stocker, A. (2003). The molecular basis of vitamin E retention: structure of human α -tocopherol transfer protein. *Journal of molecular biology*, 331(3), 725-734.
- Md, A., Nahar, L., Lijon Md, B., Imran, S., & Rhaman, M. S. (2023). The Technique for Excessive-Results of Recombinant Protein Purification led to GST-tag Affinity Chromatography: A Review. *J Microb Biochem Technol*, 15, 584.
- Min, K. C. (2007). Structure and Function of α -Tocopherol Transfer Protein: Implications for Vitamin E Metabolism and AVED. *Vitamins & Hormones*, 76, 23-43.
- Min, K. C., Kovall, R. A., & Hendrickson, W. A. (2003). Crystal structure of human α -tocopherol transfer protein bound to its ligand: implications for ataxia with vitamin E deficiency. *Proceedings of the National Academy of Sciences*, 100(25), 14713-14718.
- Morales, E. S., Parcerisa, I. L., & Ceccarelli, E. A. (2019). A novel method for removing contaminant Hsp70 molecular chaperones from recombinant proteins. *Protein Science*, 28(4), 800-807.

- Muniz Correa, M. V. (2023). The Optimization of a Time-Resolved, Vesicle-Based Fluorescence Assay for the Activity of the Lipid Kinase PI4K-III β and the Effect of Lipid Transfer Proteins on Enzyme Activity.
- Niki, E., & Abe, K. (2019). Vitamin E: Structure, properties and functions.
- Niki, E., & Traber, M. G. (2012). A history of vitamin E. *Annals of Nutrition and Metabolism*, 61(3), 207-212.
- Pollard, T. D. (2010). A guide to simple and informative binding assays. *Molecular biology of the cell*, 21(23), 4061-4067.
- Ray, J., Sapp, D. G., & Fairn, G. D. (2024). Phosphatidylinositol 3, 4-bisphosphate: Out of the shadows and into the spotlight. *Current Opinion in Cell Biology*, 88, 102372.
- Rial, D. V., & Ceccarelli, E. A. (2002). Removal of DnaK contamination during fusion protein purifications. *Protein expression and purification*, 25(3), 503-507.
- Schasfoort, R. B. (Ed.). (2017). *Handbook of surface plasmon resonance*. Royal Society of Chemistry.
- Schäfer, F., Seip, N., Maertens, B., Block, H., & Kubicek, J. (2015). Purification of GST-tagged proteins. In *Methods in enzymology* (Vol. 559, pp. 127-139). Academic Press.
- Schmölz, L., Birringer, M., Lorkowski, S., & Wallert, M. (2016). Complexity of vitamin E metabolism. *World journal of biological chemistry*, 7(1), 14.
- Schneider, C. (2005). Chemistry and biology of vitamin E. *Molecular nutrition & food research*, 49(1), 7-30.
- Shahidi, F., Pinaffi-Langley, A. C. C., Fuentes, J., Speisky, H., & de Camargo, A. C. (2021). Vitamin E as an essential micronutrient for human health: Common, novel, and unexplored dietary sources. *Free Radical Biology and Medicine*, 176, 312-321.
- Stoll, V. S., & Blanchard, J. S. (2009). Buffers: principles and practice. In *Methods in enzymology* (Vol. 463, pp. 43-56). Academic Press.
- Sure, B. (1924). Dietary requirements for reproduction: II. The existence of a specific vitamin for reproduction. *Journal of Biological Chemistry*, 58(3), 693-709.
- Szymańska, R., Nowicka, B., Trela, A., & Kruk, J. (2020). Vitamin E: Structure and forms. In *Molecular nutrition* (pp. 67-90). Academic Press.
- Thapa, S., Shah, S., Chand, S., Sah, S. K., Gyawali, P., Paudel, S., & Khanal, P. (2022). Ataxia due to vitamin E deficiency: A case report and updated review. *Clinical Case Reports*, 10(9), e6303.
- Traber, M. G. (2007). Vitamin E regulatory mechanisms. *Annu. Rev. Nutr.*, 27(1), 347-362.

Ulatowski, L. M., & Manor, D. (2015). Vitamin E and neurodegeneration. *Neurobiology of disease*, 84, 78-83.

Usuki, F., & Maruyama, K. (2000). Ataxia caused by mutations in the α -tocopherol transfer protein gene. *Journal of Neurology, Neurosurgery & Psychiatry*, 69(2), 254-256.

Van Der Merwe, P. A. (2001). Surface plasmon resonance. *Protein-ligand interactions: hydrodynamics and calorimetry*, 1, 137-170.

Van Meer, G., Voelker, D. R., & Feigenson, G. W. (2008). Membrane lipids: where they are and how they behave. *Nature reviews Molecular cell biology*, 9(2), 112-124.

Wang, X., & Quinn, P. J. (1999). Vitamin E and its function in membranes. *Progress in lipid research*, 38(4), 309-336.

Waugh, D. S. (2011). An overview of enzymatic reagents for the removal of affinity tags. *Protein expression and purification*, 80(2), 283-293.

Zhang, W. X., Thakur, V., Lomize, A., Pogozeva, I., Panagabko, C., Cecchini, M., ... & Atkinson, J. (2011). The contribution of surface residues to membrane binding and ligand transfer by the α -tocopherol transfer protein (α -TTP). *Journal of molecular biology*, 405(4), 972-988.

6 Appendix

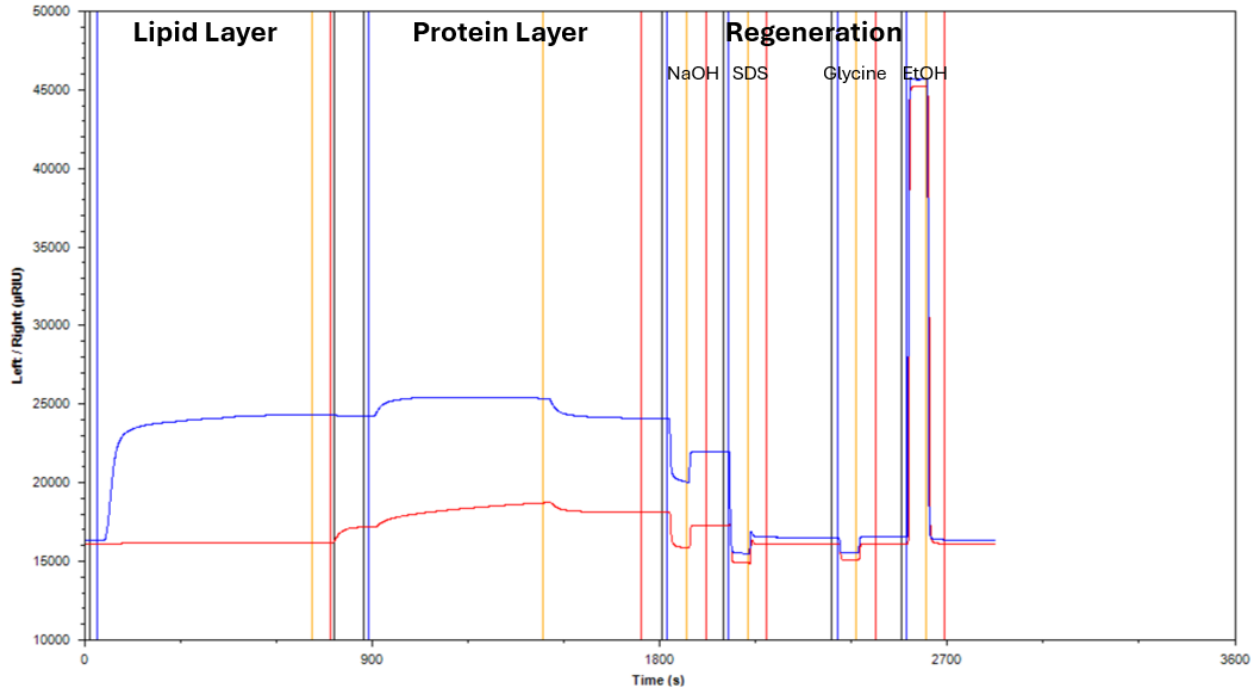


Figure 30. Representative Sensorgram of SPR Injections and Chip Regeneration Cycle.

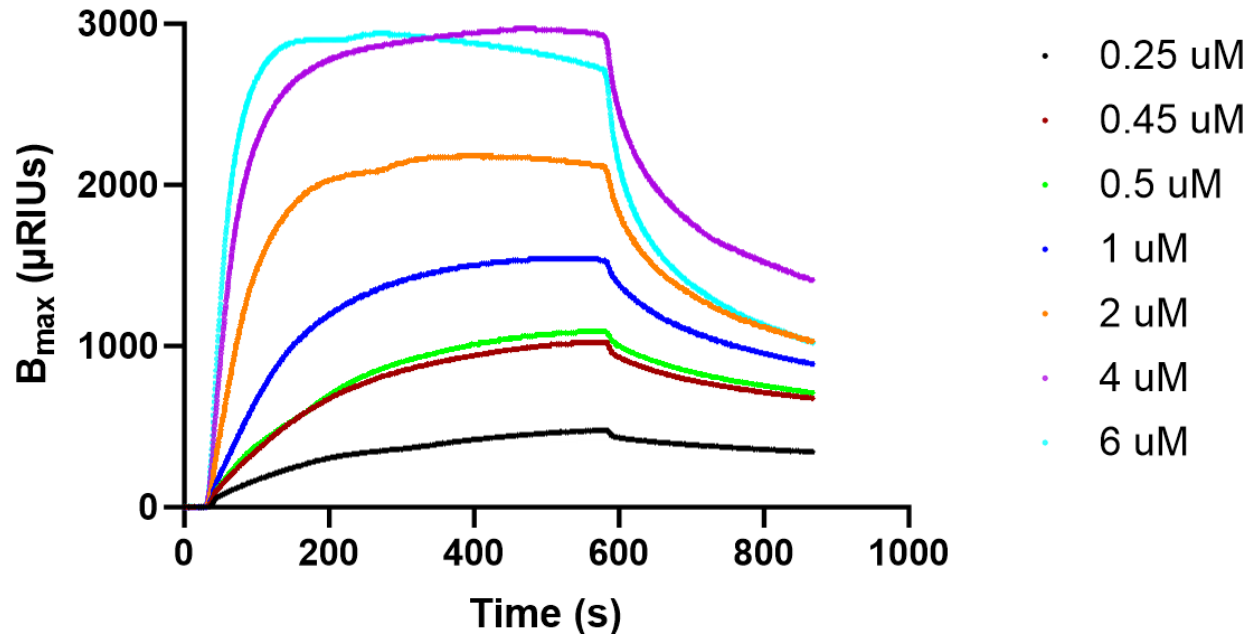


Figure 31. Raw Data Used to Generate the Concentration Binding Curve in Figure 21.

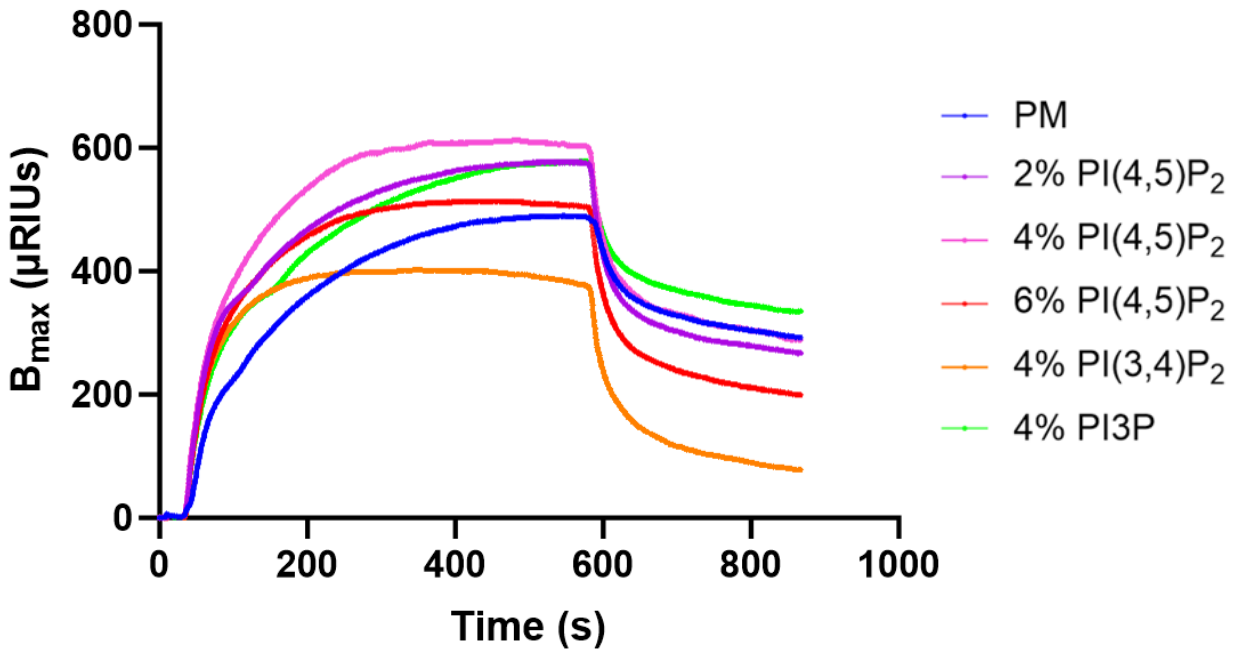


Figure 32. Raw Data of SPR Injections of wtTTP Used to Generate Figure 22.

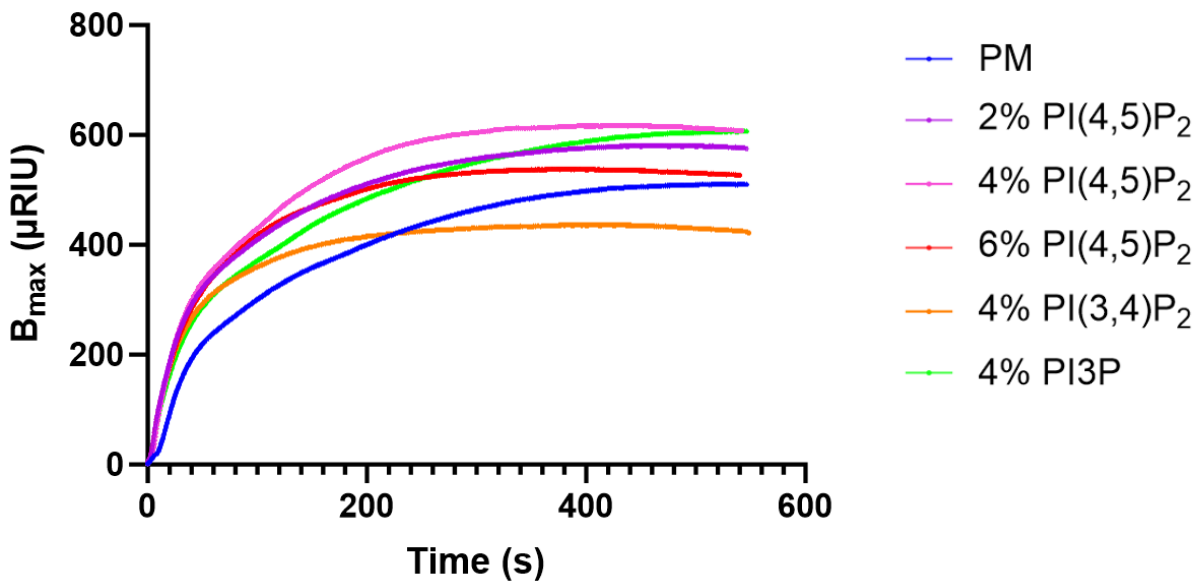


Figure 33. Non-normalized SPR Injections of wtTTP Used to Generate Figure 22.

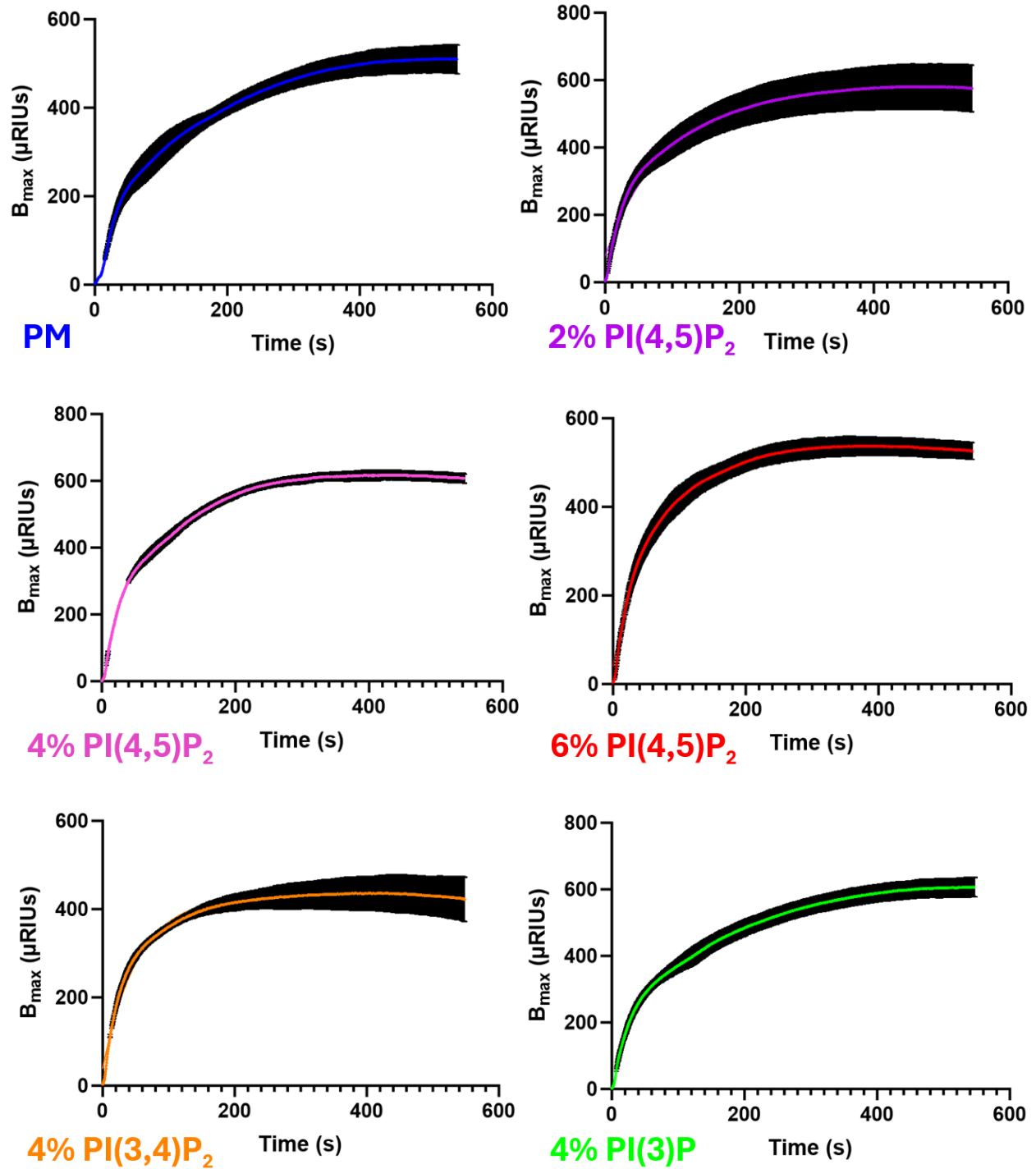


Figure 34. SPR Injections of wtTTP Depicting Error Bars Used to Generate Figure 22.

Table 8. Parameter Values of wtTTP Injections.

	wtTTP					
	PM	2% PI(4,5)P2	4% PI(4,5)P2	6% PI(4,5)P2	4% PI(3,4)P2	4% PI(3)P
B_{max} (μRIU)	516.2 ± 2.0	576.8 ± 2.8	617.0 ± 1.0	532.9 ± 1.0	429.3 ± 1.2	610.8 ± 2.1
Normalized B_{max} (μRIU)	1.000 ± 0.004	1.117 ± 0.005	1.195 ± 0.001	1.032 ± 0.002	0.832 ± 0.002	1.183 ± 0.004
k_{on} (s⁻¹)	0.00765 ± 0.00014	0.01103 ± 0.00035	0.01174 ± 0.00011	0.01503 ± 0.00021	0.01896 ± 0.00049	0.00750 ± 0.00013
R²	0.9648	0.8675	0.9849	0.9675	0.8995	0.9664

Table 9. P Values of Rate Constants for wtTTP Injections.

	PM	2% PI(4,5)P2	4% PI(4,5)P2	6% PI(4,5)P2	4% PI(3,4)P2	4% PI(3)P
PM		0.0991 (ns)	0.0556 (ns)	0.0025 (**)	< 0.0001 (****)	0.9395 (ns)
2% PI(4,5)P2	0.0991 (ns)		0.7460 (ns)	0.0661 (ns)	0.0012 (**)	0.0868 (ns)
4% PI(4,5)P2	0.0556 (ns)	0.7460 (ns)		0.1167 (ns)	0.0021 (**)	0.0484 (*)
6% PI(4,5)P2	0.0025 (**)	0.0661 (ns)	0.1167 (ns)		0.0468 (*)	0.0022 (**)
4% PI(3,4)P2	< 0.0001 (****)	0.0012 (**)	0.0021 (**)	0.0468 (*)		< 0.0001 (****)
4% PI(3)P	0.9395 (ns)	0.0868 (ns)	0.0484 (*)	0.0022 (**)	< 0.0001 (****)	

ns = not significant, * = $p < 0.05$, ** = $p < 0.01$, *** = $p < 0.001$, **** = $p < 0.0001$

Table 10. P Values of B_{max} Values for wtTTP Injections.

	PM	2% PI(4,5)P2	4% PI(4,5)P2	6% PI(4,5)P2	4% PI(3,4)P2	4% PI(3)P
PM		0.0611 (ns)	0.0053 (**)	0.5866 (ns)	0.0139 (*)	0.0079 (**)
2% PI(4,5)P2	0.0611 (ns)		0.2066 (ns)	0.1577 (ns)	0.0003 (****)	0.2856 (ns)
4% PI(4,5)P2	0.0053 (**)	0.2066 (ns)		0.0148 (*)	< 0.0001 (****)	0.8313 (ns)
6% PI(4,5)P2	0.5866 (ns)	0.1577 (ns)	0.0148 (*)		0.0049 (**)	0.0222 (*)
4% PI(3,4)P2	0.0139 (*)	0.0003 (****)	< 0.0001 (****)	0.0049 (**)		< 0.0001 (****)
4% PI(3)P	0.0079 (**)	0.2856 (ns)	0.8313 (ns)	0.0222 (*)	< 0.0001 (****)	

ns = not significant, * = $p < 0.05$, ** = $p < 0.01$, *** = $p < 0.001$, **** = $p < 0.0001$

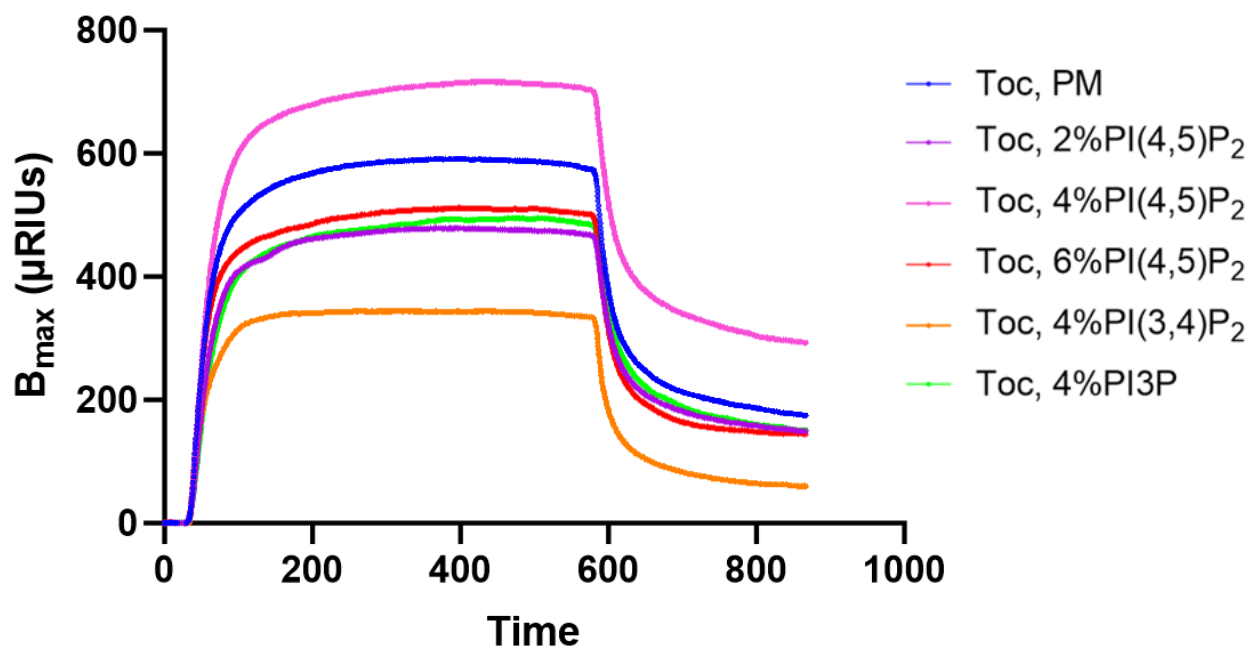


Figure 35. Raw Data of SPR Injections of wtTTP Preincubated with α -Tocopherol Used to Generate Figure 24.

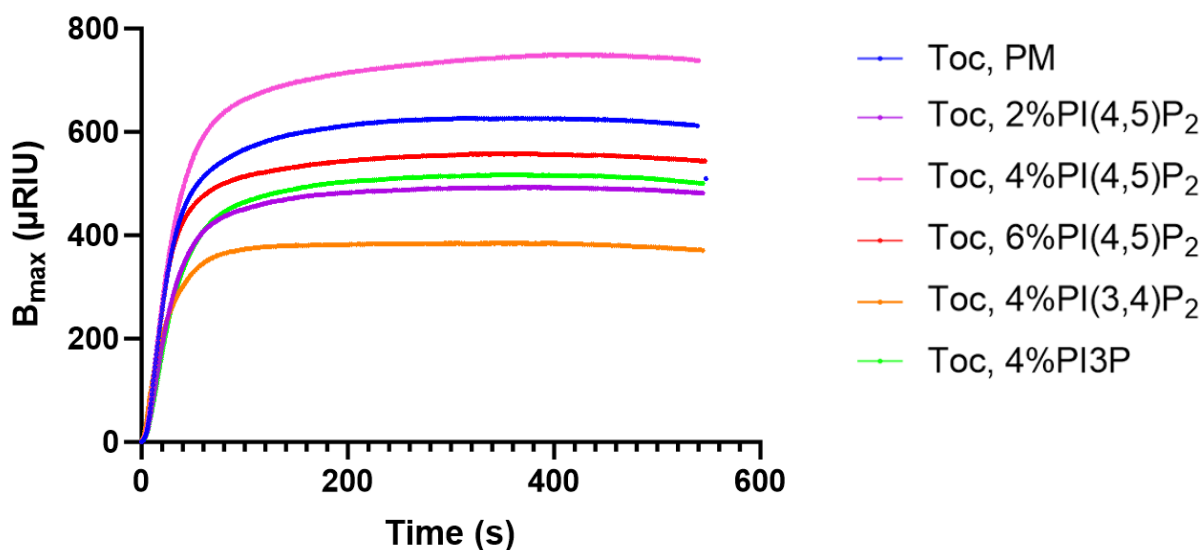


Figure 36. Non-normalized SPR Injections of wtTTP Preincubated with α -Tocopherol.

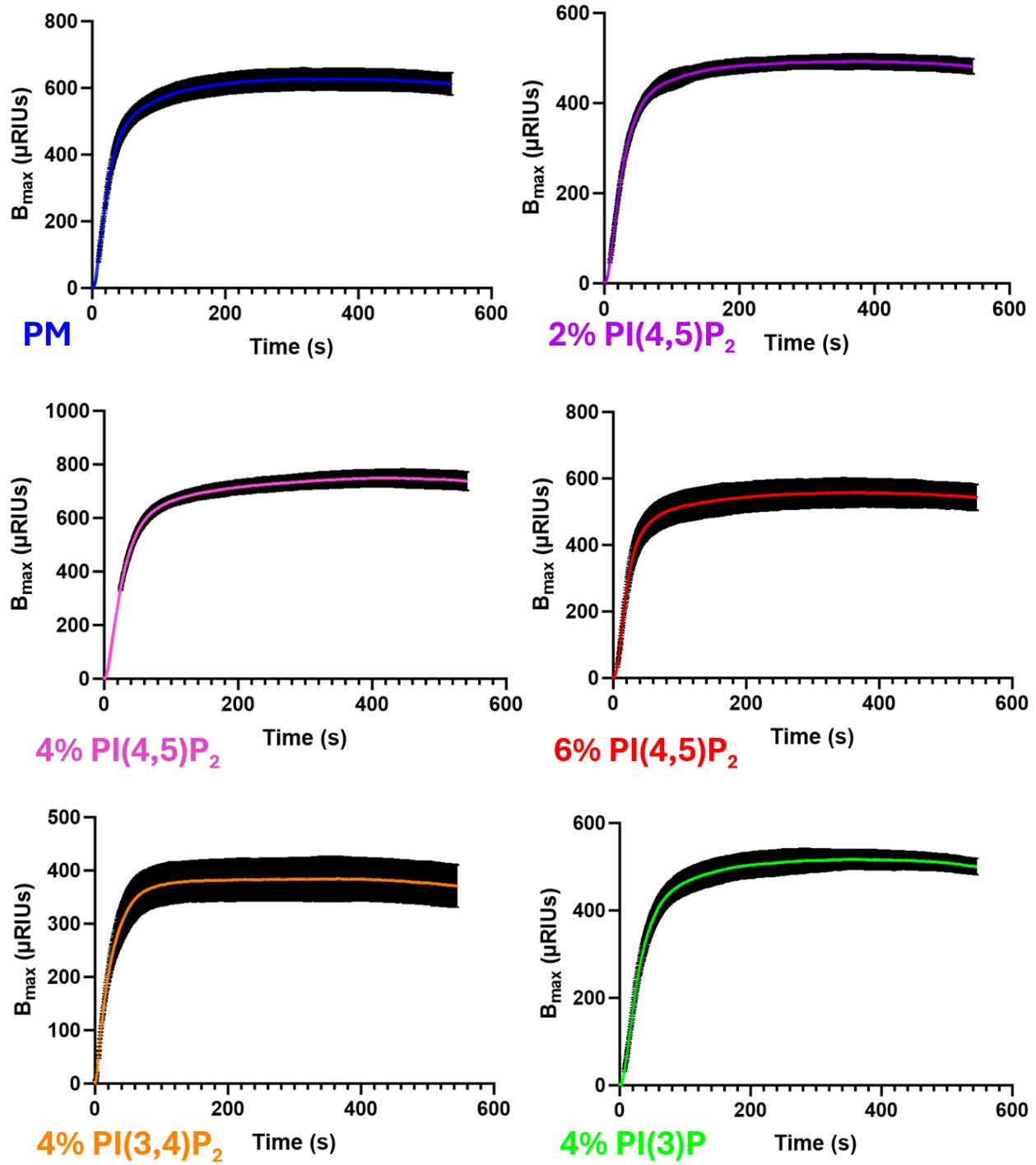


Figure 37. SPR Injections of wtTTP Preincubated with α -Tocopherol Depicting Error Bars Used to Generate Figure 24.

Table 11. Parameter Values of wtTTP Preincubated with α -Tocopherol Injections.

	wtTTP + α-Tocopherol					
	PM	2% PI(4,5)P2	4% PI(4,5)P2	6% PI(4,5)P2	4% PI(3,4)P2	4% PI(3)P
B_{max} (μRIU)	618.2 \pm 1.0	486.9 \pm 0.6	734.7 \pm 1.1	548.4 \pm 1.4	381.2 \pm 1.2	510.3 \pm 0.9
Normalized B_{max} (μRIU)	1.198 \pm 0.003	0.9433 \pm 0.0011	1.423 \pm 0.002	1.062 \pm 0.002	0.738 \pm 0.002	0.986 \pm 0.001
<i>k_{on}</i> (s⁻¹)	0.03023 \pm 0.00056	0.03015 \pm 0.00036	0.02646 \pm 0.00040	0.03598 \pm 0.00104	0.04031 \pm 0.00149	0.02678 \pm 0.00042
R²	0.9417	0.9731	0.9613	0.8647	0.7711	0.9532

Table 12. P Values of Rate Constants for wtTTP Preincubated with α -Tocopherol Injections.

	PM	2% PI(4,5)P2	4% PI(4,5)P2	6% PI(4,5)P2	4% PI(3,4)P2	4% PI(3)P
PM		0.9084 (ns)	0.0307 (*)	0.0037 (**)	< 0.0001 (****)	0.0395 (*)
2% PI(4,5)P2	0.9084 (ns)		0.0380 (*)	0.0030 (**)	< 0.0001 (****)	0.0488 (*)
4% PI(4,5)P2	0.0307 (*)	0.0380 (*)		< 0.0001 (****)	< 0.0001 (****)	0.8918 (ns)
6% PI(4,5)P2	0.0037 (**)	0.0030 (**)	< 0.0001 (****)		0.0166 (*)	< 0.0001 (****)
4% PI(3,4)P2	< 0.0001 (****)	< 0.0001 (****)	< 0.0001 (****)	0.0166 (*)		< 0.0001 (****)
4% PI(3)P	0.0395 (*)	0.0488 (*)	0.8918 (ns)	< 0.0001 (****)	< 0.0001 (****)	

ns = not significant, * = $p < 0.05$, ** = $p < 0.01$, *** = $p < 0.001$, **** = $p < 0.0001$

Table 13. P Values of B_{max} Values for wtTTP Preincubated with α -Tocopherol Injections.

	PM	2% PI(4,5)P2	4% PI(4,5)P2	6% PI(4,5)P2	4% PI(3,4)P2	4% PI(3)P
PM		0.0004 (***)	0.0009 (***)	0.0237 (*)	< 0.0001 (****)	0.0017 (**)
2% PI(4,5)P2	0.0004 (***)		< 0.0001 (****)	0.0408 (*)	0.0020 (**)	0.4009 (ns)
4% PI(4,5)P2	0.0009 (***)	< 0.0001 (****)		< 0.0001 (****)	< 0.0001 (****)	< 0.0001 (****)
6% PI(4,5)P2	0.0237 (*)	0.0408 (*)	< 0.0001 (****)		< 0.0001 (****)	0.1807 (ns)
4% PI(3,4)P2	< 0.0001 (****)	0.0020 (**)	< 0.0001 (****)	< 0.0001 (****)		0.0004 (***)
4% PI(3)P	0.0017 (**)	0.4009 (ns)	< 0.0001 (****)	0.1807 (ns)	0.0004 (***)	

ns = not significant, * = $p < 0.05$, ** = $p < 0.01$, *** = $p < 0.001$, **** = $p < 0.0001$

MS Instrument: Bruker HCTplus Ion-Trap

Sample Name: NBD- α -tocopherol C9-2014 Ion Source Type(Polarity): ESI+/-

File Name: JAH6362

Solvent : MeOH

Please read through the 7-page report.

ESI-

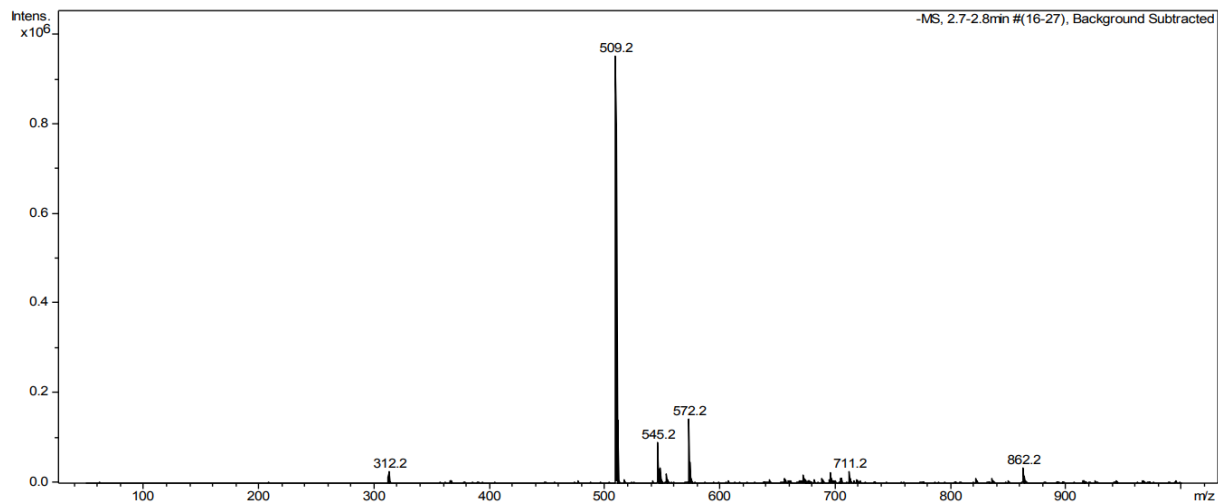


Figure 38. Mass Spectrum of NBD- α -Tocopherol Stock Solution.